NASA Technical Paper 1503

An Experimental and Theoretical Investigation of the Effect of Nonmetric Over-the-Wing Nacelles on Wing-Body Aerodynamics

David E. Reubush

AUGUST 1979

NASA

NASA Technical Paper 1503

An Experimental and Theoretical Investigation of the Effect of Nonmetric Over-the-Wing Nacelles on Wing-Body Aerodynamics

David E. Reubush
Langley Research Center
Hampton, Virginia

National Aeronautics
and Space Administration

**Scientific and Technical
Information Branch**

1979

SUMMARY

An investigation was conducted in the Langley 16-foot transonic tunnel to study drag reduction benefits due to blowing the jet exhausts over the wing for a transport-type wing-body configuration. In this investigation a combination of a wing-body model and a powered-nacelle test rig was tested at Mach numbers of 0.50 and 0.80 at angles of attack from -2° to 4° and jet total-pressure ratios from jet off to 3 or 4 (depending on Mach number) for a variety of nacelle locations relative to the wing. In addition, the experimental results were compared with the predictions obtained from several theoretical techniques. Results from this investigation indicate that positioning of the nacelles (nonmetric) can have large effects on the wing-body drag. Some positions yielded higher drag than the baseline position, whereas others yielded lower drag than the baseline position. Results from the theoretical investigation indicate that the theoretical method which utilized a quasi-vortex-lattice for the wing and wing-jet interaction in combination with a jet entrainment model gave generally reasonable predictions of the drag increments.

INTRODUCTION

The nation's fleet of transport aircraft is becoming evermore dependent on foreign oil for its fuel supply. There are also increasing demands for the fleet to be more environmentally acceptable. The need for technology to design and build a new generation of transport aircraft to meet the twin challenges of reduced fuel consumption and environmental acceptability has become acute. As a part of an overall program to develop this technology, NASA has a concerted effort underway in the area of propulsion system integration, one area of emphasis concentrating on unconventional engine arrangements. One of the most promising of these unconventional configurations is the over-the-wing (OTW) arrangement in which the engine nacelles are supported on pylons above the wing upper surface. The effect of blowing a jet above a lifting surface was first investigated during World War II (ref. 1) in regard to jet flow over tail surfaces. However, it was not until recently that this type of configuration was considered for transports. (See refs. 2 and 3.) This consideration was due primarily to the expected noise reduction resulting from the shielding of the jet exhaust by the wing. In these investigations, it was discovered that, in addition to the anticipated noise reduction, this type of configuration arrangement resulted in increased lift and reduced drag. As a result of these aerodynamic gains, the VFW 614 was designed and built with OTW nacelles. (See ref. 3.) More recently, this configuration arrangement has been investigated for supersonic transport (SST) configurations. (See refs. 4 to 6.)

Although the VFW 614 is flying with OTW nacelles and data have been published for SST configurations with OTW nacelles, there is a scarcity of published data on subsonic transport configurations. This lack of available experimental data has hindered the verification of the various theoretical techniques (refs. 7 to 12) which have been developed to predict the performance

gains from these types of engine arangements. In an effort to alleviate this problem and to gain further insight into the mechanisms involved, an experimental investigation was initiated in the Langley 16-foot transonic tunnel. In this investigation the movable nacelle support mechanism first used in the investigation of reference 4 was modified to incorporate nacelles typical of high-bypass-ratio turbofan engines. By use of this mechanism, an existing wing-body model typical of a subsonic transport configuration was tested with the nacelles positioned over the wing in several locations. The results of this investigation were reported in reference 13. Unfortunately, interference from the supporting/translating mechanism for the nacelles invalidated the measured total drag data, and only induced drag data were presented. These data, however, showed that the induced drag for most OTW nacelle configurations tested was lower than that for the basic wing-body. Because of these favorable effects, a second investigation was initiated. In this investigation, the results of which are presented herein, the boattailed aft fuselage of the model of reference 13 was replaced by a cylindrical aft fuselage with body and base-pressure instrumentation. With this type of fuselage, the interference from the nacelle supporting/translating mechanism should be limited to changes in base pressures. It should, therefore, be possible to eliminate the nacelle supporting/translating mechanism interference on the model drag by correcting for these base-pressure differences. The revised model was tested in the Langley 16-foot transonic tunnel at Mach numbers of 0.5 and 0.8 at angles of attack of -2° to 4° with jet total-pressure ratios from jet off to a maximum of 4, depending on Mach number and using room-temperature high-pressure air to simulate the jet exhaust. The locations of the nacelles relative to the wing were chosen on the basis of the data of reference 13.

SYMBOLS AND ABBREVIATIONS

b	wing span, 91.44 cm
C_D	drag coefficient
$C_{D,o}$	drag coefficient at zero lift
ΔC_D	drag coefficient increment, $C_D - C_{D,o}$
C_L	lift coefficient
C_m	pitching-moment coefficient
C_p	pressure coefficient, $\frac{p - p_\infty}{q_\infty}$
$\bar{c}$	wing mean aerodynamic chord, 16.21 cm
D	nacelle exit diameter, 5.08 cm
Exp	experimental

J.O. jet off

l axial distance from nose of fuselage, positive aft

M Mach number

NPR nozzle pressure ratio, $p_{t,j}/p_\infty$

OTW over the wing

p static pressure on fuselage

$p_{t,j}$ jet total pressure

p_∞ free-stream static pressure

q_∞ free-stream dynamic pressure

R radial distance from centerline of nacelle

S wing area, 0.139 m^2

s axial distance from model station 80.77 cm, positive aft

x axial position of nacelle exit with respect to local wing leading edge, positive aft

x_n axial distance from nose of nacelle, positive aft

y spanwise position of nacelle exit with respect to model centerline

z vertical position of nacelle exit with respect to wing chord plane, positive up

α angle of attack

ϕ meridional angle about model axis, positive clockwise when viewed from rear, 0° at top of model

APPARATUS AND PROCEDURE

Wind Tunnel

The investigation was conducted in the Langley 16-foot transonic tunnel, which is a single-return, continuous-flow, atmospheric tunnel. The test section is a regular octagon in cross section, with slots at the corners of the octagon. The tunnel speed can be varied continuously from a Mach number of 0.20 to a Mach number of 1.30. Further description of the Langley 16-foot transonic tunnel can be found in references 14 to 16.

Models and Support System

The wing-body model with nacelles and nacelle supporting/translating apparatus mounted in the Langley 16-foot transonic tunnel is shown in figure 1. A sketch of the wing-body model is shown in figure 2. The body of the model was 123.95 cm long and had a maximum diameter of 12.45 cm. The wing was swept back 35^{o} at the quarter chord and had a wing area S of 0.139 m^2, an aspect ratio of 6, an NACA 63A008 airfoil section, a span of 91.4 cm, a root chord of 21.77 cm, a tip chord of 8.71 cm, and a mean aerodynamic chord of 16.21 cm. The two nacelles were each 44.45 cm long and had a maximum diameter of 7.11 cm and a jet exit diameter of 5.08 cm. The nacelle supporting/translating apparatus allowed 3 degrees of translational freedom in locating the nacelles relative to the wing.

Instrumentation and Tests

The wing-body model was mounted on a six-component strain-gage balance which was used to measure the aerodynamic forces and moments. The nacelles and their supporting/translating apparatus were nonmetric. In addition to the balance, the top of the aft fuselage was instrumented with 17 static-pressure taps, 2.54 cm apart, in a row starting at model station 80.77 cm. The base was instrumented with four base-pressure orifices, and the balance cavity was instrumented with two static-pressure taps to facilitate adjustments to the balance data to free-stream static pressure at the base and in the cavity.

Tests were conducted in the Langley 16-foot transonic tunnel at Mach numbers of 0.5 and 0.8, at angles of attack from -2^{o} to 4^{o}, with nozzle total-pressure ratios from jet off to 3 at $M = 0.5$ and jet off to 4 at $M = 0.8$ to simulate realistic plume shapes at these Mach numbers. To facilitate the determination of propulsion induced increments, if desired, the lowest jet on nozzle pressure ratios tested (1.2 at $M = 0.5$ and 1.5 at $M = 0.8$) were chosen to simulate those from a flow-through nacelle. Grit was applied to the nose and wings of the model according to the methods of references 17 and 18 to insure turbulent flow at all test conditions. With the nacelle support apparatus allowing 3 degrees of translational freedom in locating the nacelles relative to the wing, the wing-body model was tested with the centerline of the nacelle exits in a variety of locations as shown in the following table:

x/D	z/D of -			
	0.5	1.0	1.5	1.0
	0.25b/2			0.5b/2
-1		x		
0	x	x	x	x
1		x		x
1.5		x		
2		x		
3		x		

PRESENTATION OF RESULTS

The results from this investigation are presented in the following figures:

DISCUSSION

Baseline Determination

To assess the effectiveness of OTW nacelles in reducing drag, a baseline must be established with which comparisons can be made. In reference 13, model total drag coefficients were not presented. Only induced drag coefficients were presented because of an interference effect from the nacelle supporting/translating apparatus which propagated forward and changed the pressure field felt by the boattailed aft fuselage. This change in the pressure field thus changed the measured drag on the model. Thus, interference varied with nacelle position as the supporting/translating apparatus changed position. Since there was no pressure instrumentation on this aft fuselage, there was no way to correct the drag coefficient data for this effect. For the current investigation, a new cylindrical aft fuselage was constructed with extensive pressure instrumentation. With this cylindrical fuselage, the primary area affected by the drag interference should be the base, and with the base-pressure measurements, correction for this interference is possible. To assess the effect of the nacelle support system, the nacelles, nacelle support booms, and pylons were removed, leaving only the aft supporting/translating mechanisms. Tests were made with these supports in the locations corresponding to the locations for the various nacelle positions (a total of 10). The data obtained are shown in figure 3 at both $M = 0.5$ and $M = 0.8$. As can be seen, the lift, drag, and

pitching-moment coefficients, after correction for base-drag effects, are not significantly affected at either Mach number by movement of this supporting/translating apparatus. Virtually all the data fall within the normal wind-tunnel accuracy of ±0.5 percent. Therefore, the average coefficient curves (both M = 0.5 and 0.8) for the 10 runs, plotted as solid lines in figure 3, will be used as the baseline for comparison purposes in succeeding figures. In addition, as a further check on the effectiveness of the base and cavity corrections, the wing-body was tested with the supporting/translating apparatus removed, and these data are plotted as the dashed lines in figure 3. Again, these data fall well within ±0.5 percent.

Effect of Nozzle Pressure Ratio

Wing-body lift, drag, and pitching-moment characteristics of the various configurations are shown in figures 4 to 13 for the various nozzle pressure ratios investigated at both M = 0.5 and 0.8. The effect of nozzle pressure ratio on each individual configuration will not be discussed but the effects on a typical configuration ($x/D = 1$, $2y/b = 0.25$, $z/D = 1$) shown in figure 6 are discussed. For the range of pressure ratios investigated, a large increase in drag coefficient occurs when the jet is first turned on, with generally only slight changes as the pressure ratio is increased above the simulated flow-through nozzle pressure ratios. When compared with the baseline, it appears from these data that the solid blockage interference effect of the presence of the nacelles and low energy wake is highly beneficial to the wing-body drag, and operation of the jet tends to reduce this beneficial effect. Although the large beneficial interference effect of the installation of the nacelles was not totally anticipated, the effect is seen for most of the 10 nacelle positions tested. Whether there is a corresponding detrimental effect on the nacelles themselves is unknown since the nacelles were, of necessity, nonmetric. Another interesting but smaller effect is seen, especially at M = 0.8; the drag curves remain essentially the same for jet-on nozzle pressure ratios of 3 and below, whereas the drag at a nozzle pressure ratio of 4 is higher. It is believed that this phenomenon is an indication that the jet plume has spread sufficiently at the high nozzle pressure ratio so that it hits the wing and results in a scrubbing drag and possibly a wave drag that are not found at the lower nozzle pressure ratios. Care should, therefore, be exercised in the design of full-scale aircraft configurations to insure that the plume at the engine operating nozzle pressure ratio will not impinge on the wing.

As with drag coefficient, there is a relatively large effect on nose-down pitching moment when the jet is turned on, and then only very minor changes with increases in nozzle pressure ratio. Jet operation has only a small effect on the stability of the configuration. The lift curves generally show only small changes in level with nozzle pressure ratio but retain approximately the same slope. These results are encouraging in that there are no large changes in stability which would have to be dealt with for a configuration utilizing this type of engine arrangement.

Since changes in nozzle pressure ratio, once the jet has been turned on, have only small effects on wing-body aerodynamic characteristics, all further comparisons between various nacelle positions will be presented at constant

values of nozzle pressure ratio. It is anticipated that a typical future high-bypass-ratio engine will deliver a constant total-pressure rise factor of approximately 1.6 over its subsonic Mach number operating envelope. This total-pressure rise factor translates into nozzle pressure ratios approximately 2.0 at $M = 0.5$ and 2.5 at $M = 0.8$. These, then, are the nozzle pressure ratios at which the comparison data will be presented.

Effect of Nacelle Height

The effects of nacelle-exit vertical location on wing-body characteristics at Mach numbers of 0.5 and 0.8 for configurations with the nacelle exits at $x/D = 0$ and $2y/b = 0.25$ are shown in figure 14. As would be expected, the configuration with the nacelle exits at $z/D = 0.5$ (equivalent to upper surface blowing) has the highest drag because of the scrubbing drag associated with the jet washing the wing. The two other configurations exhibit progressively lower drag as the nacelles are raised above the wing. The trend for nacelle height above the wing, therefore, is that as the nacelles are raised above the wing, and hence as the jet moves away from the surface of the wing, the drag is reduced. However, in the range of cruise lift coefficients around 0.3, the drag of the $z/D = 1.5$ configuration is not much lower than that of the $z/D = 1$ configuration, especially at $M = 0.5$. The effects of nacelle-exit vertical position on the wing-body lift and pitching-moment characteristics are small at both Mach numbers.

Effect of Nacelle Span Location

Nacelle-exit span-location effects (span locations of $2y/b = 0.25$ and 0.5) on wing-body aerodynamic characteristics for configurations with $z/D = 1$, $x/D = 0$, and $x/D = 1$ at Mach numbers of 0.5 and 0.8 are shown in figures 15 and 16. For both $x/D = 0$ and $x/D = 1$ configurations, there are significant reductions in drag when the nacelles are moved outboard. It is believed that there are at least two factors which contribute to the benefits seen from the outboard location. The beneficial solid blockage interference from the presence of the nacelles can propagate further over the wing before interacting with the effect of the body. Also, the flow-channeling effect due to the proximity of the nacelle and body is eliminated by the outboard placement.

At this point, it should be mentioned that at lift coefficients near 0.3, the drag of the $x/D = 0$ configuration with the nacelle exits at $z/D = 1$ and $2y/b = 0.5$ is lower at both $M = 0.5$ and 0.8 than that for the baseline wing-body. At $x/D = 1$, both the $2y/b = 0.25$ and $2y/b = 0.5$ configurations have lower drag than the baseline wing-body over almost the whole C_L range, the $2y/b = 0.5$ configuration having substantially lower drag than the baseline in the range of lift coefficients for cruise. Since it was shown in figure 6 that for the conditions considered herein, jet operation has a detrimental effect on wing-body drag, these improvements in drag over the baseline wing-body must be due to a very large beneficial interference effect on the wing caused by the presence of the nacelles. As mentioned before, whether there is a corresponding detrimental effect on the nacelles themselves is unknown since the nacelles

were, of necessity, nonmetric. Further research is necessary to determine the corresponding forces and moments on the nacelles of configurations incorporating this type of engine arrangement.

Although there are large effects of span location on drag, the lift and pitching-moment characteristics for these configurations (as well as previously discussed configurations, which do not exhibit reductions in drag that are as significant as these) change only slightly, if at all. The trend in pitching-moment coefficient with span location for both $x/D = 0$ and $x/D = 1$ configurations is for the configurations to have more nose-down moments at $2y/b = 0.5$ than at $2y/b = 0.25$, whereas the slope remains about the same at both positions. The slopes of the pitching-moment coefficient curves for all four configurations are somewhat less than that for the wing-body alone. The effect of spanwise movement of the nacelles on the wing-body lift coefficient is small at both $x/D = 0$ and $x/D = 1$. In addition, the lift curves for all four configurations are very close to that of the baseline wing-body.

Effect of Nacelle Longitudinal Location

Figures 17 and 18 present the effect of nacelle longitudinal location on wing-body aerodynamic characteristics for configurations with the nacelles at $2y/b = 0.25$ and 0.5, respectively ($z/D = 1$ for all configurations). As can be seen from figure 17, this position variable was extensively investigated at $2y/b = 0.25$. This extensive investigation was due in part to the results from the test reported in reference 13 which indicated that moving the nacelles aft caused a reduction in induced drag. The current data indicate that as the nacelles are moved aft from $x/D = -1$, the drag polars initially tend to change so that the drag coefficients at cruise lift coefficients (e.g., 0.3) are lower as the nacelles are moved aft. At nacelle exit locations of $x/D \geq 1$ aft of the leading edge, the shape of the drag polars begins to change so that there are cross-overs in relative position with different nacelle exit positions having lower drag at different lift coefficients. Also the relative positions of the polars are not exactly the same at both Mach numbers. However, at both $M = 0.5$ and 0.8 and at lift coefficients above approximately 0.2, the $x/D = 1.5$ configuration has the lowest drag of any of this series. In addition, when the nacelle exits are moved from $x/D = 2$ to $x/D = 3$, the general trend of a reduction in drag with aft movement is reversed. The reason for the reversal in trend is not clear at present. It should, however, be noted that several of the configurations with nacelle exits aft of the leading edge have drag coefficients in the cruise range which are lower than the baseline wing-body drag coefficients for both Mach numbers investigated. This result again indicates that at these positions, the beneficial interference effect from the presence of the nacelles more than overcomes the adverse effects of jet operation.

At the 50-percent semispan position (fig. 18), only two axial nacelle-exit locations were investigated: $x/D = 0$ and $x/D = 1$. As with the $2y/b = 0.25$ configurations, the $x/D = 1$ configuration has substantially lower drag than the $x/D = 0$ configuration at both Mach numbers. Although the optimum axial location at $2y/b = 0.5$ was not determined, the $x/D = 1$ configuration does

have the lowest drag of any of the nacelle-exit positions tested, and the drag is substantially below that of the baseline wing-body.

At both $2y/b = 0.25$ and 0.5, there are only minor effects of nacelle longitudinal location on wing-body pitching-moment coefficient with the exception of the configuration with $x/D = 3$ at $2y/b = 0.25$. For this configuration, there is an increase in the nose-down pitching moment over that for the other configurations at both Mach numbers. The causes for this shift are probably the same as those for the reversal of the drag coefficient trend with this configuration and, as such, have not been identified. Aft movement of the nacelles caused an increase in lift at zero angle of attack without changing the lift-curve slope for all configurations at both $2y/b = 0.25$ and $2y/b = 0.5$.

Effect of Nacelle Position at $C_L = 0.3$

Summary plots of the trends in wing-body drag with nacelle position at a typical cruise C_L of 0.3 for both $M = 0.5$ and 0.8 are shown in figure 19. Figure 19(a) shows the effect of nacelle vertical position at $x/D = 0$ and at $2y/b = 0.25$, with the $z/D = 1.5$ configuration having the lowest drag of this series. No positions above $z/D = 1.5$ were tested, but the shape of the curves at both $M = 0.5$ and 0.8 indicate that possibly the minimum drag coefficient has been reached. Figure 19(b) shows the effect of nacelle-exit span location at both $x/D = 0$ and $x/D = 1$ for configurations with $z/D = 1$. As mentioned in the previous discussion, the trend is for the wing-body drag coefficient to be reduced as the nacelles are moved outboard. Figure 19(c) shows the effect of nacelle-exit longitudinal position on wing-body drag coefficient for configurations with $2y/b = 0.25$ and $z/D = 1$. Again, the $x/D = 1.5$ configuration has the lowest drag for this lift coefficient of all the longitudinal positions tested at $2y/b = 0.25$. Also indicated in figure 19 is the drag of the baseline wing-body configuration at $C_L = 0.3$ and, as can be seen, there are several nacelle locations with jets operating which yield lower drag than the baseline wing-body configuration.

Aft Fuselage Pressures

The pressure coefficients measured with the row of static-pressure taps along the top of the aft fuselage are shown in figure 20 at both Mach numbers and an angle of attack of about 0°. Two general comments can be made concerning these data. For all configurations, the installation of the nacelles results in higher pressure coefficients over most of the aft fuselage whereas the operation of the jets reduces the level slightly. This condition corresponds to the effects in wing-body drag, as shown in figure 6. When the nacelles were installed, the drag was substantially reduced but jet operation had a detrimental effect. Also, the two aftmost nacelle positions tested at $2y/b = 0.25$ ($x/D = 2$ and 3) show very large positive pressure rises toward the beginning of the aft fuselage with the installation of the nacelles. This result appears to provide some insight as to the possible mechanism by which the installation of the nacelles yields drag reductions, that is, by propagating a

positive pressure field over the wing and body. The configurations which have the lowest drag have this positive pressure field over the wing (e.g., $x/D = 1.5$ at $2y/b = 0.25$).

Theoretical Investigation

There are several theoretical methods which have been specifically developed to predict the drag increments due to the use of jets blowing over a wing. Comparisons of the drag increments predicted by the methods of references 7, 10, and 12 with the experimental data for the 10 configurations tested are shown in figure 21 ($M = 0.5$, $p_{t,j}/p_\infty = 2.0$ and $M = 0.8$, $p_{t,j}/p_\infty = 2.5$). The method of reference 7 uses a vortex-lattice representation of the wing lifting surface and a line sink-source distribution to simulate the effects of the jet exhaust on the wing lift and drag. The method is limited to those cases where the jet exhaust does not intersect or wash the wing. The method of reference 10 uses a quasi-vortex-lattice representation for the wing and wing-jet interaction due to differences between the jet and free-stream dynamic pressures and Mach numbers in combination with an entrainment theory for the effects of jet entrainment on the wing. The method of reference 12 is the same as that of reference 10 with the addition of the capability of including the fuselage. Both of these methods allow the jet to wash the wing. However, these three methods do not include the nacelles in the calculations.

Generally, all three methods are somewhat optimistic with regard to the predicted drag increments. The method of reference 10 generally gives reasonable predictions; the method of reference 7, somewhat worse predictions (not shown for all configurations tested); and the method of reference 12, the poorest predictions of the drag increments. The reason for the deterioration of prediction capability with the addition of the fuselage in going from the method of reference 10 to that of reference 12 is not completely clear. However, it must be noted that the instructions in reference 12 state that the wing should not intersect the fuselage, but when a test case (not shown) was run with the wing going to the centerline of the fuselage, the results were essentially the same as the results from reference 10. This result suggests that perhaps the fuselage contributions are not being handled correctly. In all cases, the addition of a method to calculate the effect of the nacelles on the configuration would probably improve the theoretical predictions since the experimental data show that the nacelles themselves have a large effect on the wing-body drag.

In addition to the comparisons which were made with the theoretical methods, a further theoretical investigation was undertaken. Since the jets in the experimental investigation were simulated by high pressure air, the nacelle inlets could not be simulated and the nacelle forebodies were smoothly faired to a point. There was some concern that this fairing would result in an unrealistic interference effect on the wing-body which would thus invalidate the drag reduction results found during the investigation. To insure that this was not the case, a three-dimensional panel aerodynamics method was exercised. (See ref. 19.) A number of configurations were examined by using this method, including fuselage alone, fuselage with nacelles and jets, fuselage with nacelles and jets with the nacelles extended far forward as cylinders to simu-

late the inlet stream-tube, wing-body with nacelles and jets, and wing-body with nacelles and jets with the nacelles extended forward. Typical fuselage pressure coefficient results from this investigation are shown in figure 22 for $\phi = 15^{\circ}$ and 165° for both the fuselage and wing-body configurations at $M = 0.5$ and $\alpha = 0^{\circ}$. As can be seen in the region of the fuselage where there is a forward-facing area, the pressure level is higher over most of this area for the configurations with the pointed-nose nacelles than for the extended nacelles. This condition means that the suction on the fuselage nose is less; hence, the drag of the configuration is greater than if the inlet had been in operation. Therefore, the drag reductions found during the experimental investigation should actually be conservative.

CONCLUDING REMARKS

The current investigation of the effect of over-the-wing nacelles on wing-body aerodynamic characteristics has indicated a number of significant results. Jet operation has a detrimental effect on wing-body drag when compared with jet-off levels for this type of configuration arrangement. However, the interference on the wing-body due to the presence of the nacelles is beneficial so that in some cases the drag of the wing-body with nacelles and jets operating is lower than that of the baseline wing-body. (It should be noted that the nacelles were not metric and, as such, it was impossible to ascertain their direct effect.) Of the configurations investigated, the one with the lowest drag had the nacelles installed at $x/D = 1$, $2y/b = 0.5$, and $z/D = 1$ where x, y, and z are the axial, spanwise, and vertical coordinates; b is wing span; and D is nacelle exit diameter. Of the configurations investigated at $2y/b = 0.25$, the configuration with $x/D = 1.5$ and $z/D = 1$, had the lowest drag in the range of typical cruise lift coefficients. Concurrent with the beneficial effects on wing-body drag, the effects of the nacelles on wing-body lift are generally small and beneficial when compared with the lift of the baseline wing-body. The effects of the nacelles on wing-body pitching moment are also generally small. Therefore, the drag benefits from this type of configuration arrangement may be accrued without any extreme trim drag penalty. Results from the theoretical portion of this investigation indicate that the theoretical method which utilized a quasi-vortex-lattice for the wing and wing-jet interaction in combination with a jet entrainment model gave generally reasonable predictions of the induced drag coefficients for this type of configuration arrangement. Also further theoretical investigation indicates that the drag reductions from the experimental data are conservative.

Langley Research Center
National Aeronautics and Space Administration
Hampton, VA 23665
July 6, 1979

REFERENCES

1. Falk, H.: The Influence of the Jet of a Propulsion Unit on Nearby Wings. NACA TM 1104, 1946.

2. Putnam, Lawrence E.: Exploratory Investigation at Mach Numbers From 0.40 to 0.95 of the Effects of Jets Blown Over a Wing. NASA TN D-7357, 1973.

3. Krenz, G.; and Ewald, B.: Airframe - Engine Interaction for Engine Configurations Mounted Above the Wing. Airframe/Propulsion Interference, AGARD-CP-150, Mar. 1975, pp. 26-1 - 26-32.

4. Mercer, Charles E.; and Carson, George T., Jr.: Upper Surface Nacelle Influence on SCAR Aerodynamic Characteristics at Transonic Speeds. Proceedings of the SCAR Conference - Part I, NASA CP-001, 1977, pp. 137-154.

5. Coe, Paul L., Jr.; McLemore, H. Clyde; and Shivers, James P.: Effects of Upper-Surface Blowing and Thrust Vectoring on Low-Speed Aerodynamic Characteristics of a Large-Scale Supersonic Transport Model. NASA TN D-8296, 1976.

6. Shrout, Barrett L.; and Hayes, Clyde: Effect of a Simulated Engine Jet Blowing Above an Arrow Wing at Mach 2.0. NASA TP-1050, 1977.

7. Putnam, Lawrence E.: An Analytical Study of the Effects of Jets Located More Than One Jet Diameter Above a Wing at Subsonic Speeds. NASA TN D-7754, 1974.

8. Ahmed, S. R.: Prediction of the Optimum Location of a Nacelle Shaped Body on the Wing of a Wing-Body Configuration by Inviscid Flow Analysis. Airframe/Propulsion Interference, AGARD-CP-150, Mar. 1975, pp. 25-1 - 25-12.

9. Lan, C. Edward; and Campbell, James F.: Theoretical Predictions of Jet Interaction Effects for USB and OWB Configurations. Powered-Lift Aerodynamics and Acoustics, NASA SP-406, 1976, pp. 197-211.

10. Lan, C. Edward; Fillman, Greg L.; and Fox, Charles H., Jr.: Computer Program for Calculating Aerodynamic Characteristics of Upper-Surface-Blowing and Over-Wing-Blowing Configurations. NASA TM X-73987, 1977.

11. Lan, C. E.; Campbell, J. F.; and Fillman, G.: Theoretical Prediction of Over-Wing-Blowing Aerodynamics. AIAA Paper 77-575, June 1977.

12. Lan, C. Edward; Mehrotra, Sudhir C.; and Fox, Charles H., Jr.: A Computer Program for Calculating Symmetrical Aerodynamic Characteristics and Lateral-Directional Stability Derivatives of Wing-Body Combinations With Blowing Jets. NASA TM-78684, 1978.

13. Reubush, David E.: An Investigation of Induced Drag Reduction Through Over-the-Wing Blowing. AIAA Paper 77-884, July 1977.

14. Ward, Vernon G.; Whitcomb, Charles F.; and Pearson, Merwin D.: Air-Flow and Power Characteristics of the Langley 16-Foot Transonic Tunnel With Slotted Test Section. NACA RM L52E01, 1952.

15. Schaefer, William T., Jr.: Characteristics of Major Active Wind Tunnels at the Langley Research Center. NASA TM X-1130, 1965.

16. Corson, Blake W., Jr.; Runckel, Jack F.; and Igoe, William B.: Calibration of the Langley 16-Foot Transonic Tunnel With Test Section Air Removal. NASA TR R-423, 1974.

17. Braslow, Albert L.; and Knox, Eugene C.: Simplified Method for Determination of Critical Height of Distributed Roughness Particles for Boundary-Layer Transition at Mach Numbers From 0 to 5. NACA TN 4363, 1958.

18. Braslow, Albert L.; Hicks, Raymond M.; and Harris, Roy V., Jr.: Use of Grit-Type Boundary-Layer-Transition Trips on Wind-Tunnel Models. NASA TN D-3579, 1966.

19. Siclari, M. J.; Barche, J.; and Migdal, D.: V/STOL Aircraft Prediction Technique Development for Jet-Induced Effects. Volume 1 - Theoretical and Empirical Development of Prediction Techniques. GAC-PDR-623-18-VOL-1 (Contract N00140-74-C-0113), Grumman Aerospace Corporation, Apr. 15, 1975. (Available from DDC as AD B005 259L.)

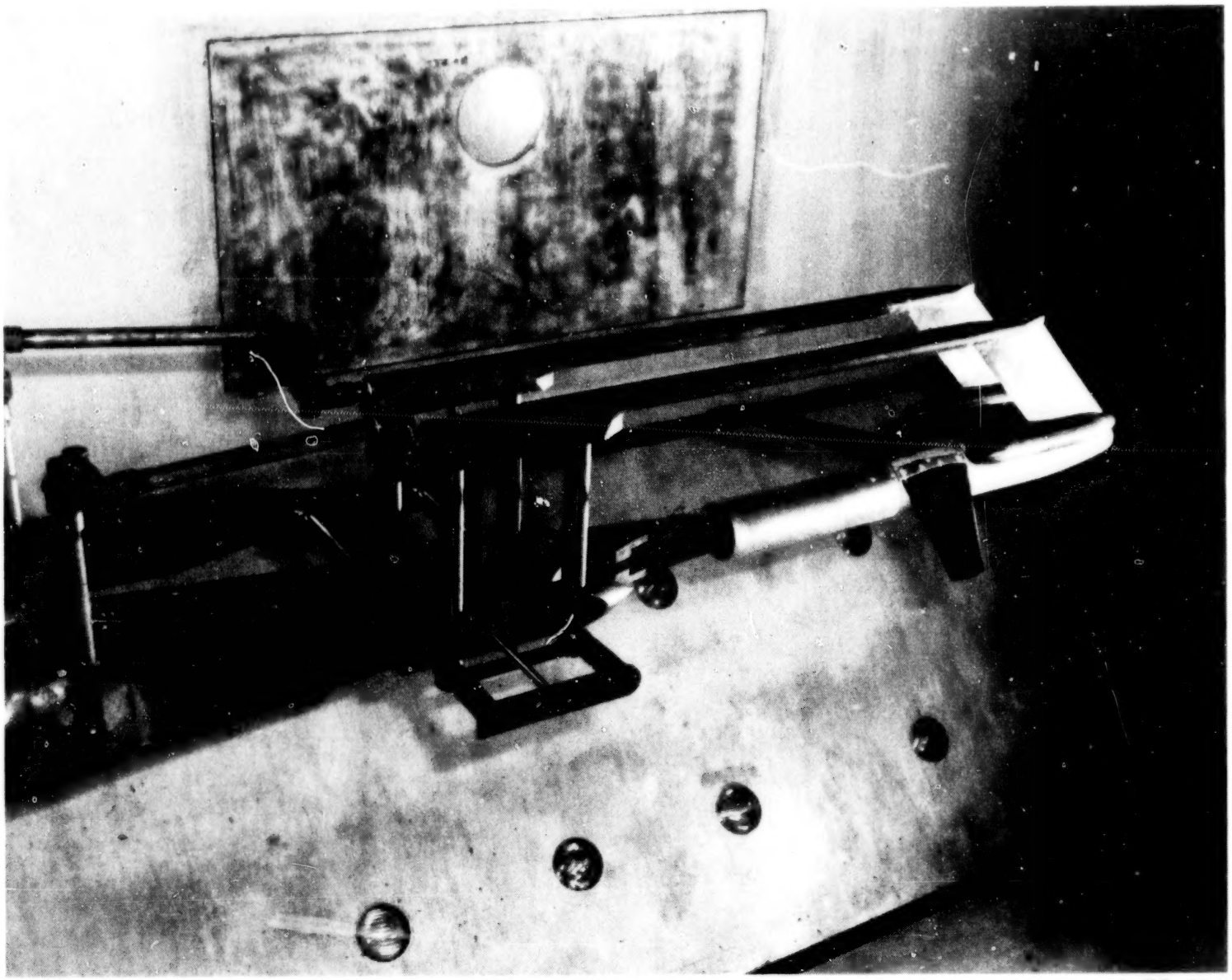

L-78-594

(a) Three-quarter rear view of model.

Figure 1.- Wing-body model with nacelles and nacelle supporting/translating apparatus installed in the Langley 16-foot transonic tunnel.

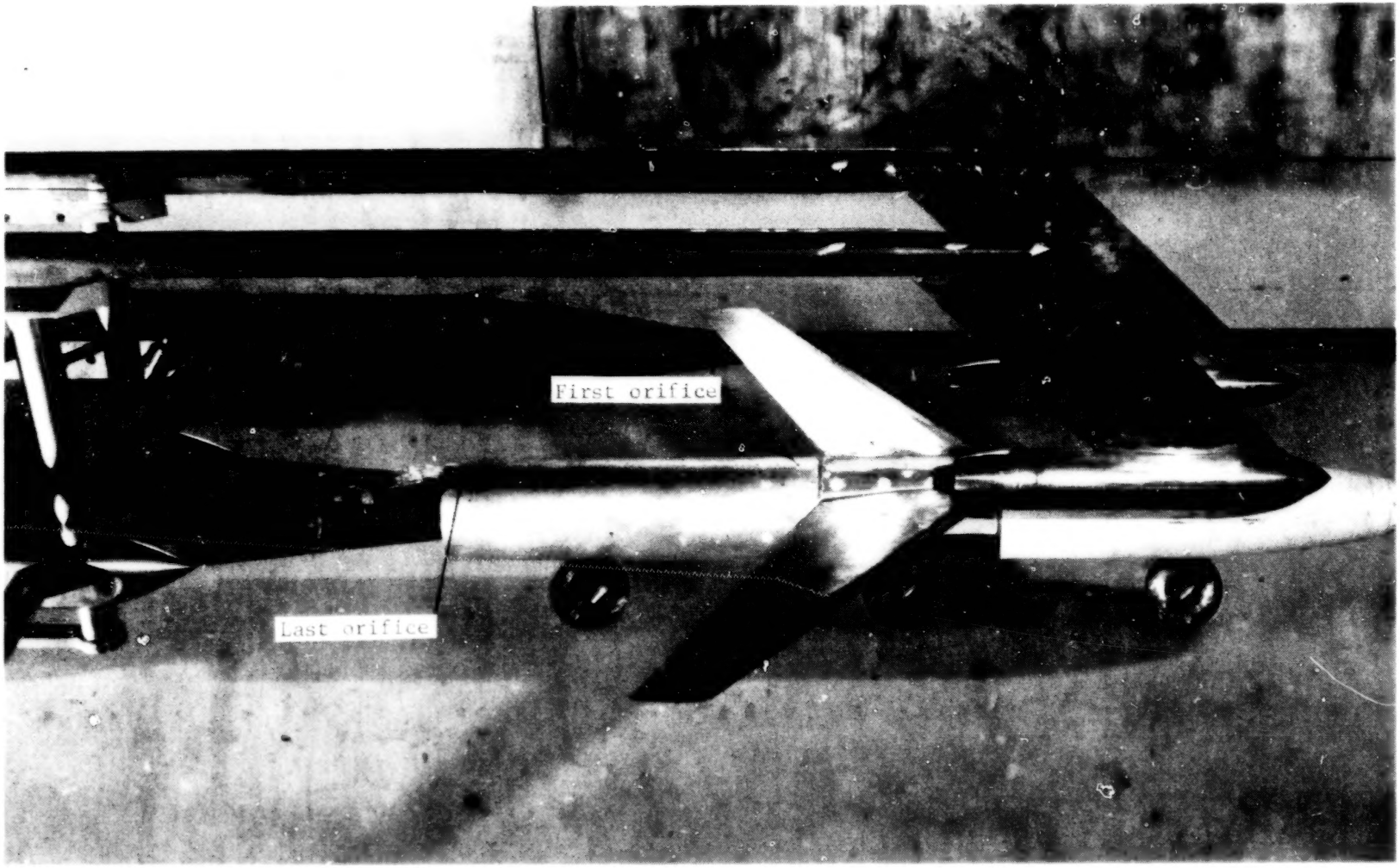

L-78-593

(b) Side view of wing-body model showing location of row of fuselage pressure orifices.

Figure 1.- Concluded.

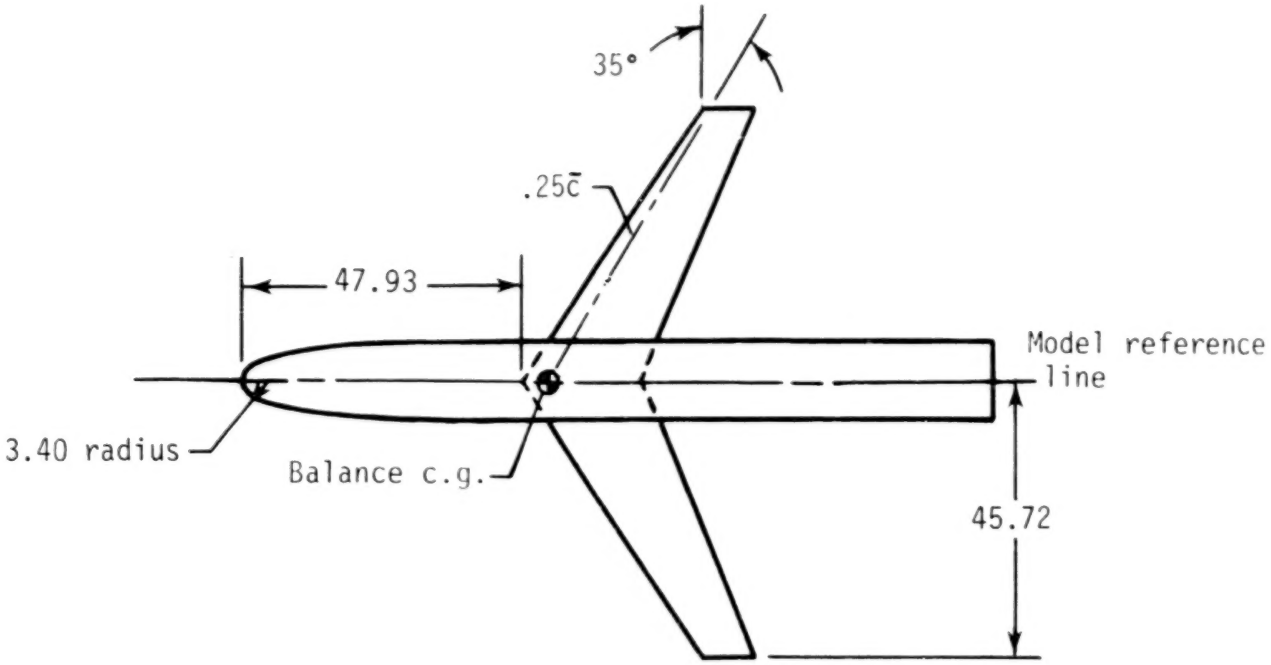

Plan view

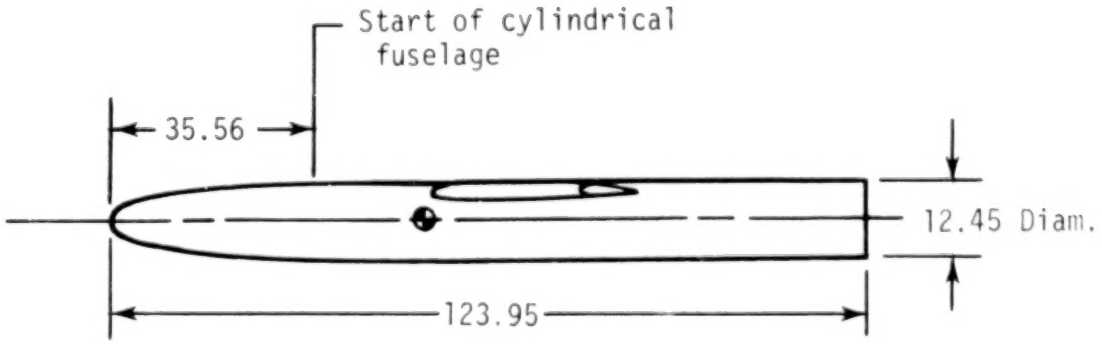

Side view

(a) Views of model.

Figure 2.- Sketch of wing-body model. All dimensions are in centimeters.

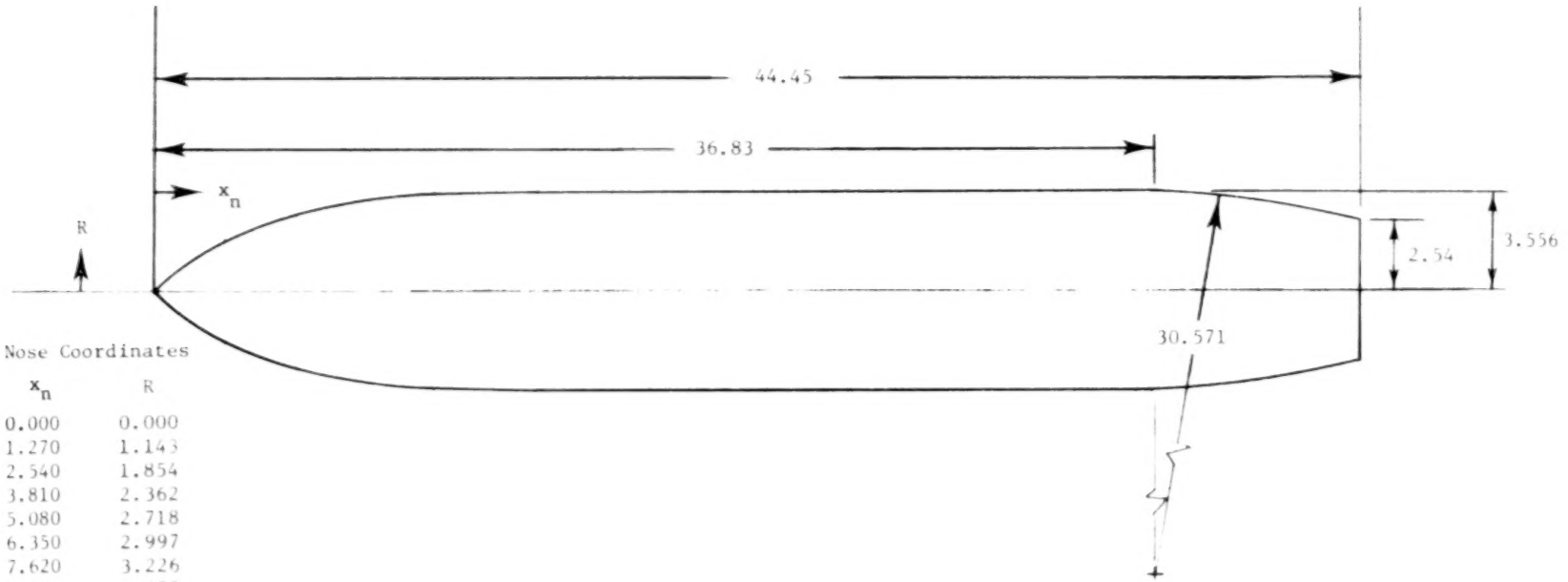

Nose Coordinates

x_n	R
0.000	0.000
1.270	1.143
2.540	1.854
3.810	2.362
5.080	2.718
6.350	2.997
7.620	3.226
8.890	3.378
10.160	3.480
11.430	3.505
12.700	3.531
13.970	3.556

(b) Nacelle details.

Figure 2.- Continued.

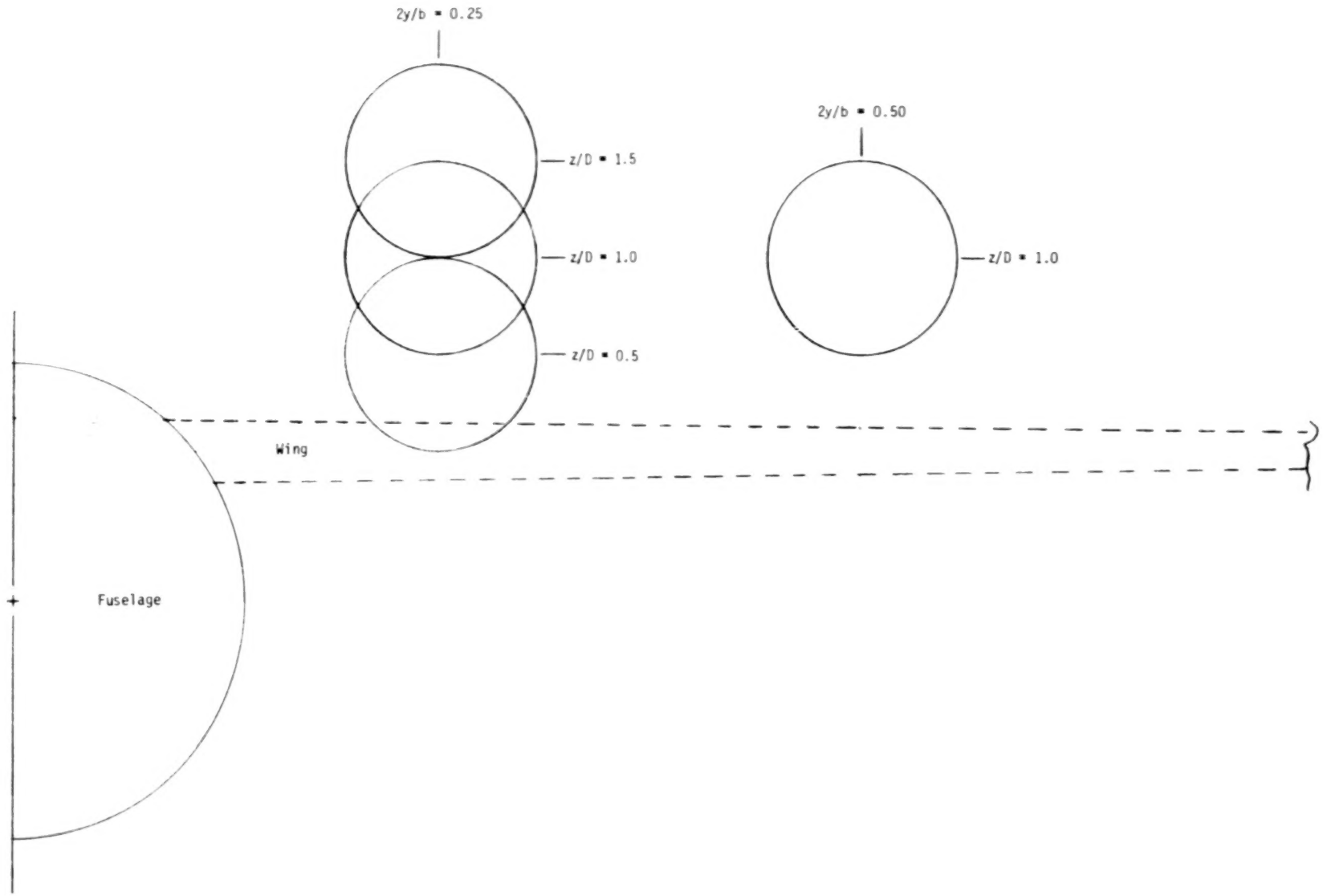

(c) Rear view showing positions of nacelle exits in y and z in relation to fuselage and wing (wing shown at maximum thickness).

Figure 2.- Continued.

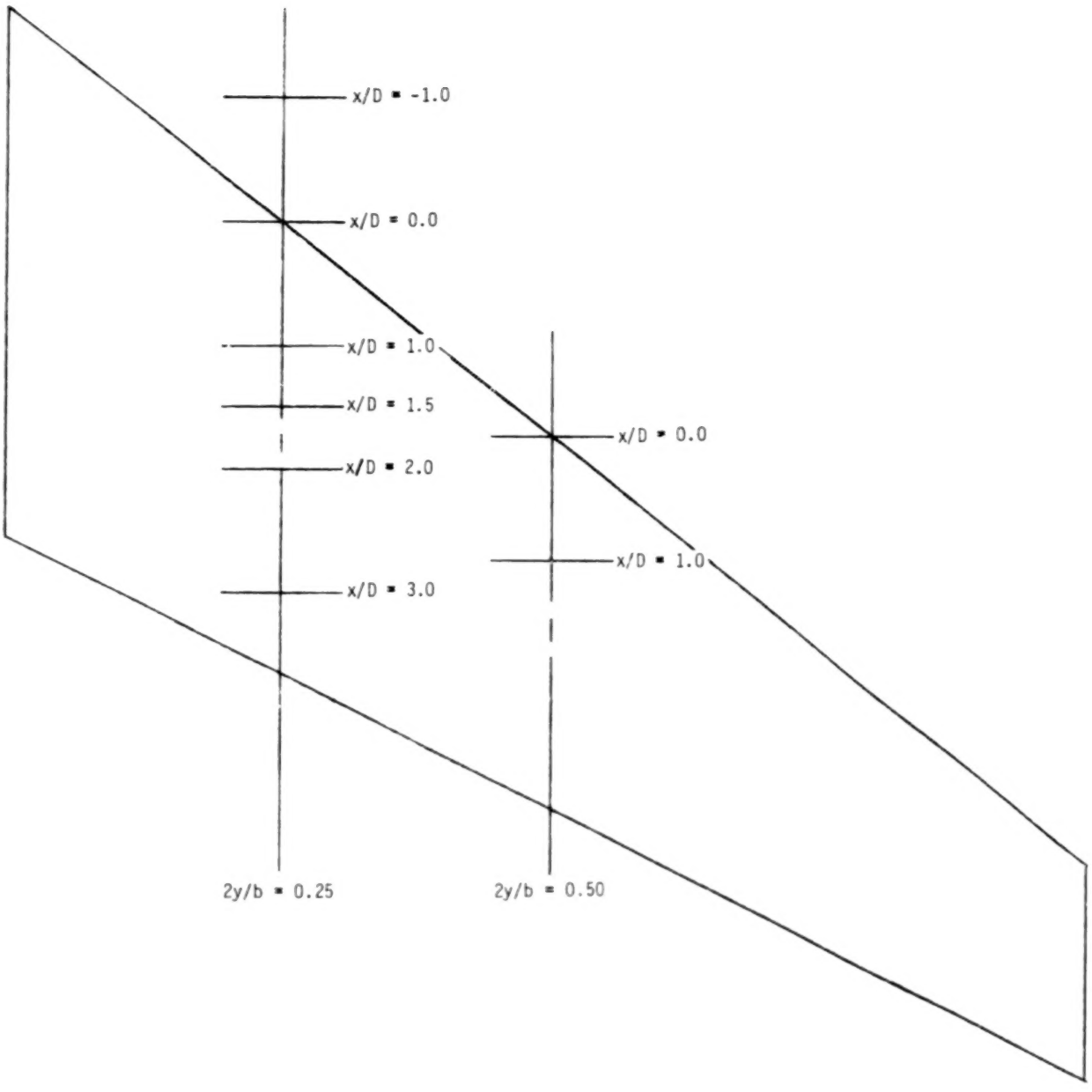

(d) Top view showing positions of nacelle exits in x and y in relation to wing.

Figure 2.- Concluded.

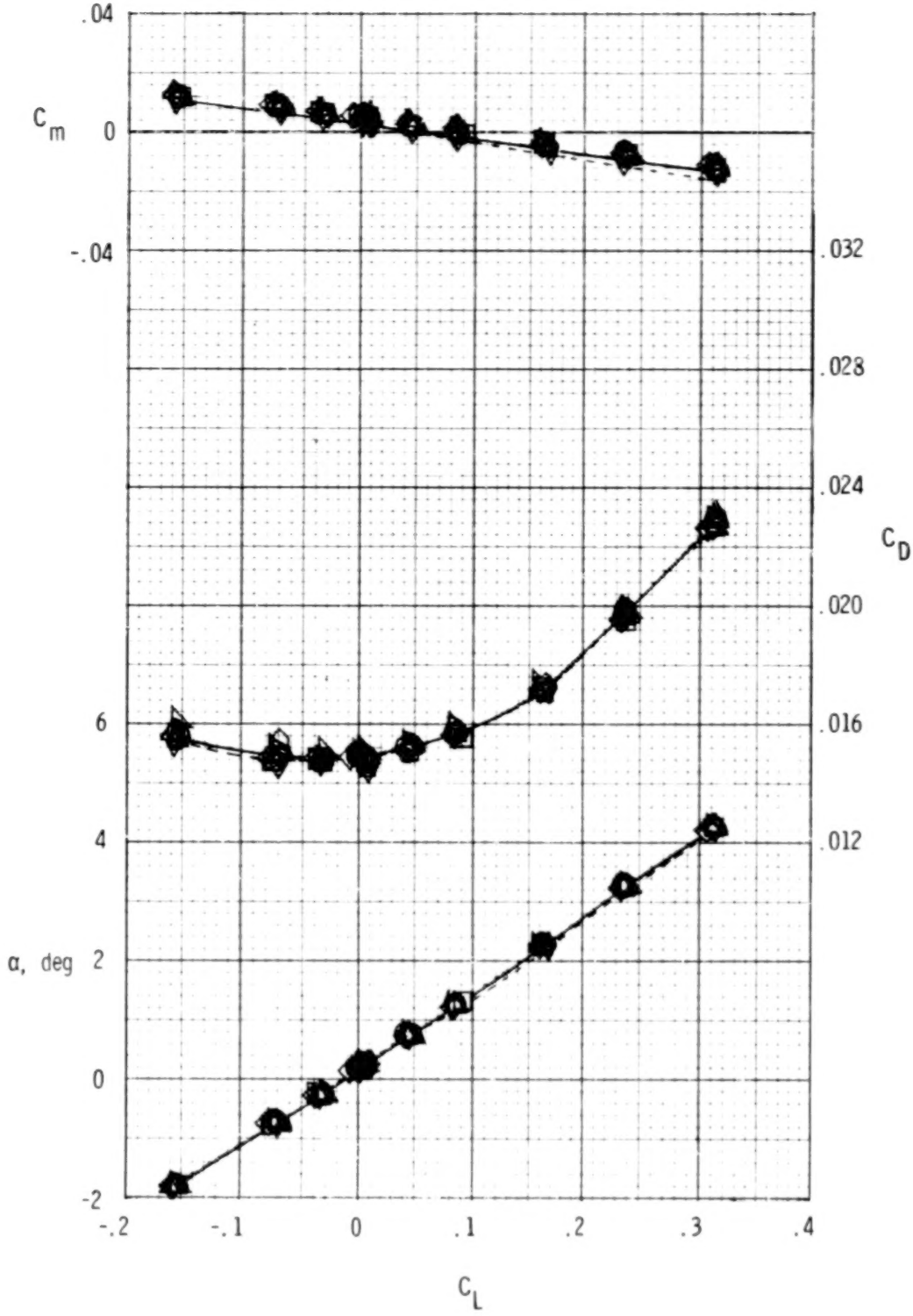

(a) M = 0.5.

Figure 3.- Wing-body aerodynamic characteristics for the 10 baseline runs with supporting/translating apparatus in positions corresponding to the 10 nacelle positions tested, each denoted by a different symbol. (Fairing is average; dashed line is with supporting/translating apparatus removed.)

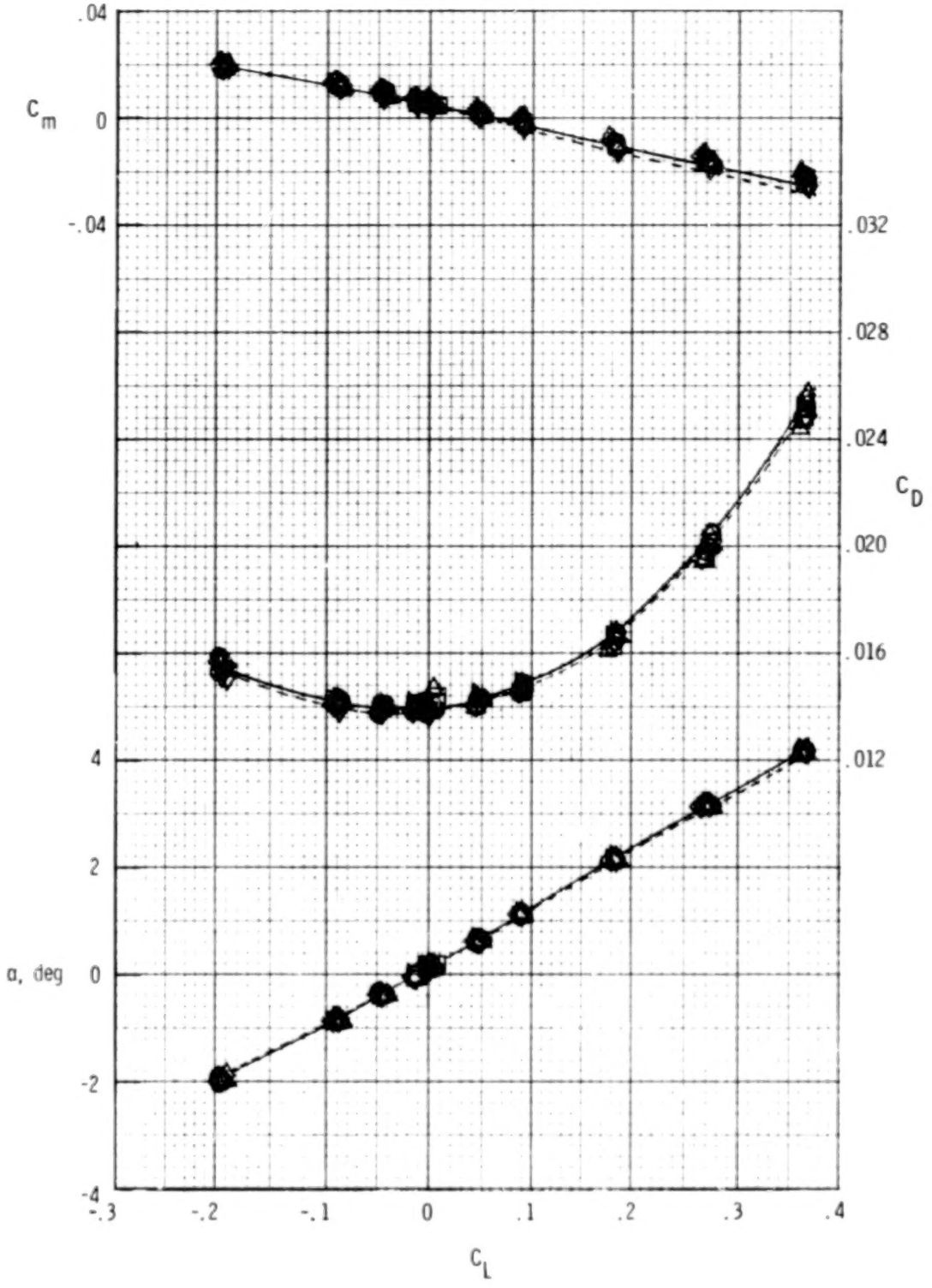

(b) M = 0.8.

Figure 3.- Concluded.

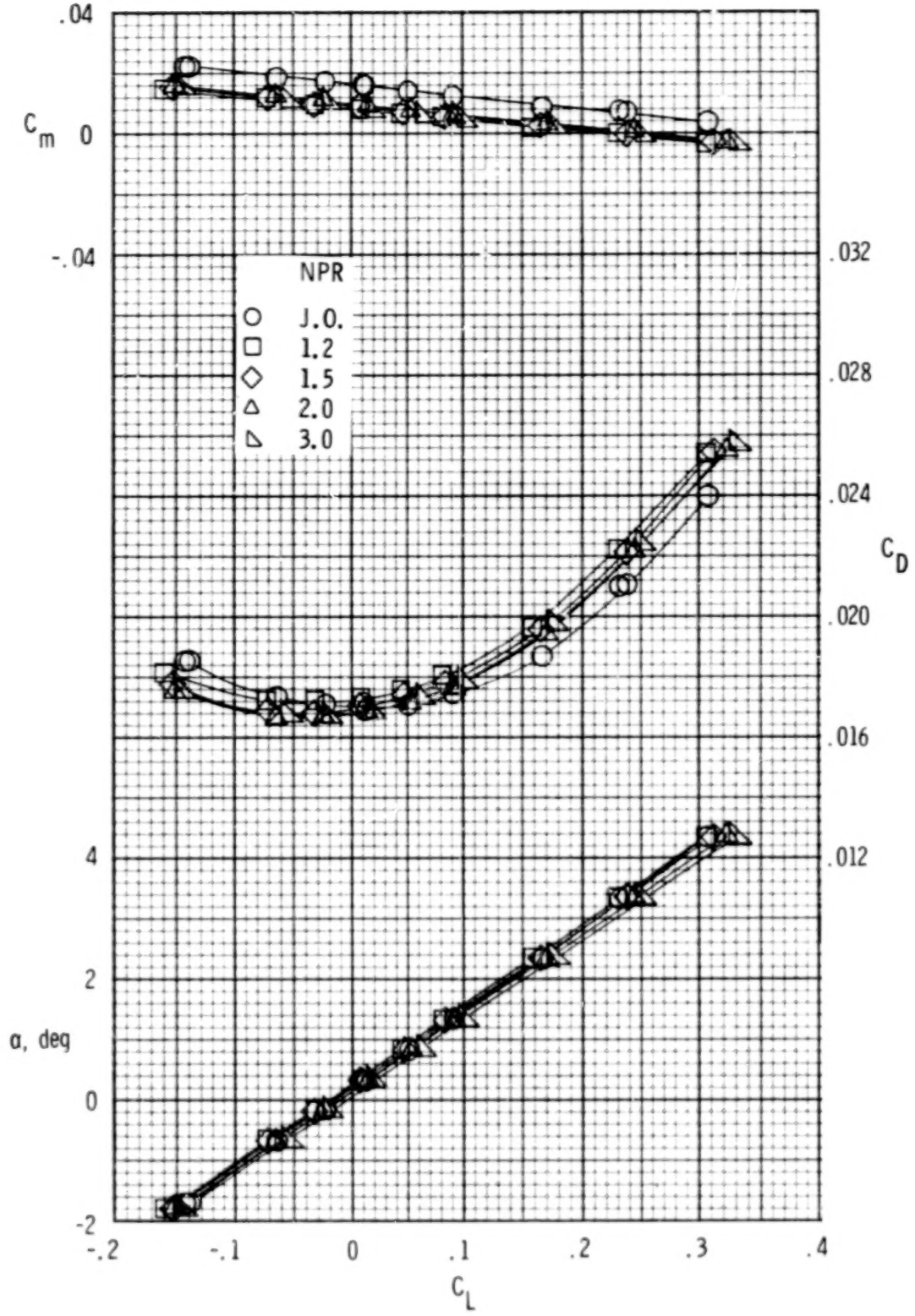

(a) M = 0.5.

Figure 4.- Effect of nozzle pressure ratio (NPR) on wing-body aerodynamic characteristics for the configuration with x/D = -1, 2y/b = 0.25, and z/D = 1. J.O. denotes jet off.

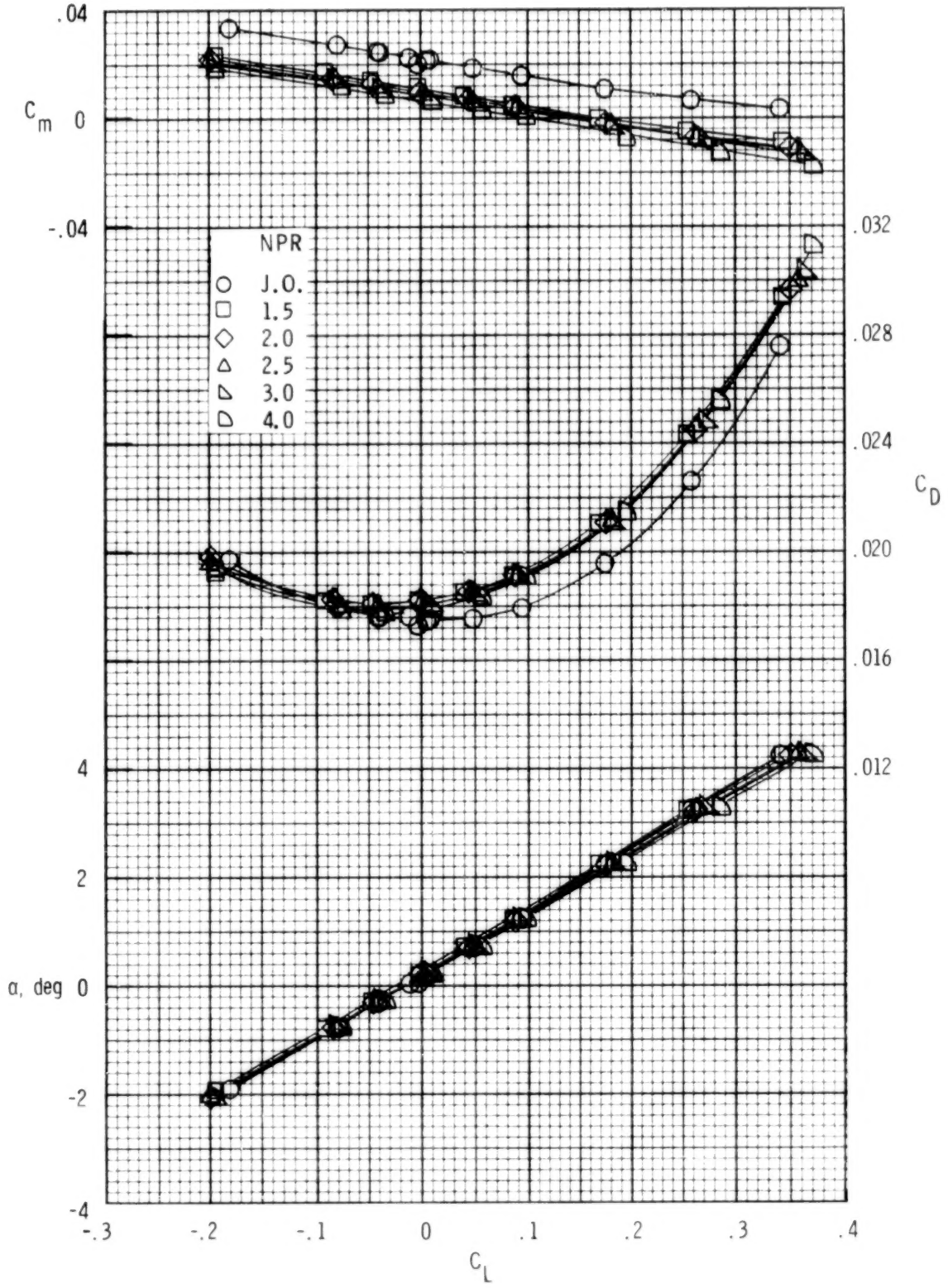

(b) M = 0.8.

Figure 4.- Concluded.

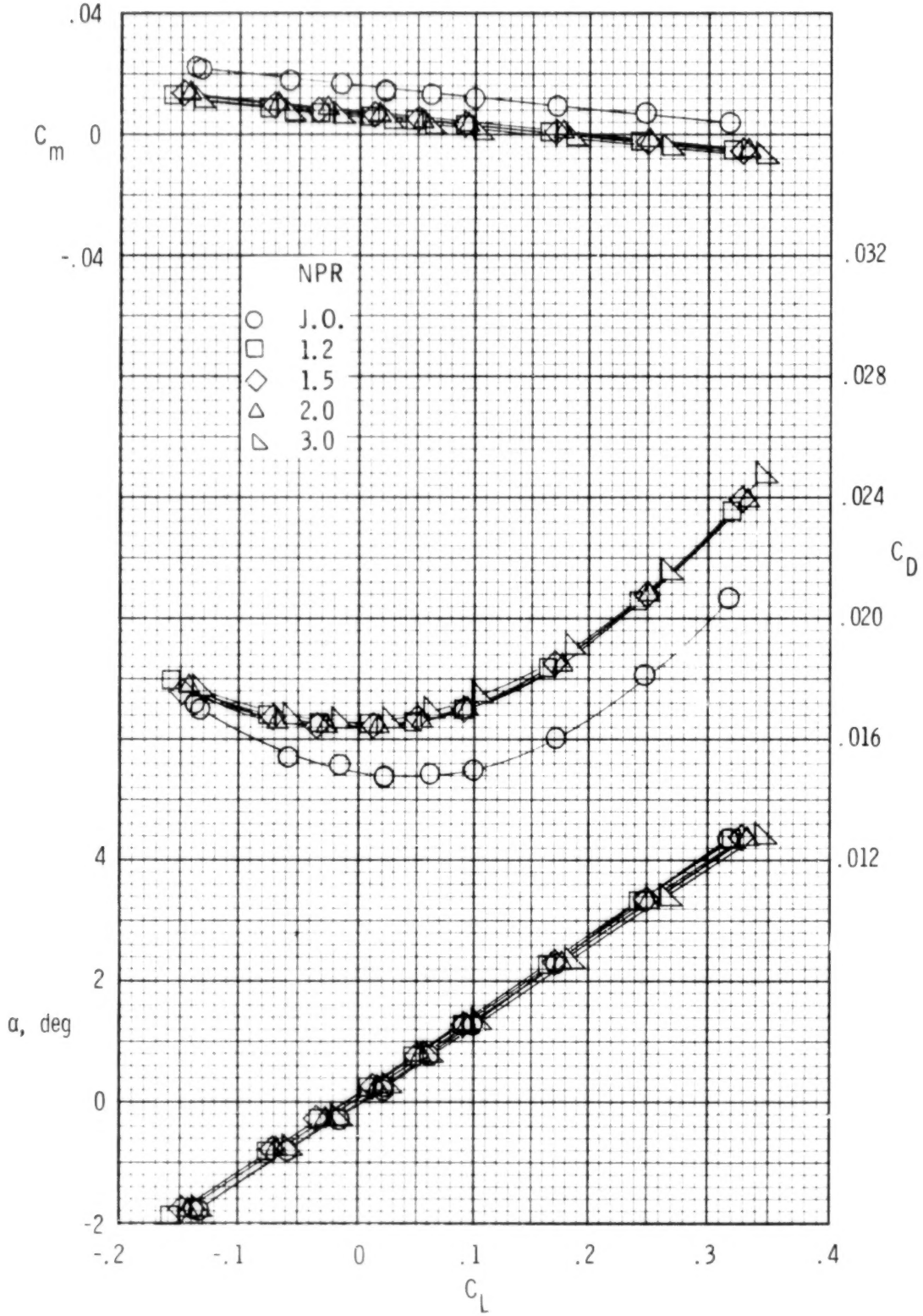

(a) M = 0.5.

Figure 5.- Effect of nozzle pressure ratio (NPR) on wing-body aerodynamic characteristics for the configuration with x/D = 0, 2y/b = 0.25, and z/D = 1. J.O. denotes jet off.

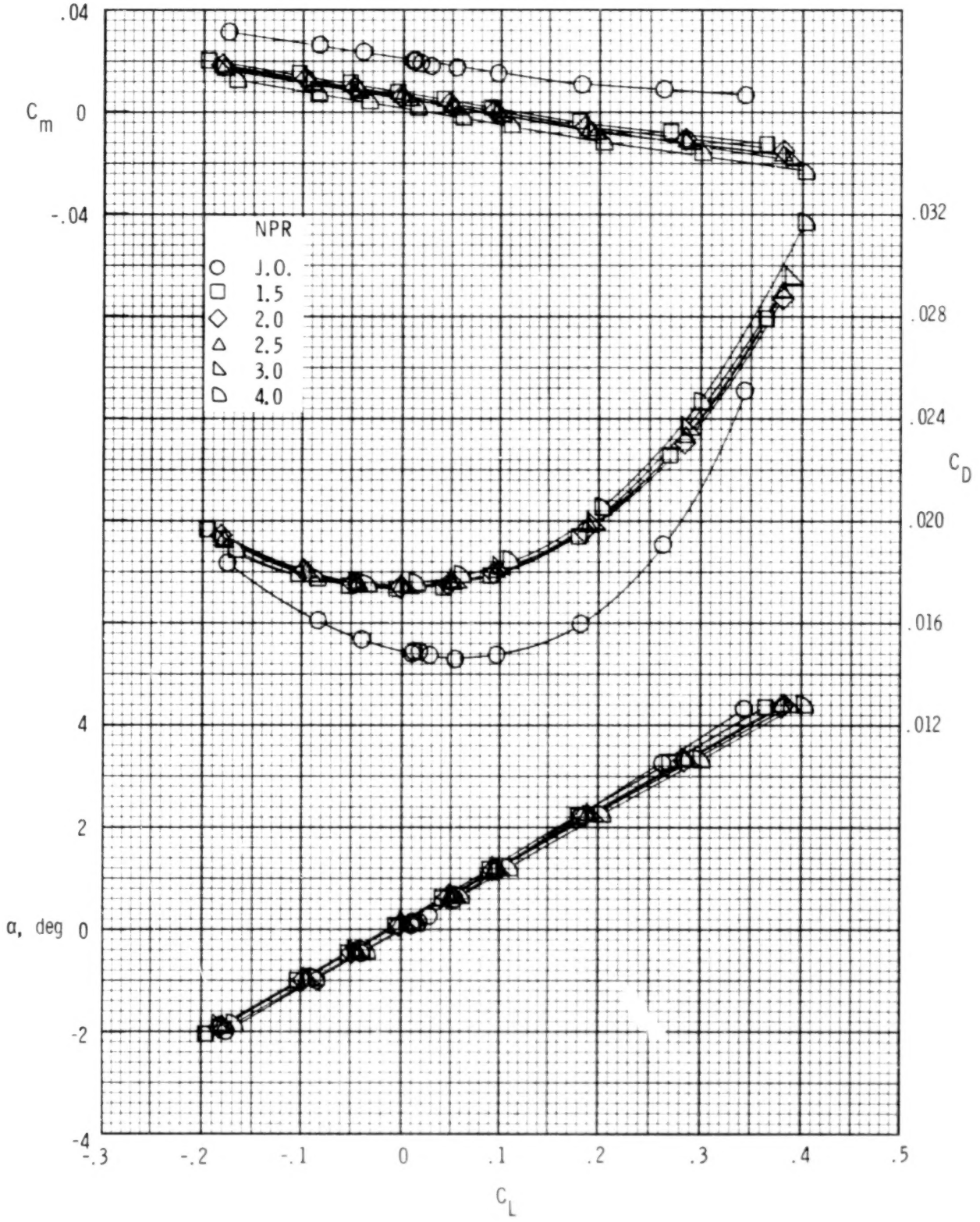

(b) M = 0.8.

Figure 5.- Concluded.

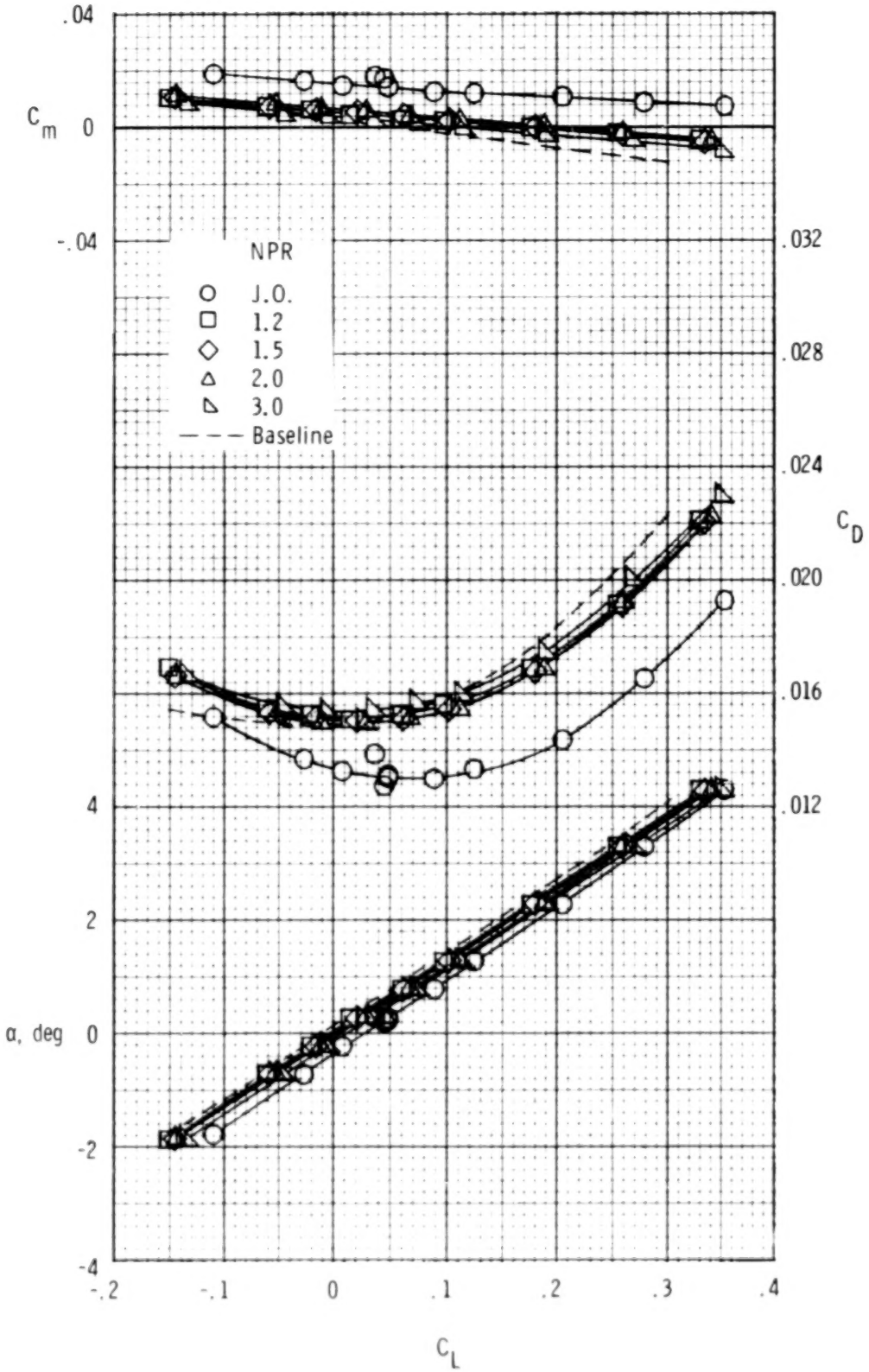

(a) M = 0.5.

Figure 6.- Effect of nozzle pressure ratio (NPR) on wing-body aerodynamic characteristics for a typical configuration (x/D = 1, 2y/b = 0.25, z/D = 1). J.O. denotes jet off.

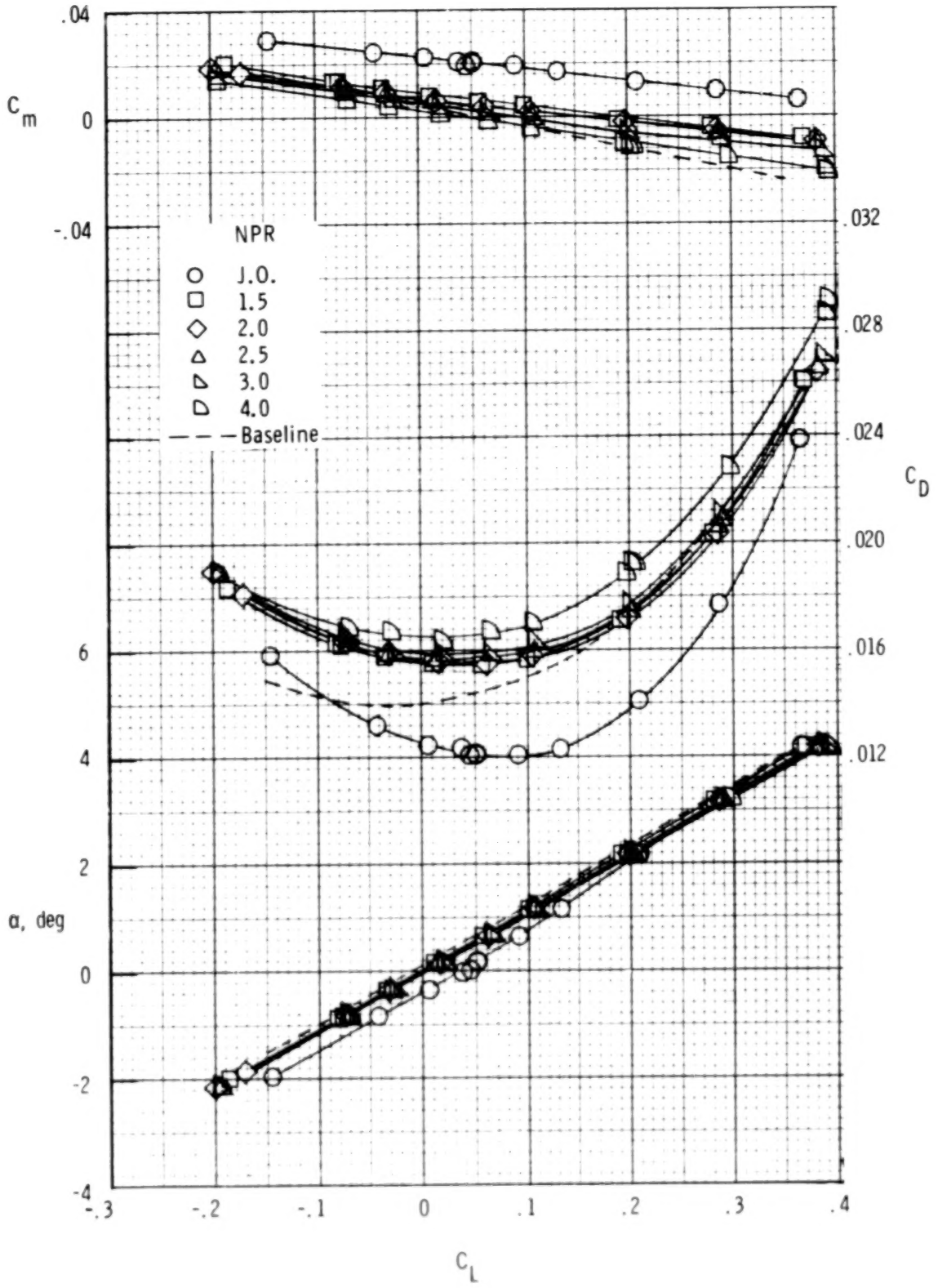

(b) M = 0.8.

Figure 6.- Concluded.

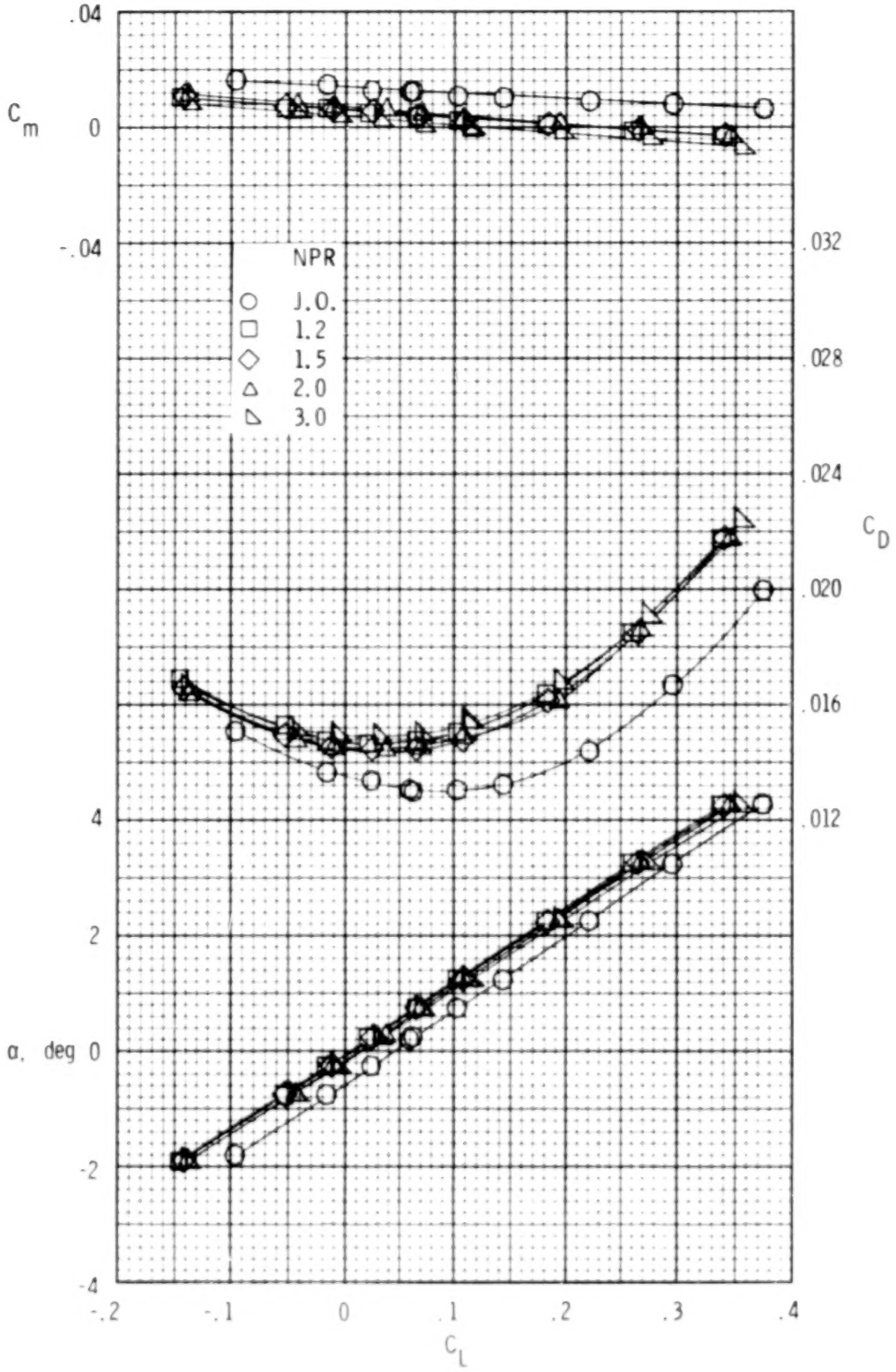

(a) M = 0.5.

Figure 7.- Effect of nozzle pressure ratio (NPR) on wing-body aerodynamic characteristics for the configuration with x/D = 1.5, 2y/b = 0.25, and z/D = 1. J.O. denotes jet off.

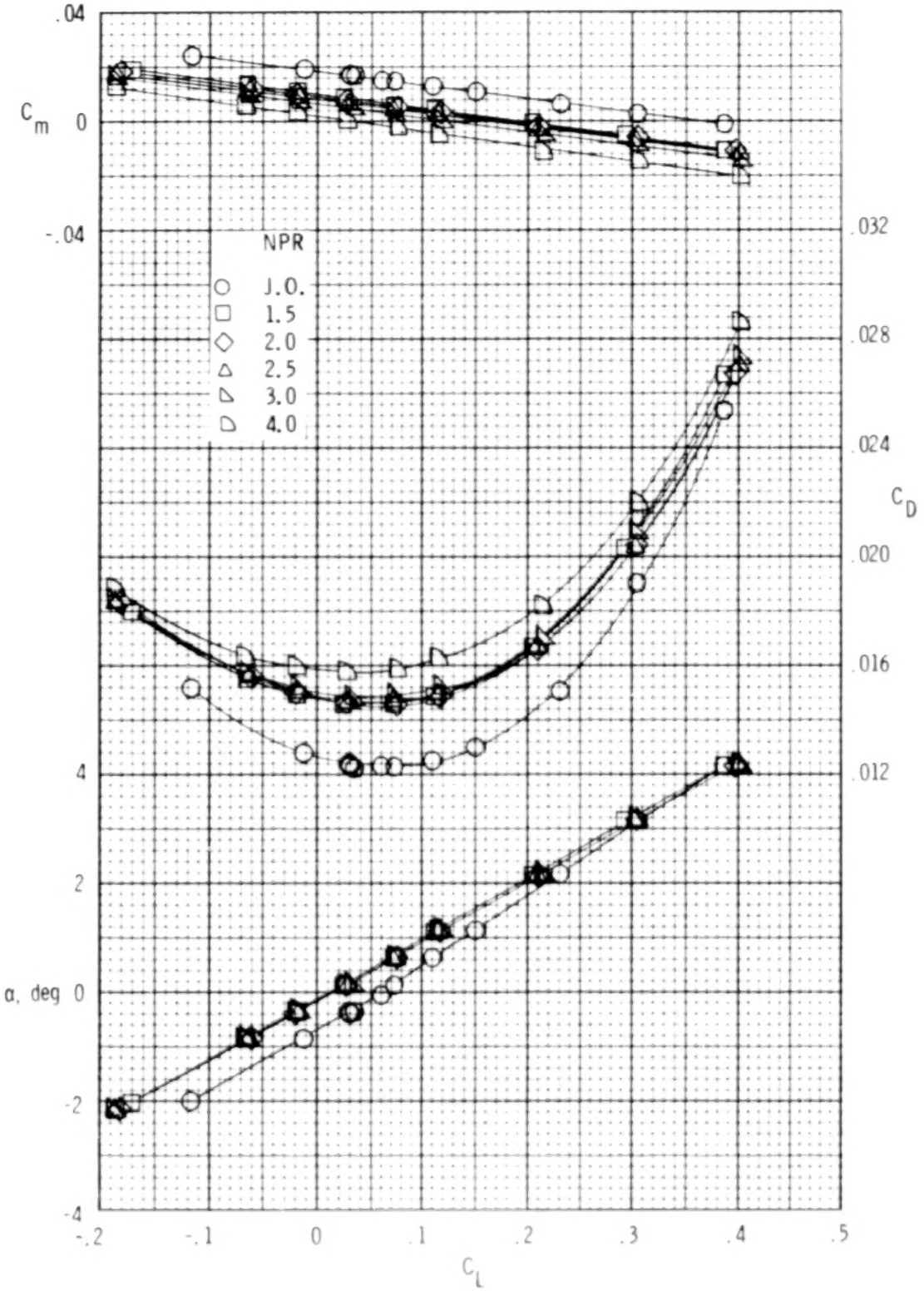

(b) M = 0.8.

Figure 7.- Concluded.

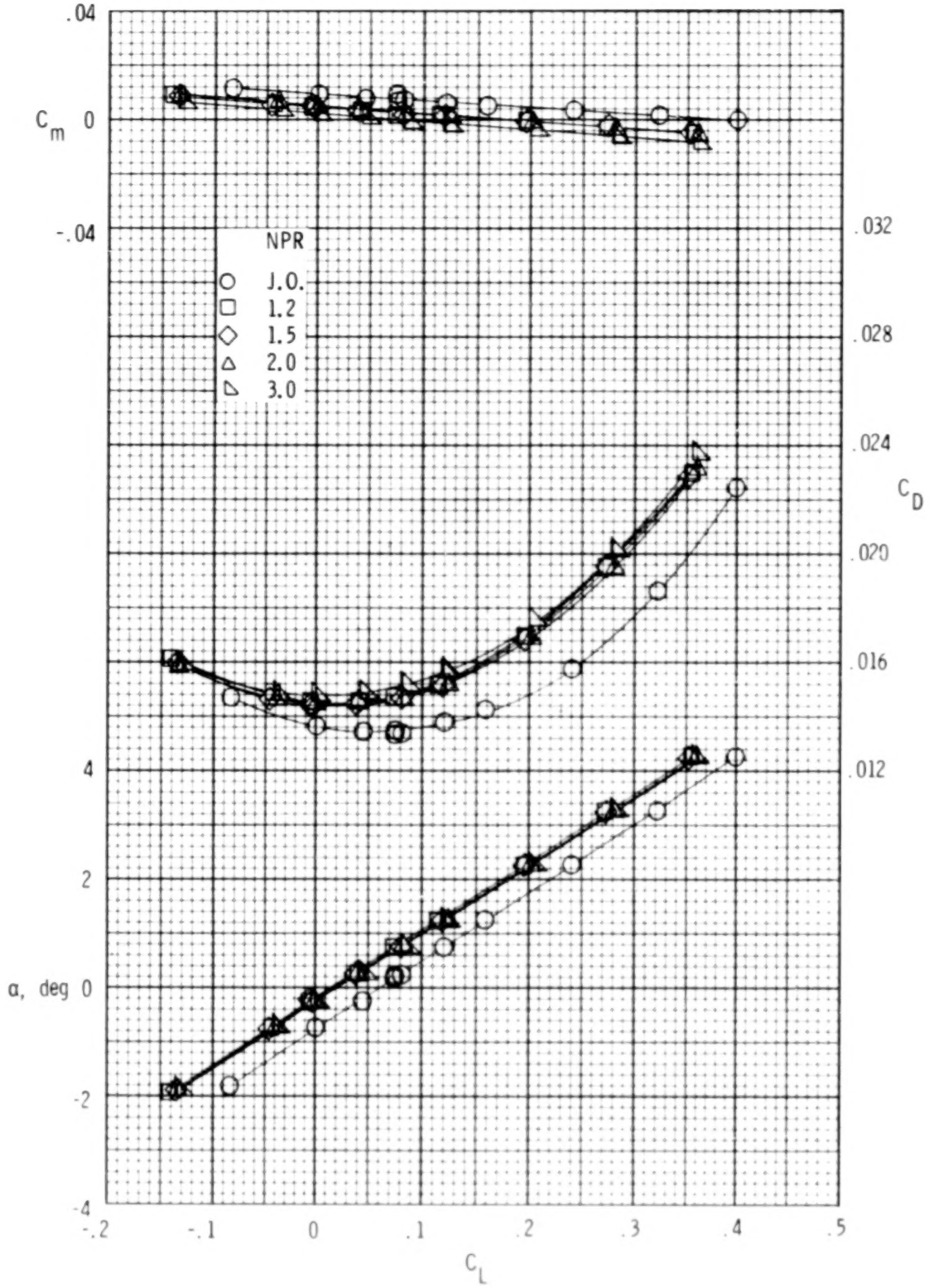

(a) M = 0.5.

Figure 8.- Effect of nozzle pressure ratio (NPR) on wing-body aerodynamic characteristics for the configuration with x/D = 2, 2y/b = 0.25, and z/D = 1. J.O. denotes jet off.

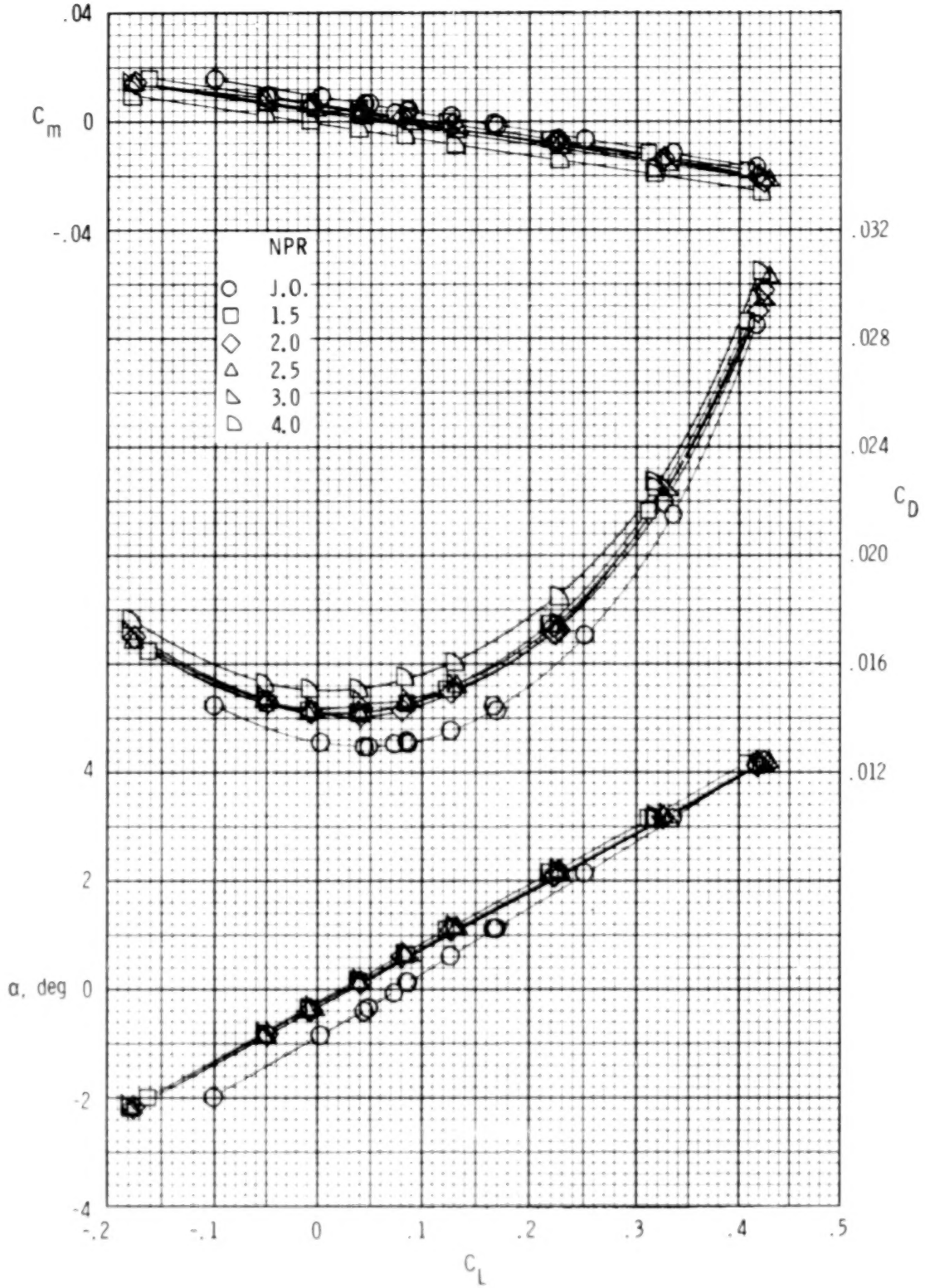

(b) M = 0.8.

Figure 8.- Concluded.

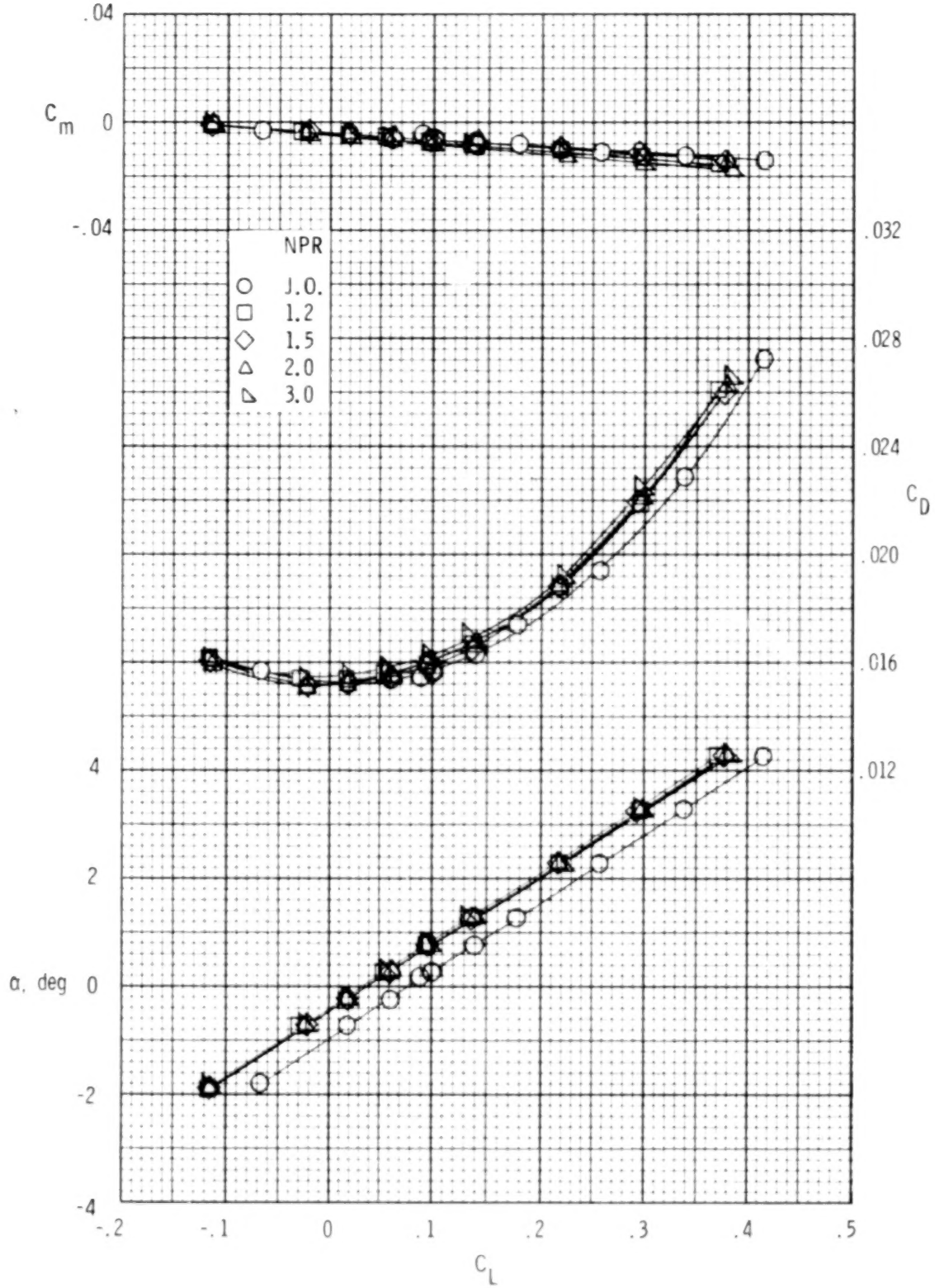

(a) M = 0.5.

Figure 9.- Effect of nozzle pressure ratio (NPR) on wing-body aerodynamic characteristics for the configuration with x/D = 3, 2y/b = 0.25, and z/D = 1. J.O. denotes jet off.

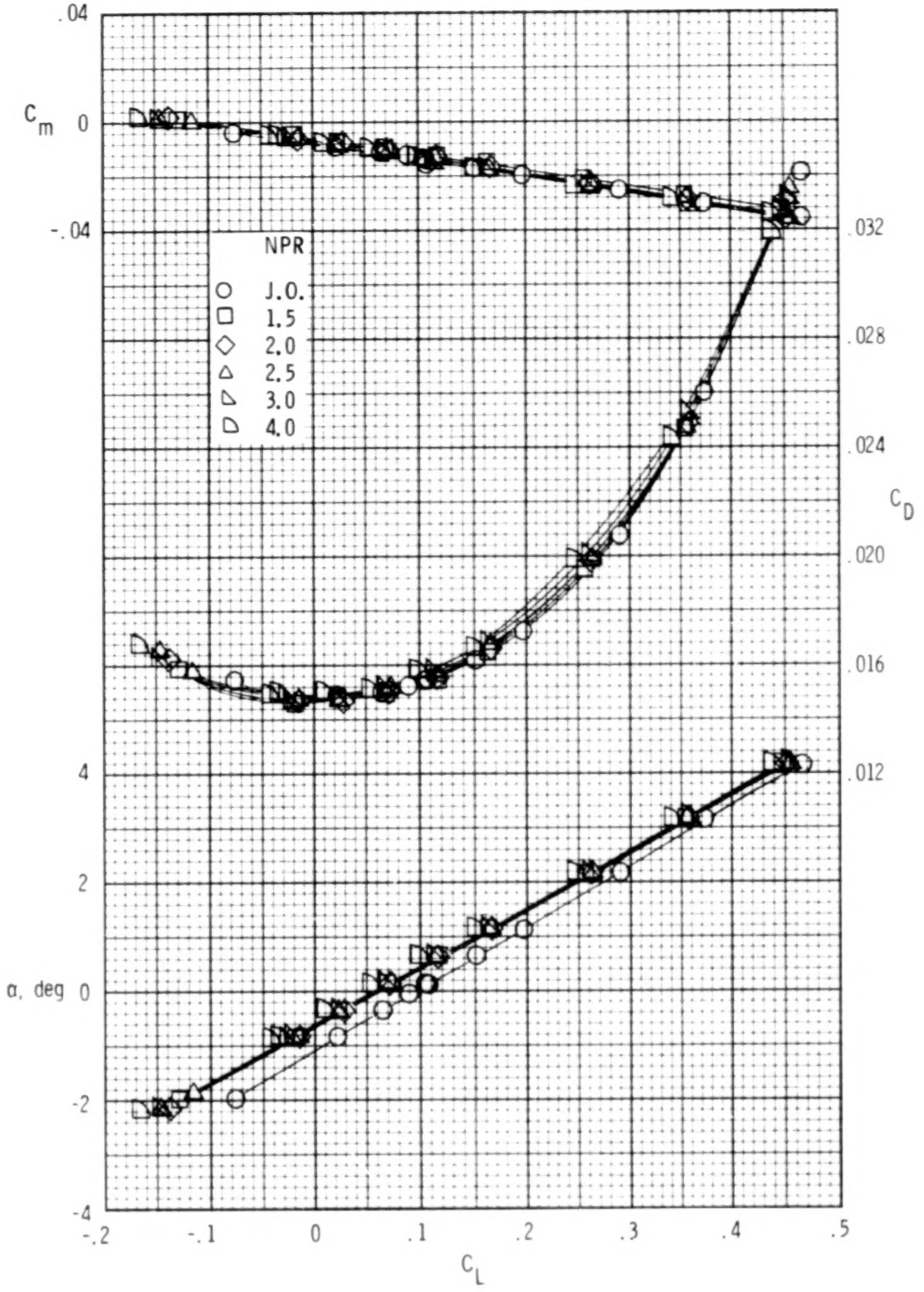

(b) M = 0.8.

Figure 9.- Concluded.

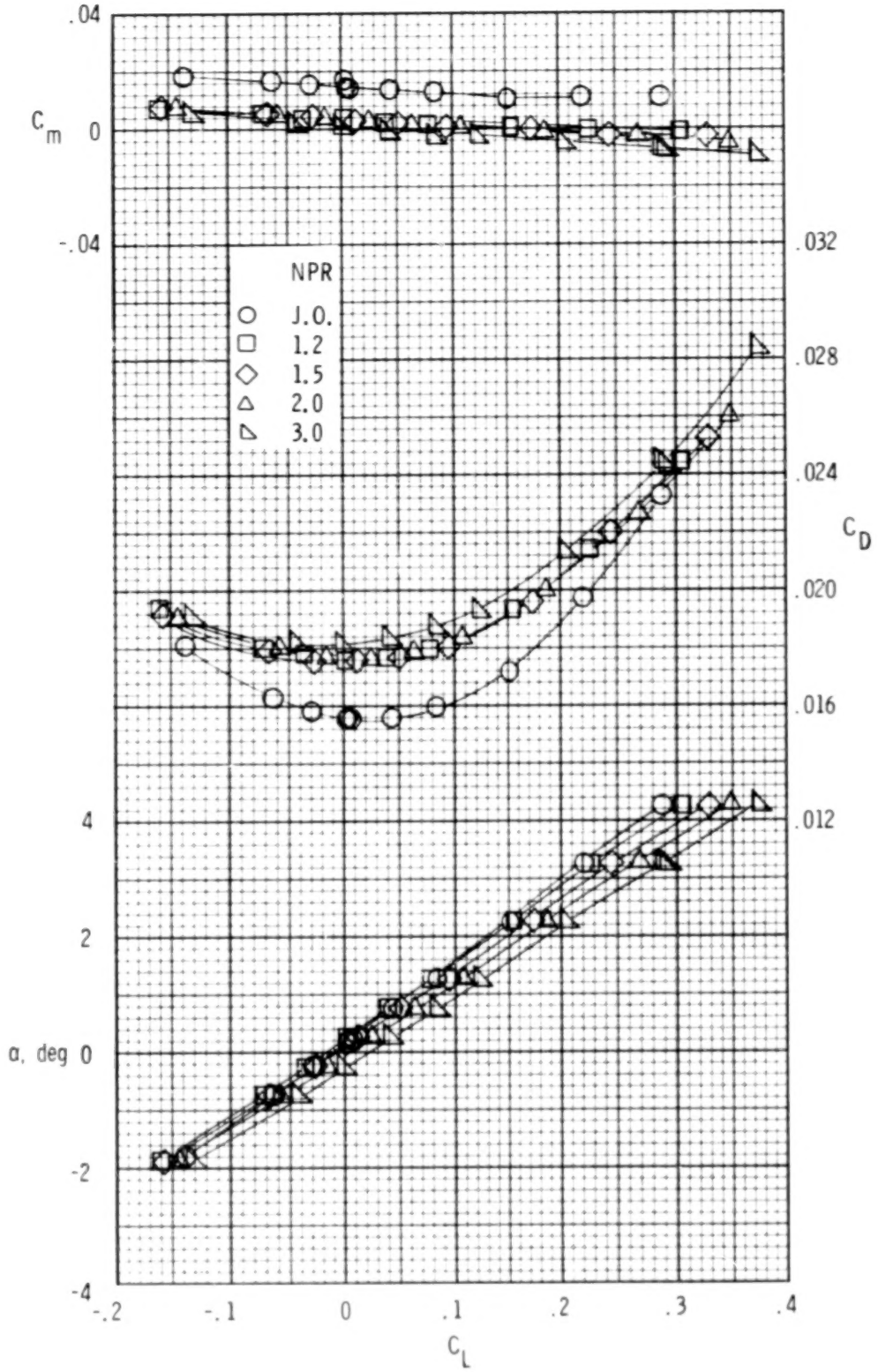

(a) M = 0.5.

Figure 10.- Effect of nozzle pressure ratio (NPR) on wing-body aerodynamic characteristics for the configuration with x/D = 0, 2y/b = 0.25, and z/D = 0.5. J.O. denotes jet off.

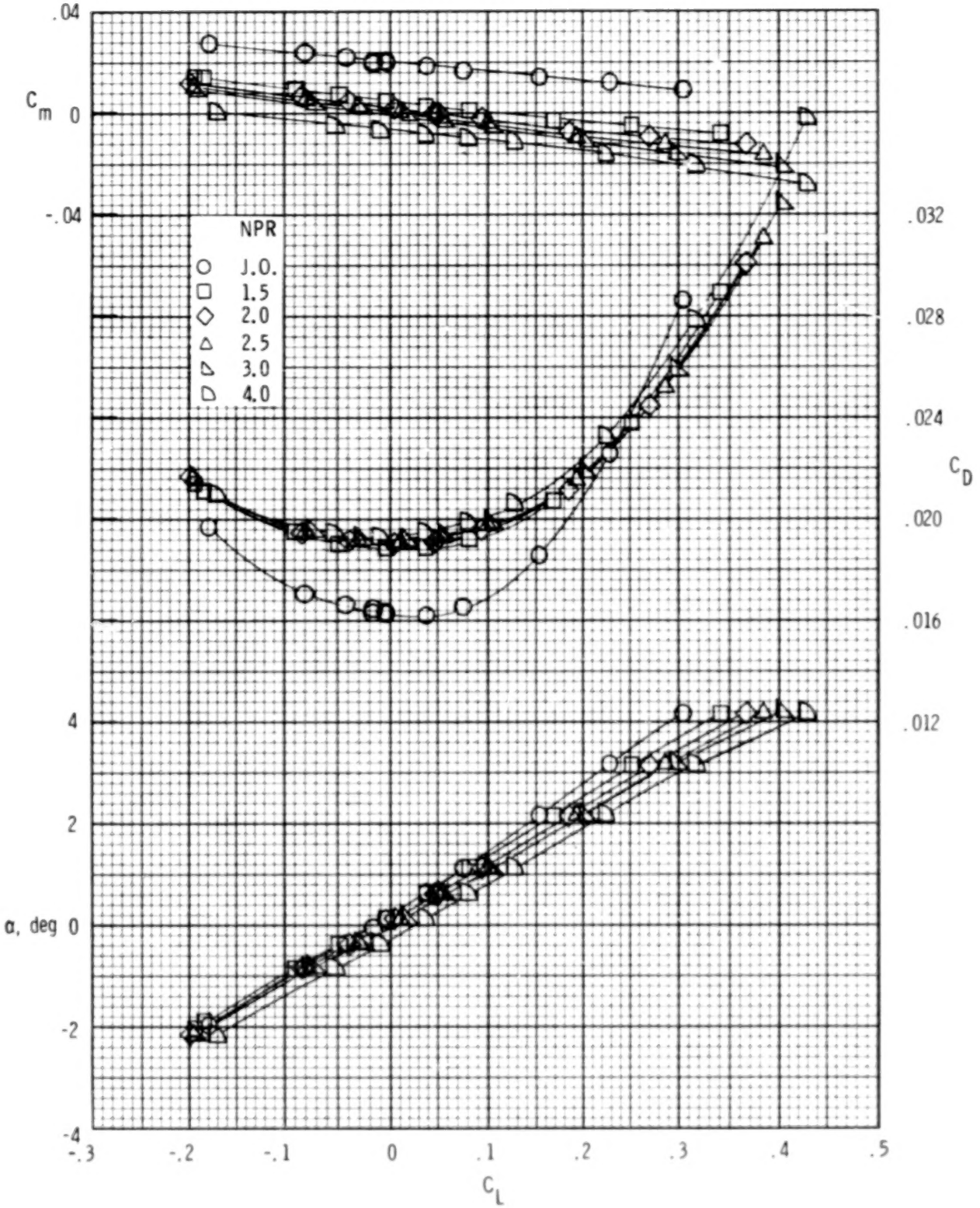

(b) M = 0.8.

Figure 10.- Concluded.

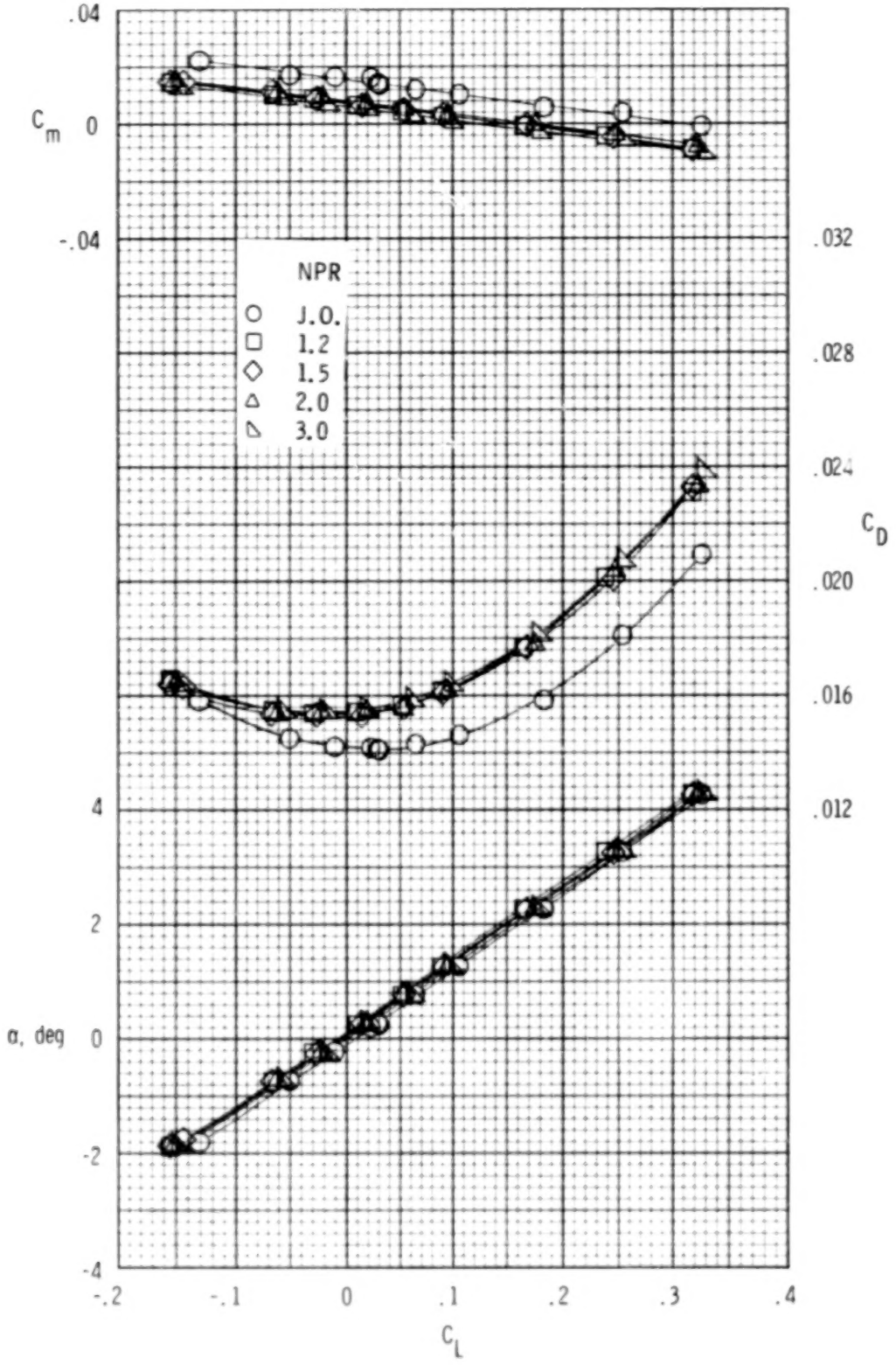

(a) M = 0.5.

Figure 11.- Effect of nozzle pressure ratio (NPR) on wing-body aerodynamic characteristics for the configuration with x/D = 0, 2y/b = 0.25, and z/D = 1.5. J.O. denotes jet off.

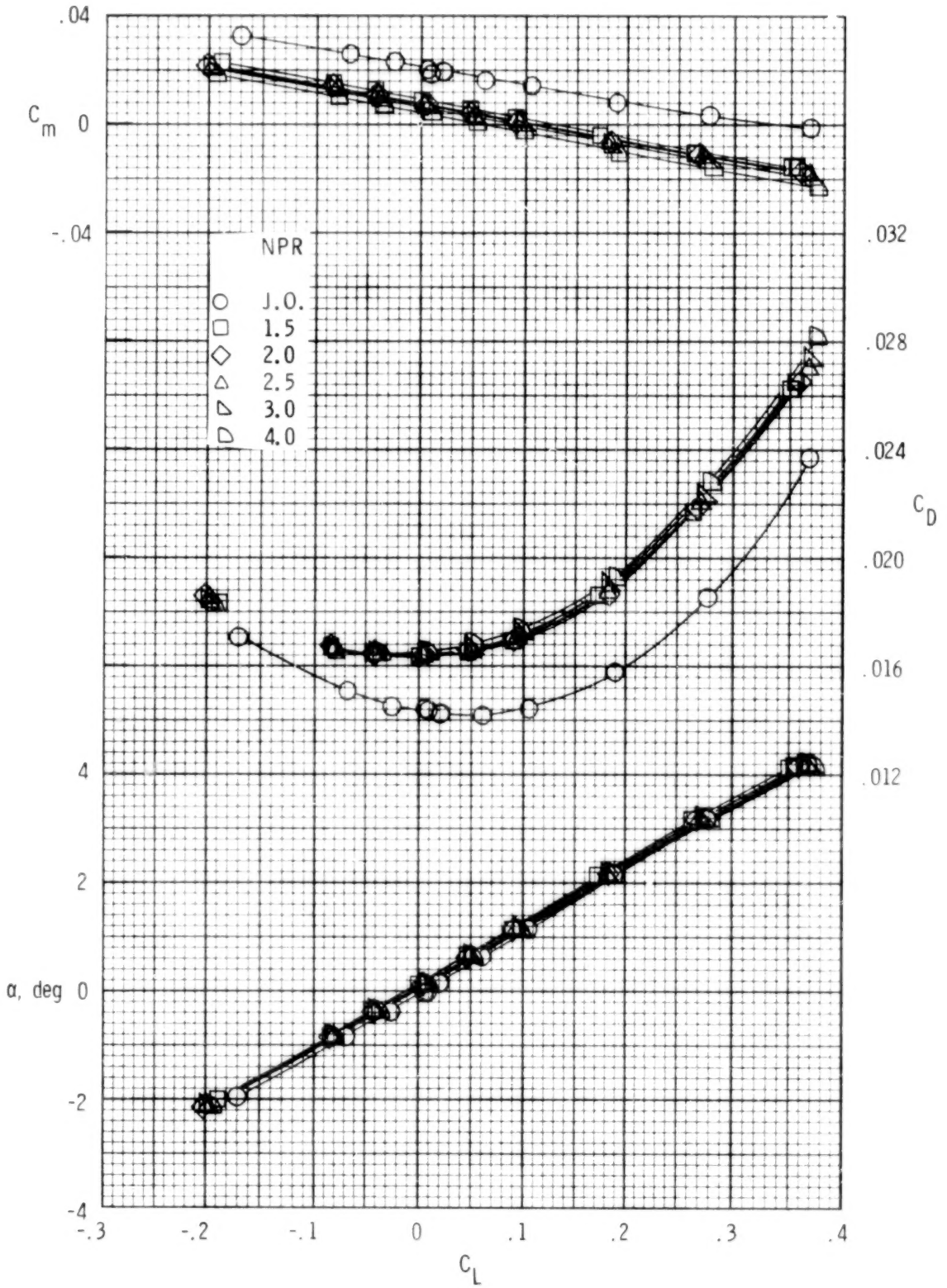

(b) M = 0.8.

Figure 11.- Concluded.

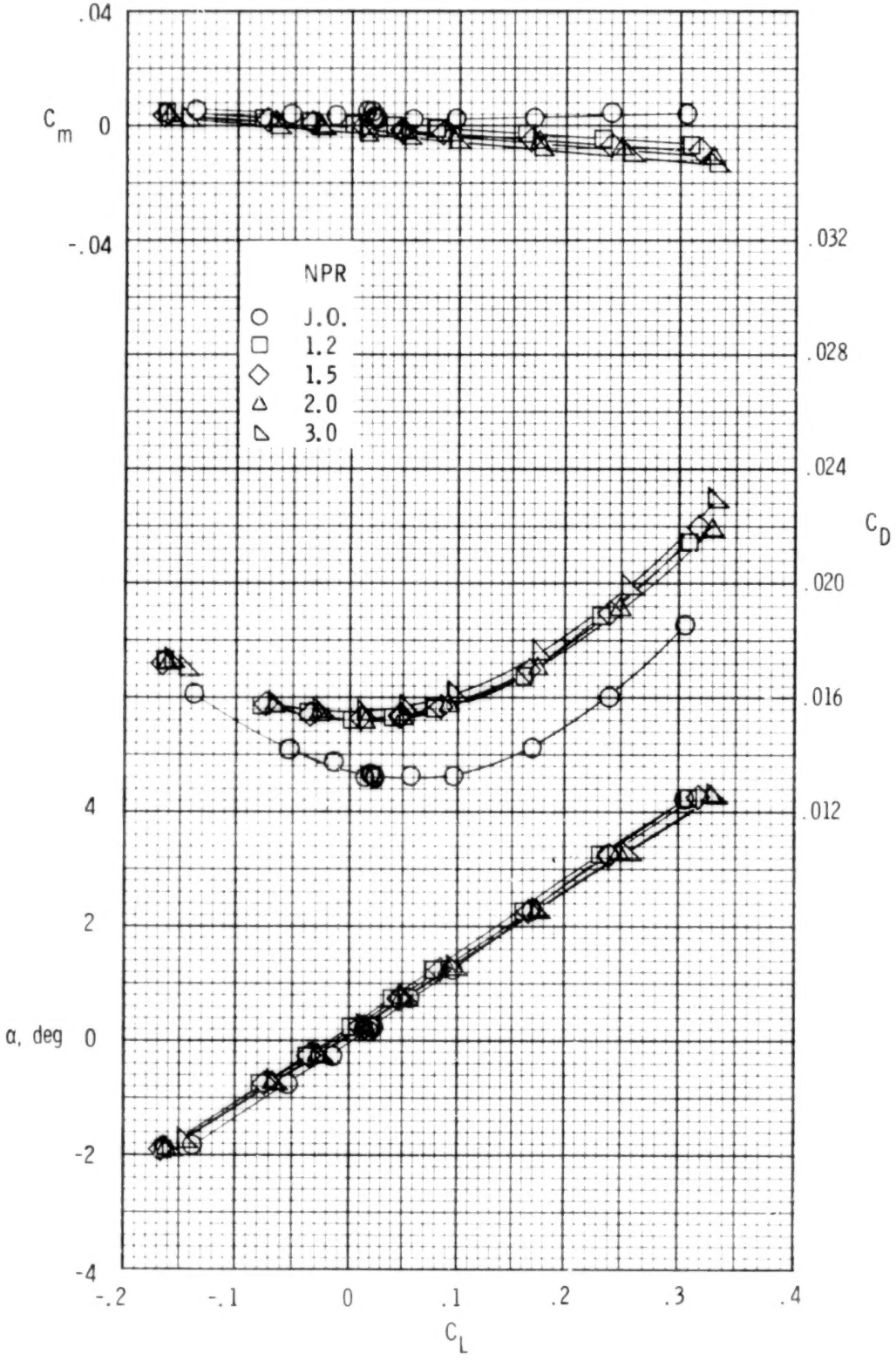

(a) M = 0.5.

Figure 12.- Effect of nozzle pressure ratio (NPR) on wing-body aerodynamic characteristics for the configuration with x/D = 0, 2y/b = 0.5, and z/D = 1. J.O. denotes jet off.

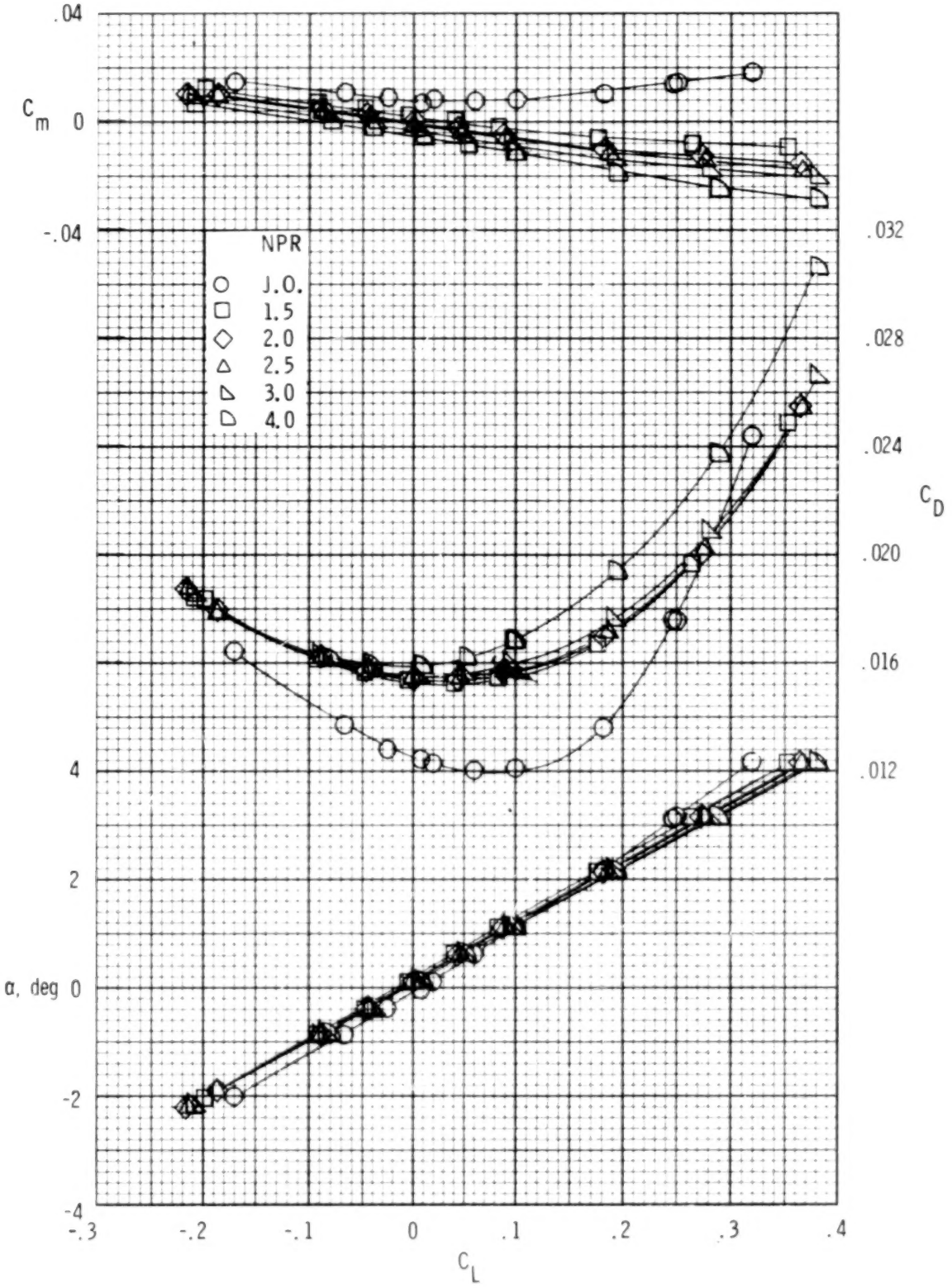

(b) M = 0.8.

Figure 12.- Concluded.

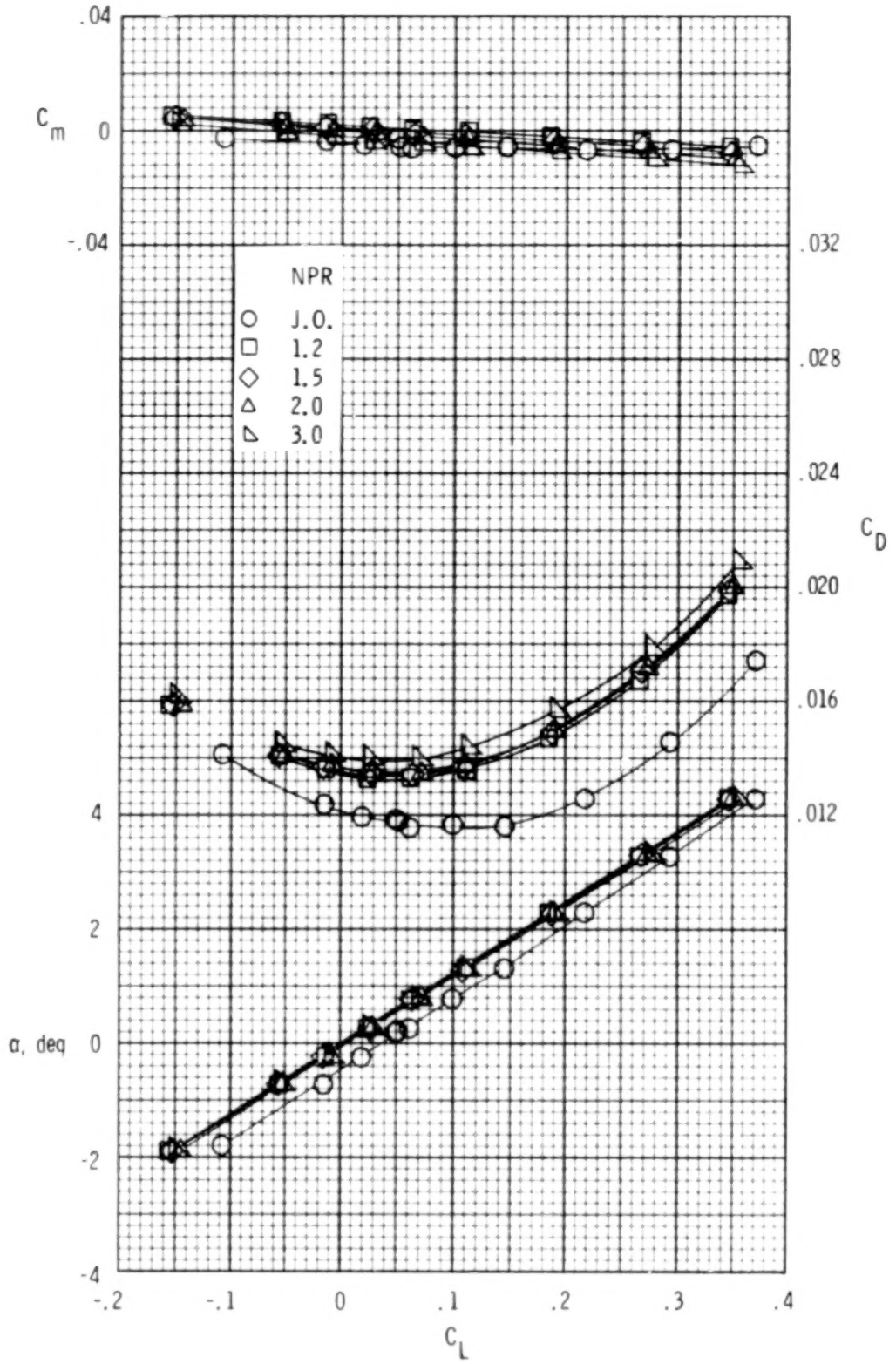

(a) M = 0.5.

Figure 13.- Effect of nozzle pressure ratio (NPR) on wing-body aerodynamic characteristics for the configuration with x/D = 1, 2y/b = 0.5, and z/D = 1. J.O. denotes jet off.

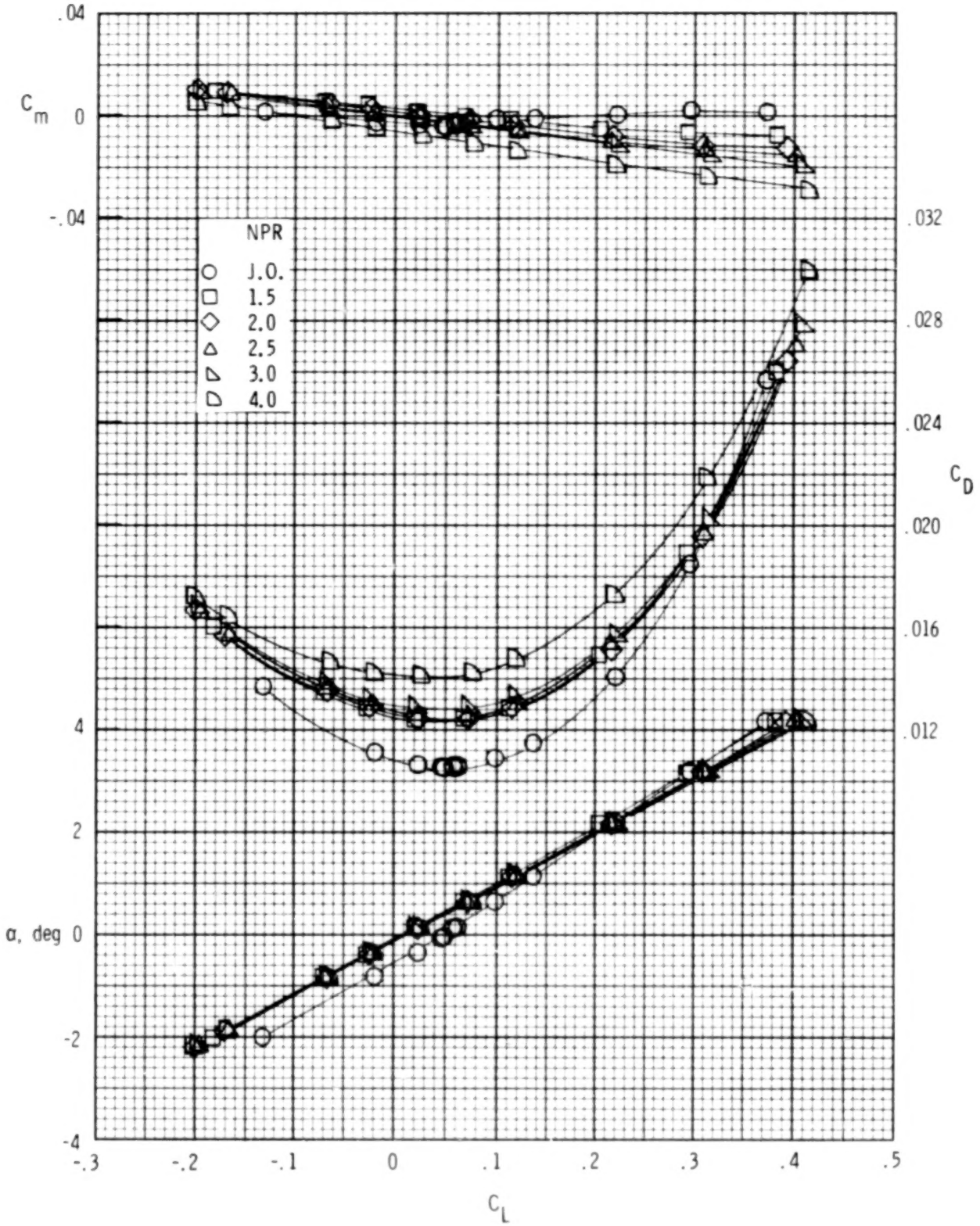

(b) M = 0.8.

Figure 13.- Concluded.

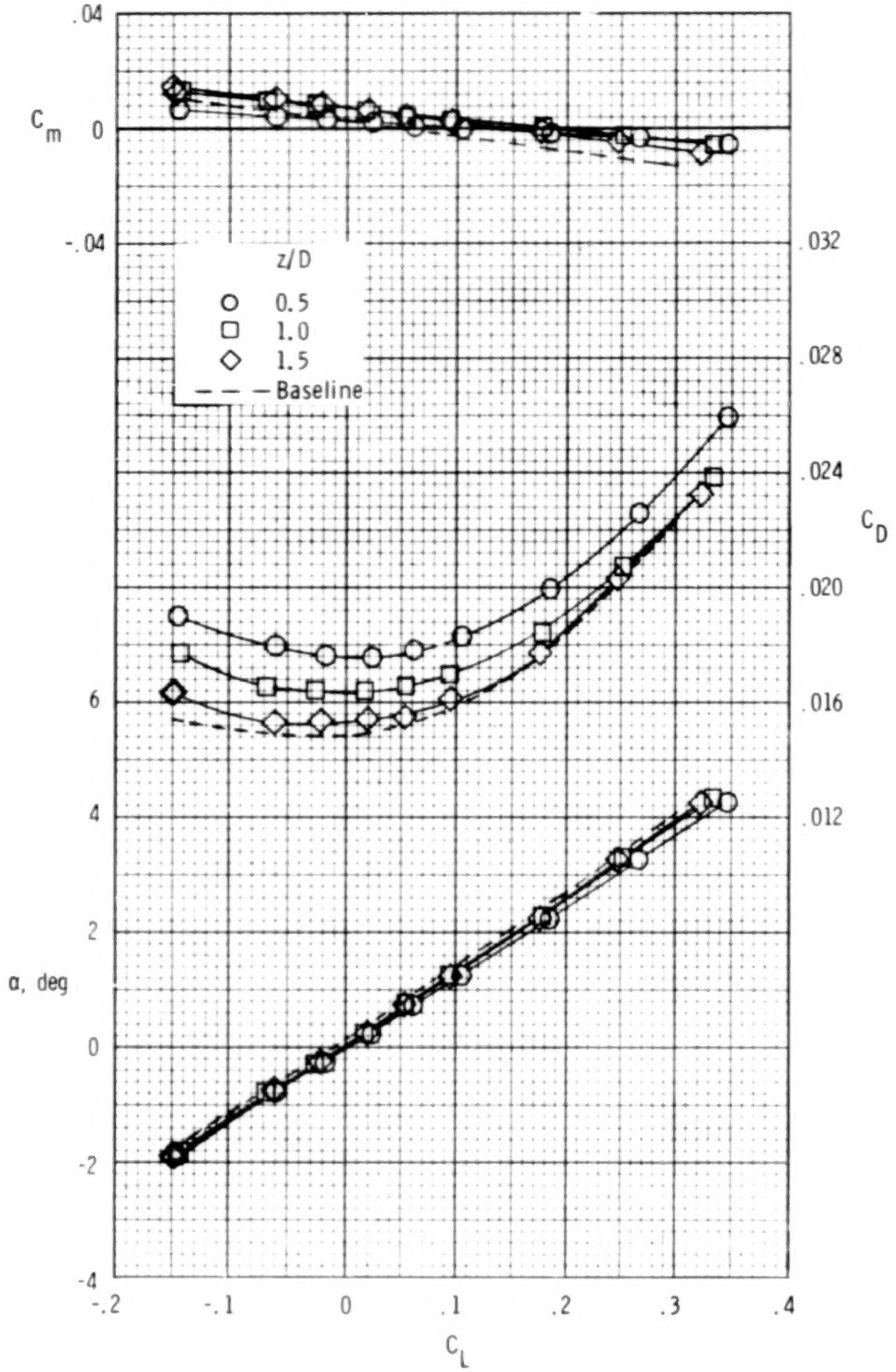

(a) M = 0.5; $p_{t,j}/p_\infty$ = 2.0.

Figure 14.- Effect of nacelle-exit vertical location on wing-body aerodynamic characteristics for configurations with x/D = 0 and 2y/b = 0.25.

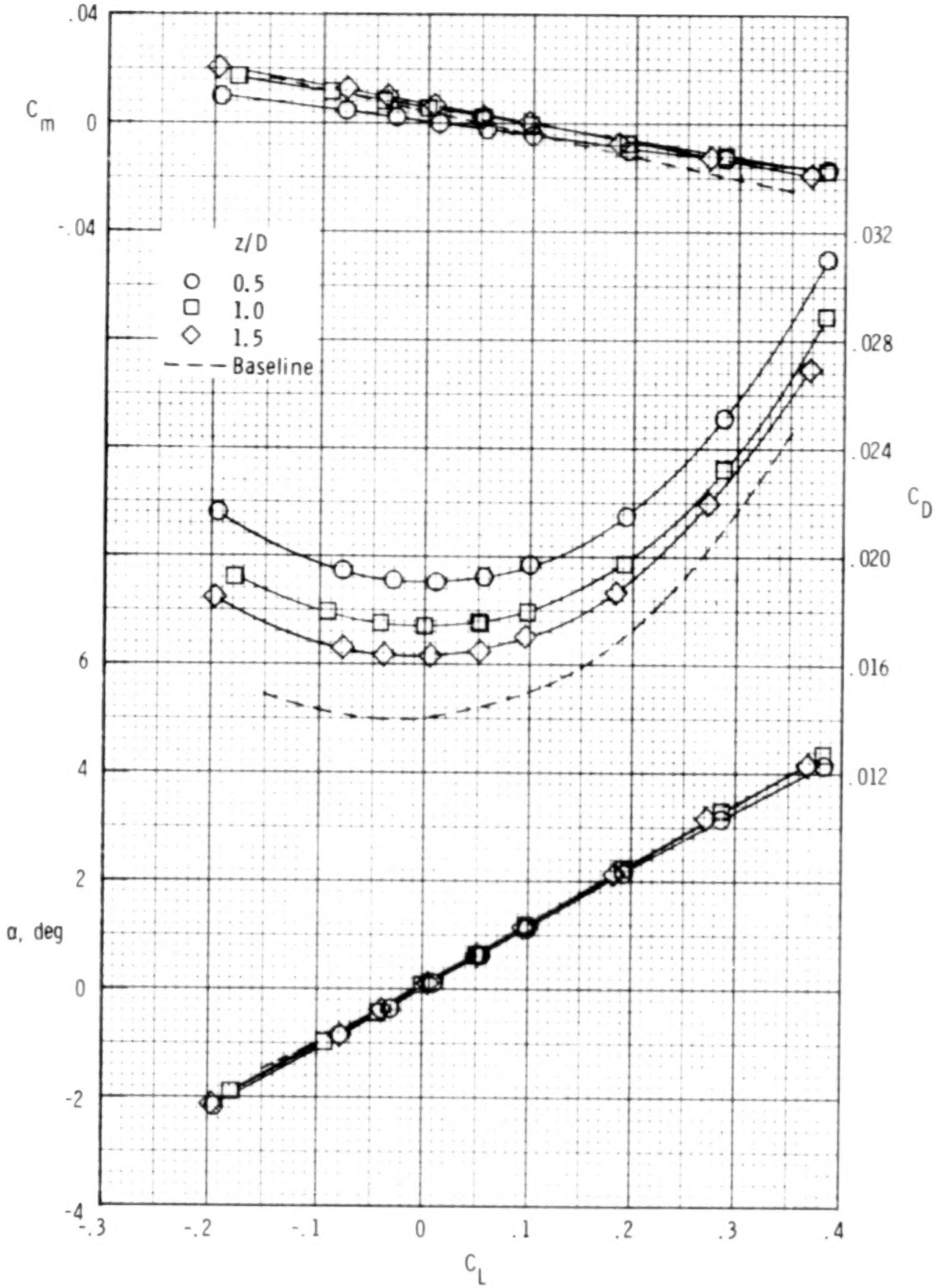

(b) M = 0.8; $p_{t,j}/p_\infty$ = 2.5.

Figure 14.- Concluded.

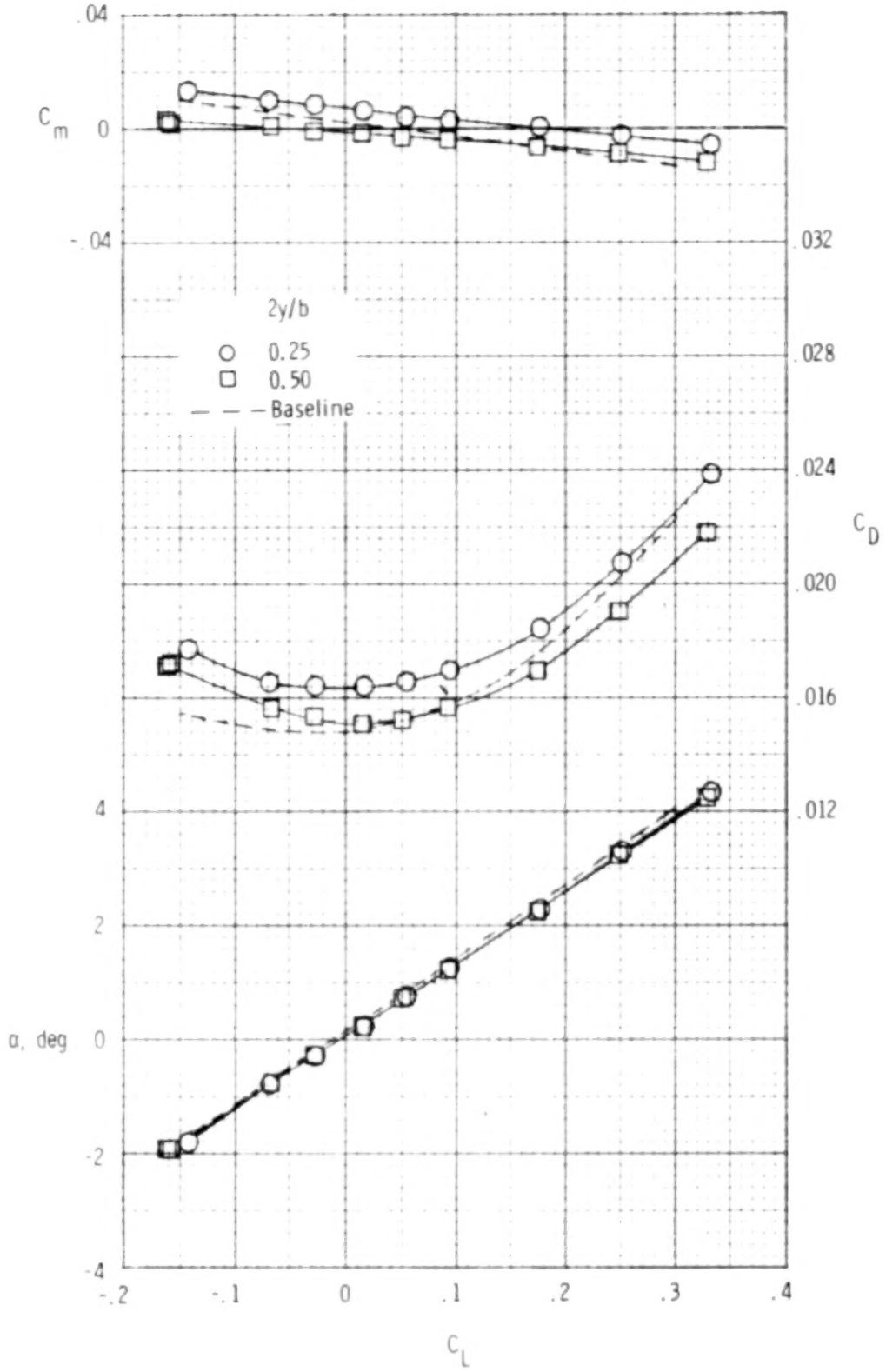

(a) M = 0.5; $p_{t,j}/p_\infty$ = 2.0.

Figure 15.- Effect of nacelle-exit span location on wing-body aerodynamic characteristics for configurations with x/D = 0 and z/D = 1.

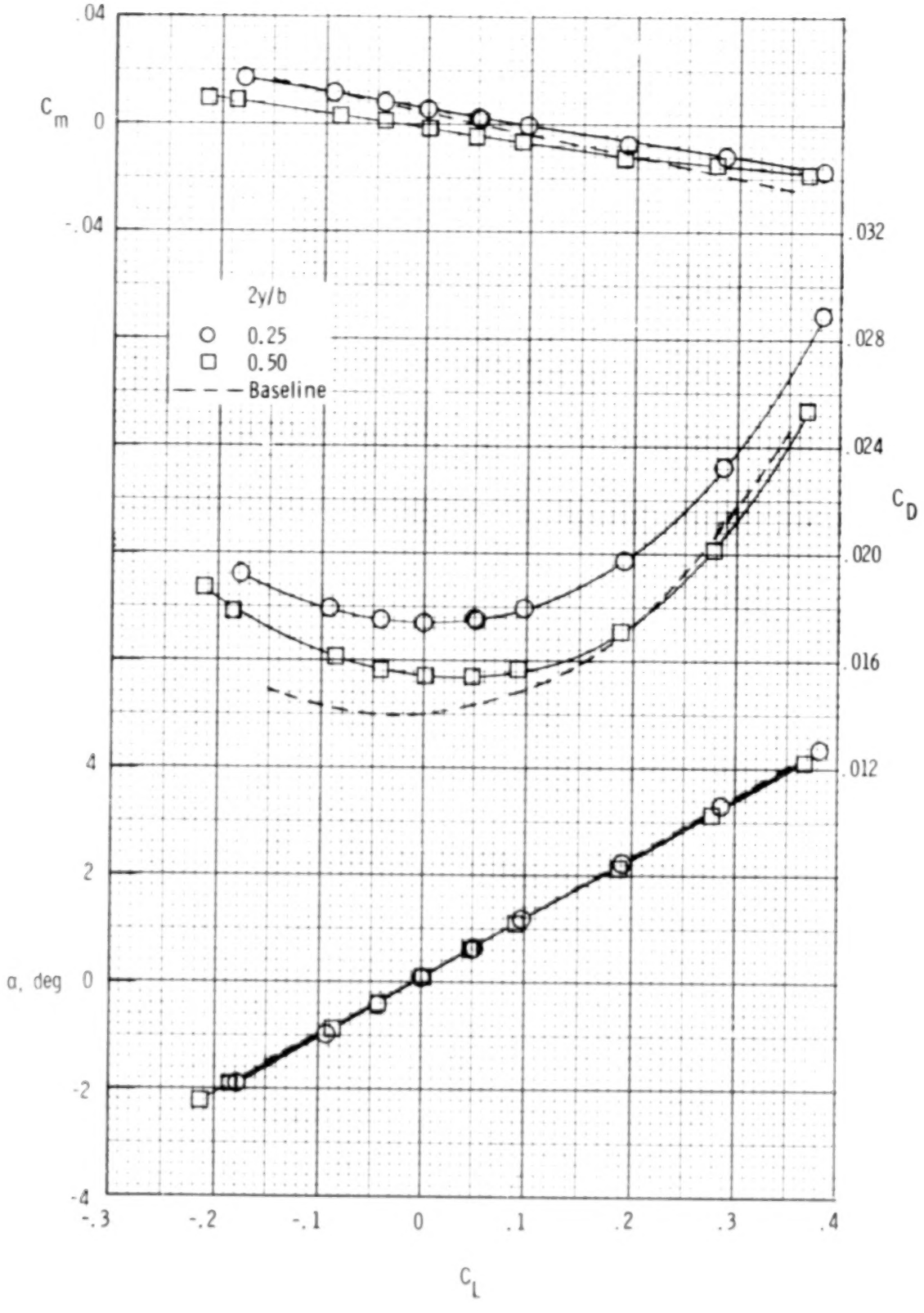

(b) M = 0.8; $p_{t,j}/p_\infty$ = 2.5.

Figure 15.- Concluded.

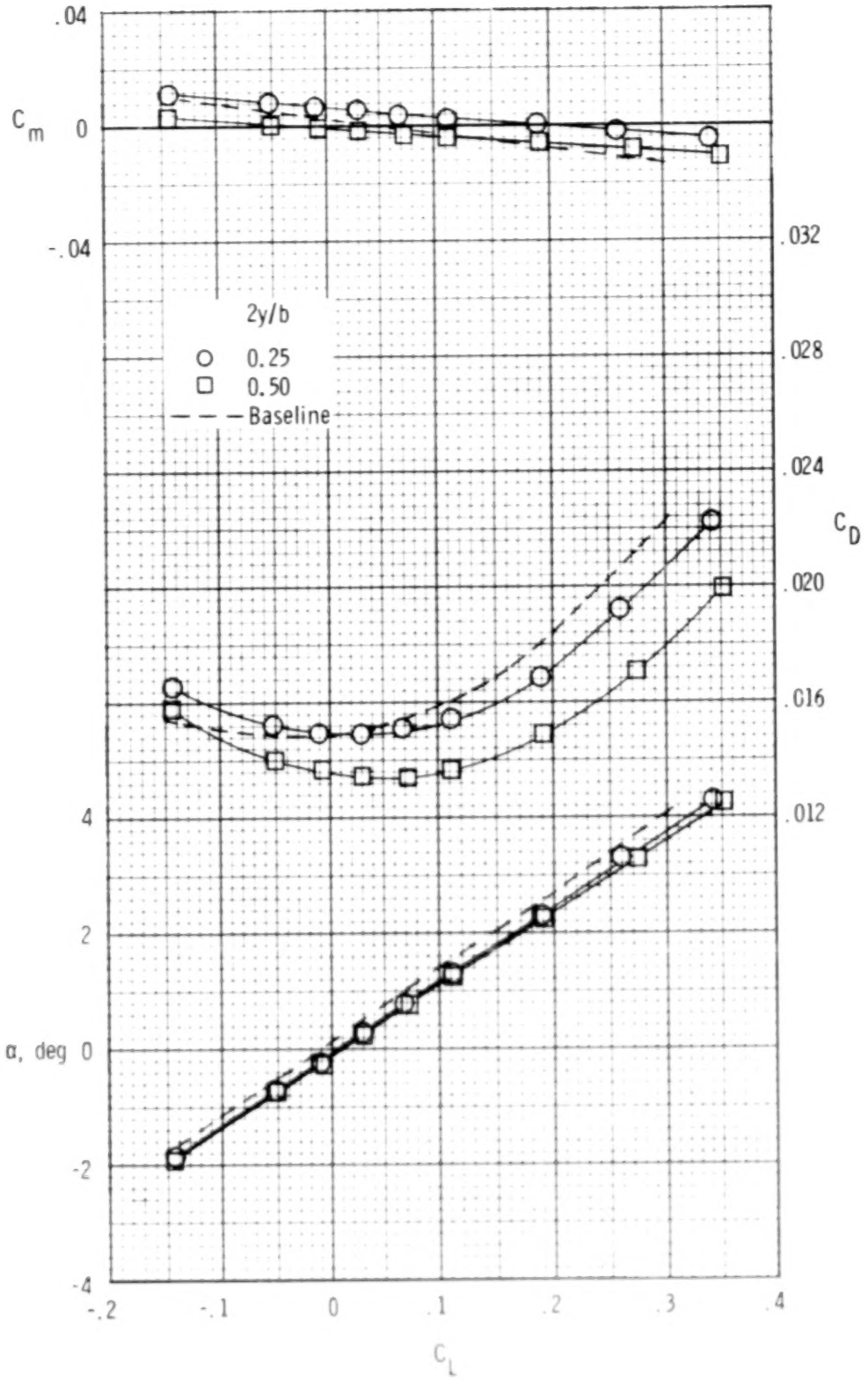

(a) M = 0.5; $p_{t,j}/p_\infty$ = 2.0.

Figure 16.- Effect of nacelle-exit span location on wing-body aerodynamic characteristics for configurations with x/D = 1 and z/D = 1.

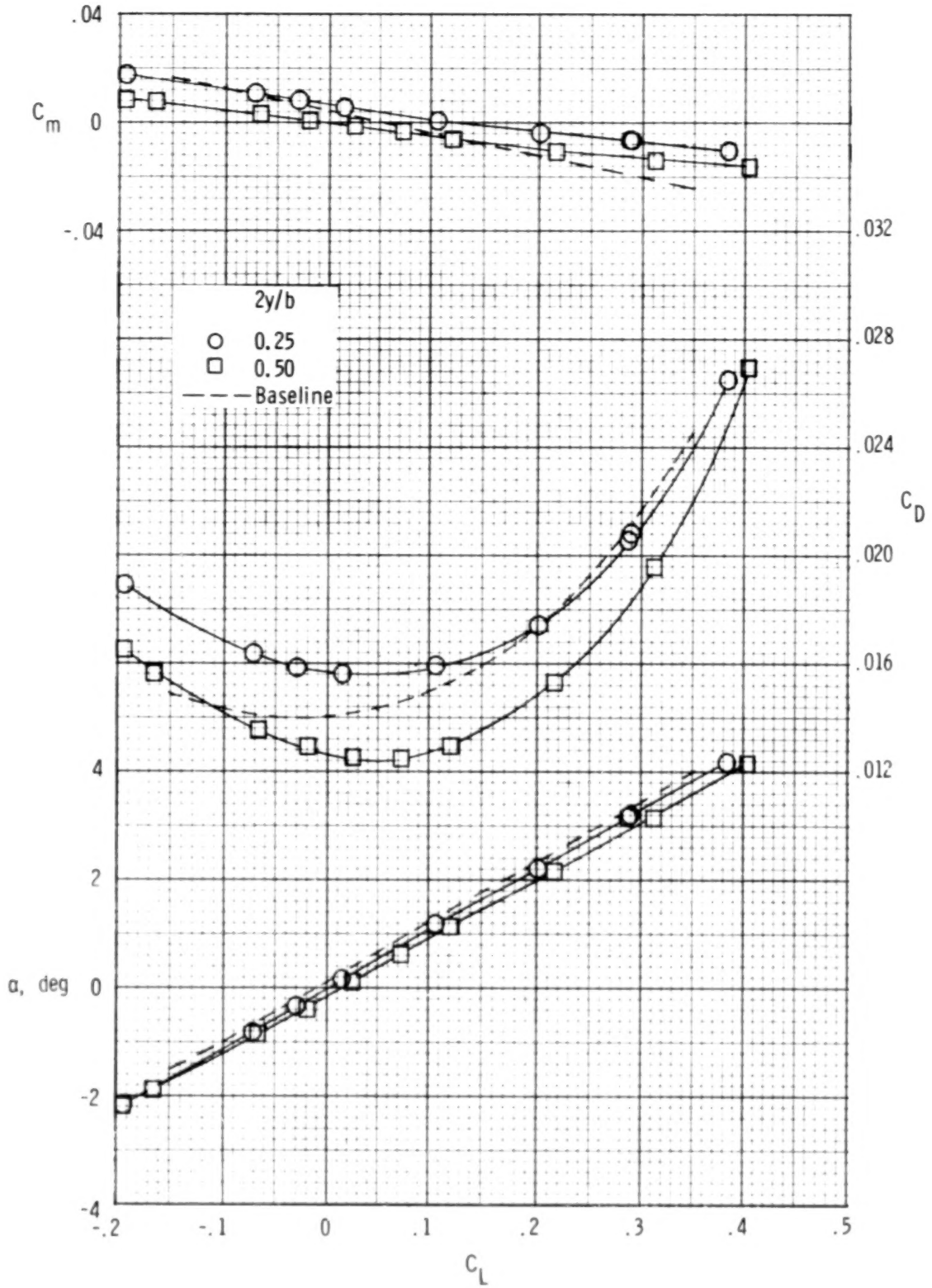

(b) M = 0.8; $p_{t,j}/p_\infty$ = 2.5.

Figure 16.- Concluded.

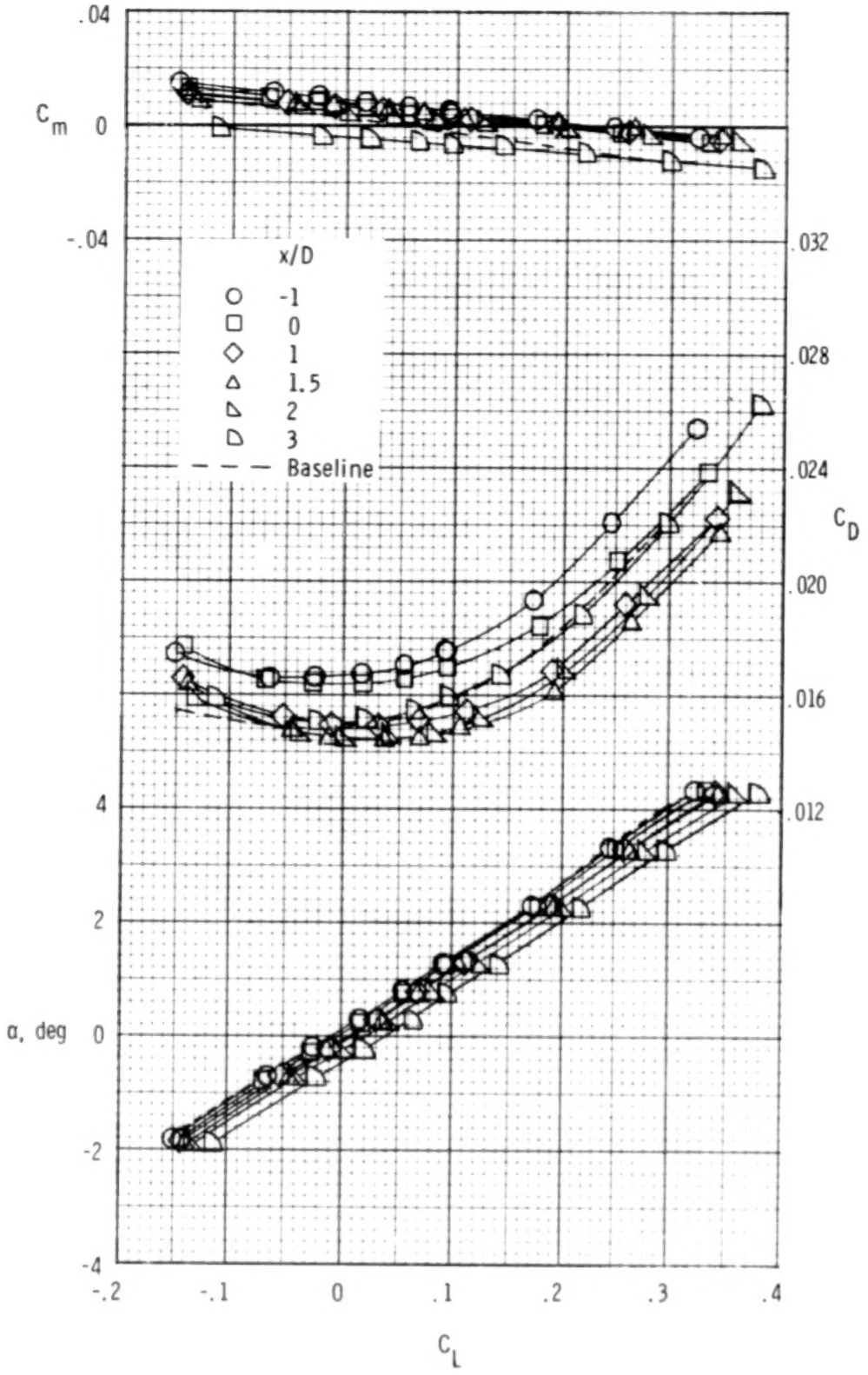

(a) M = 0.5; $p_{t,j}/p_\infty$ = 2.0.

Figure 17.- Effect of nacelle-exit longitudinal location on wing-body aerodynamic characteristics for configurations with 2y/b = 0.25 and z/D = 1.

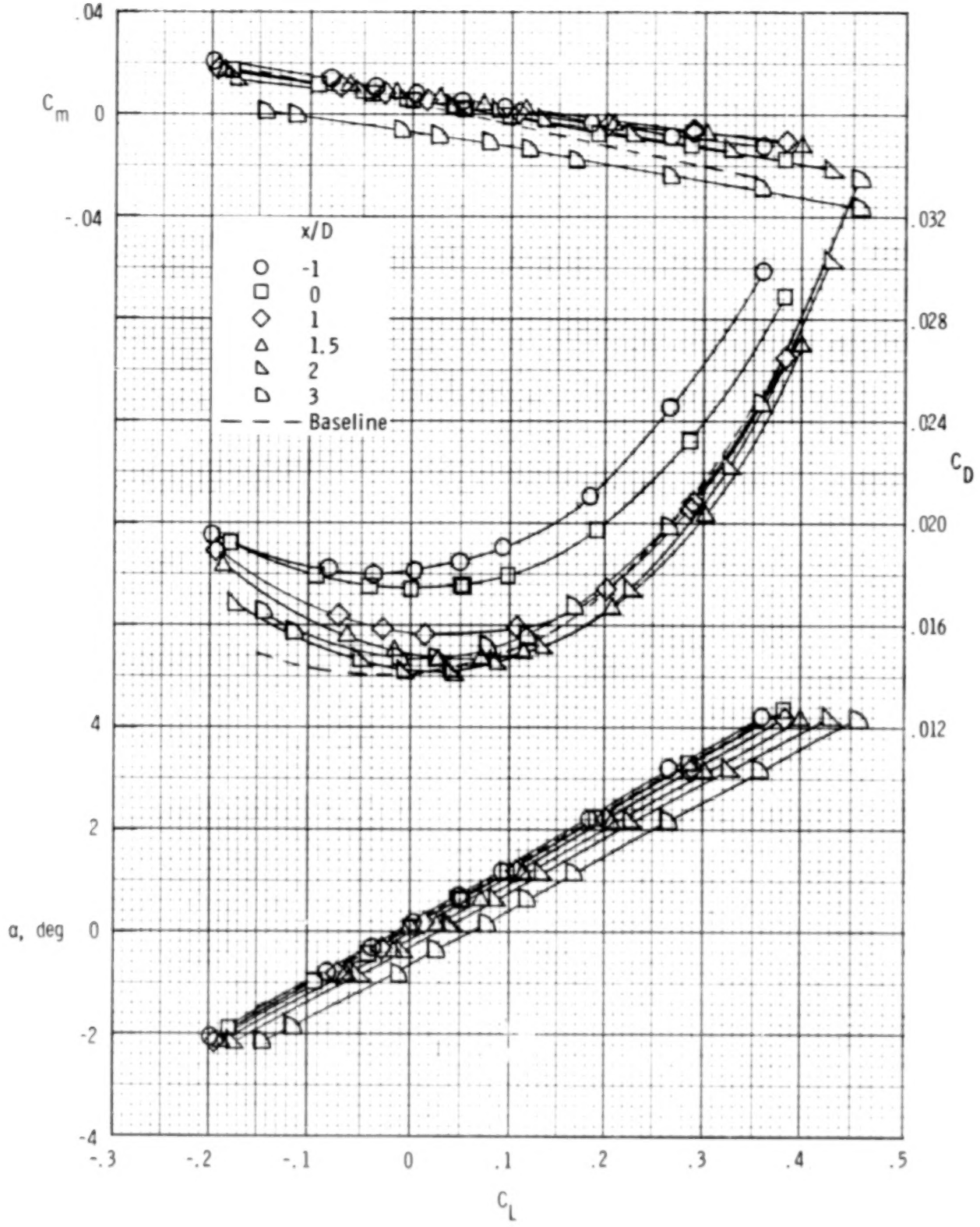

(b) M = 0.8; $p_{t,j}/p_\infty$ = 2.5.

Figure 17.- Concluded.

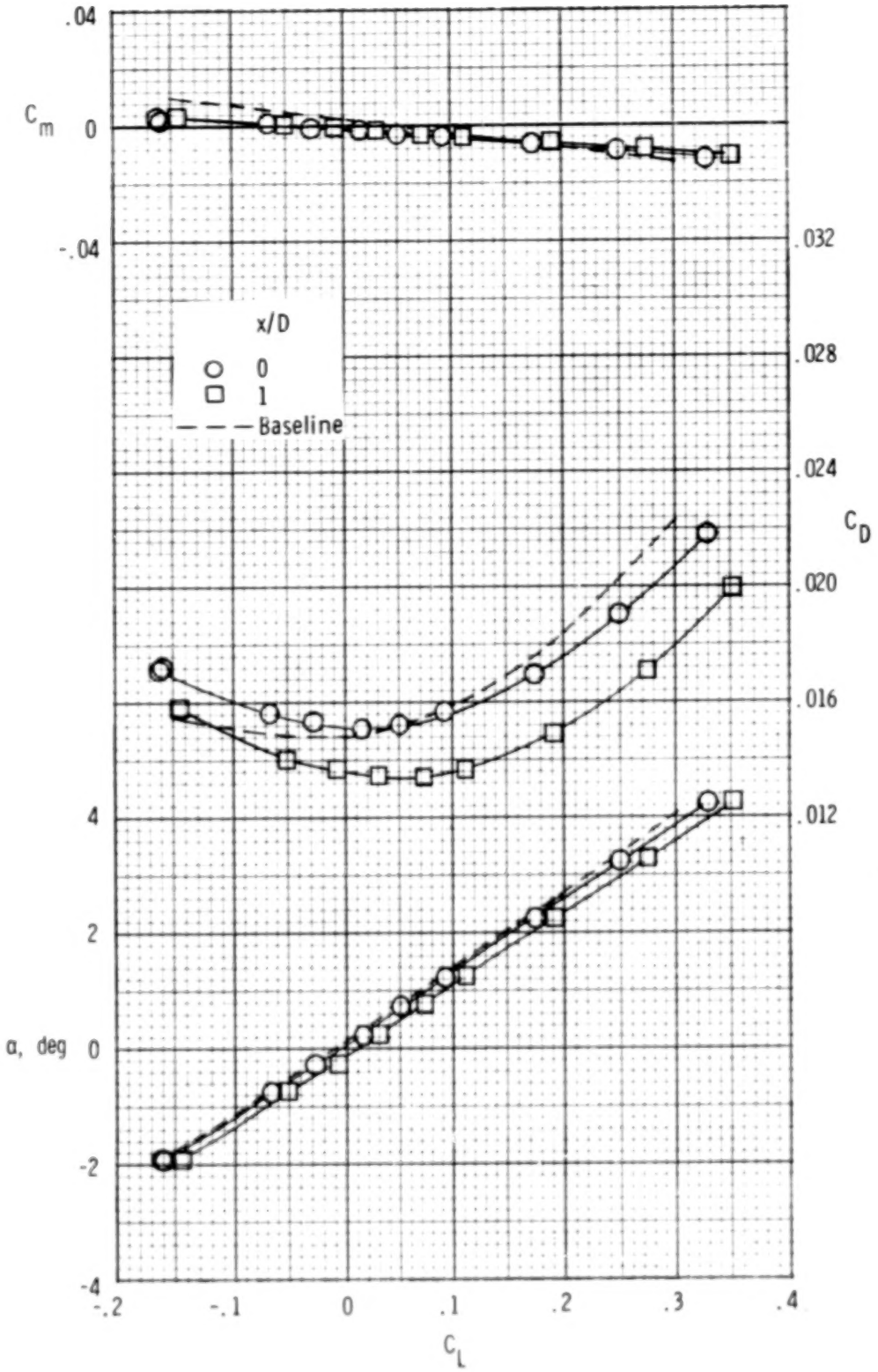

(a) M = 0.5; $p_{t,j}/p_\infty$ = 2.0.

Figure 18.- Effect of nacelle-exit longitudinal location on wing-body aerodynamic characteristics for configurations with 2y/b = 0.5 and z/D = 1.

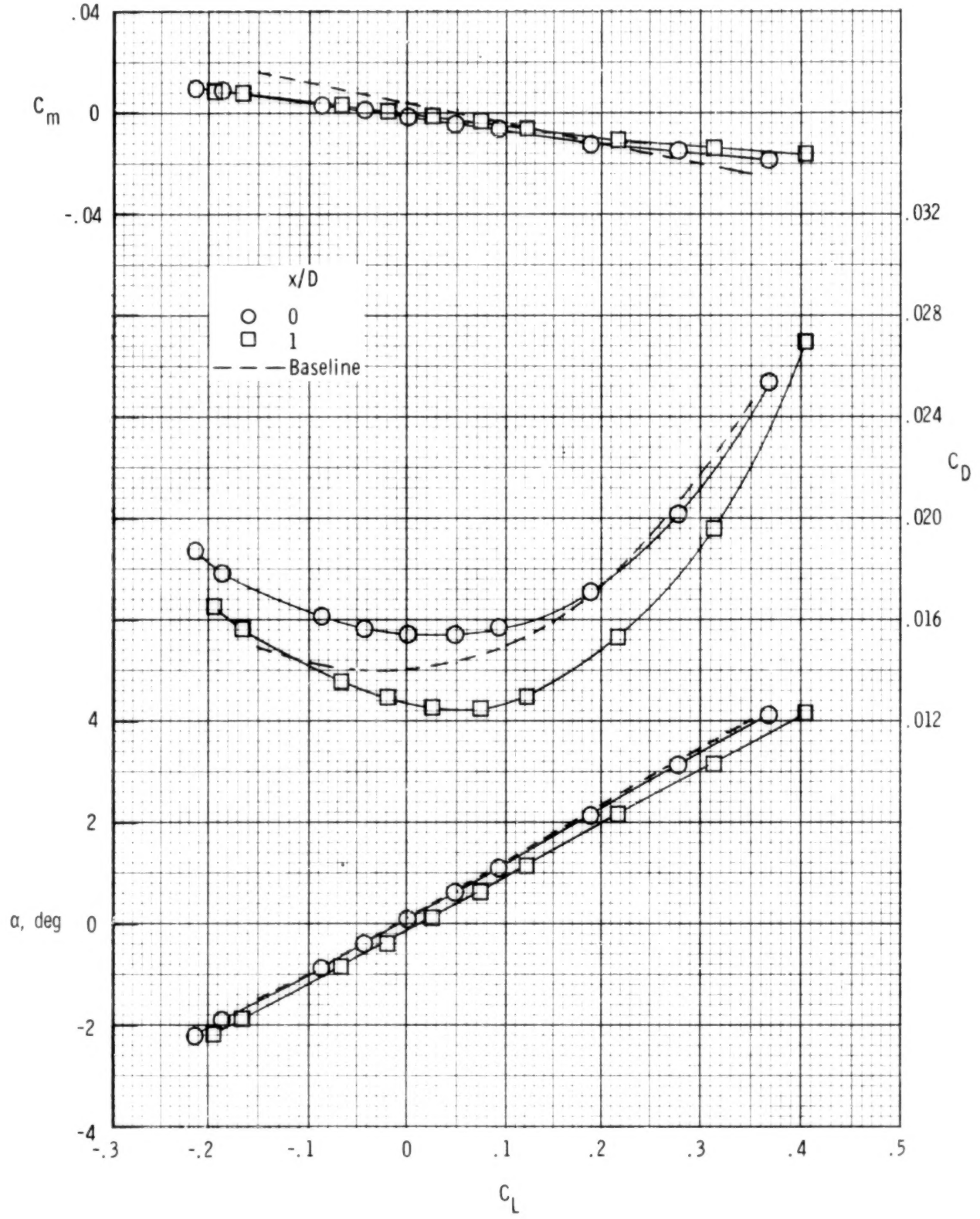

(b) M = 0.8; $p_{t,j}/p_\infty$ = 2.5.

Figure 18.- Concluded.

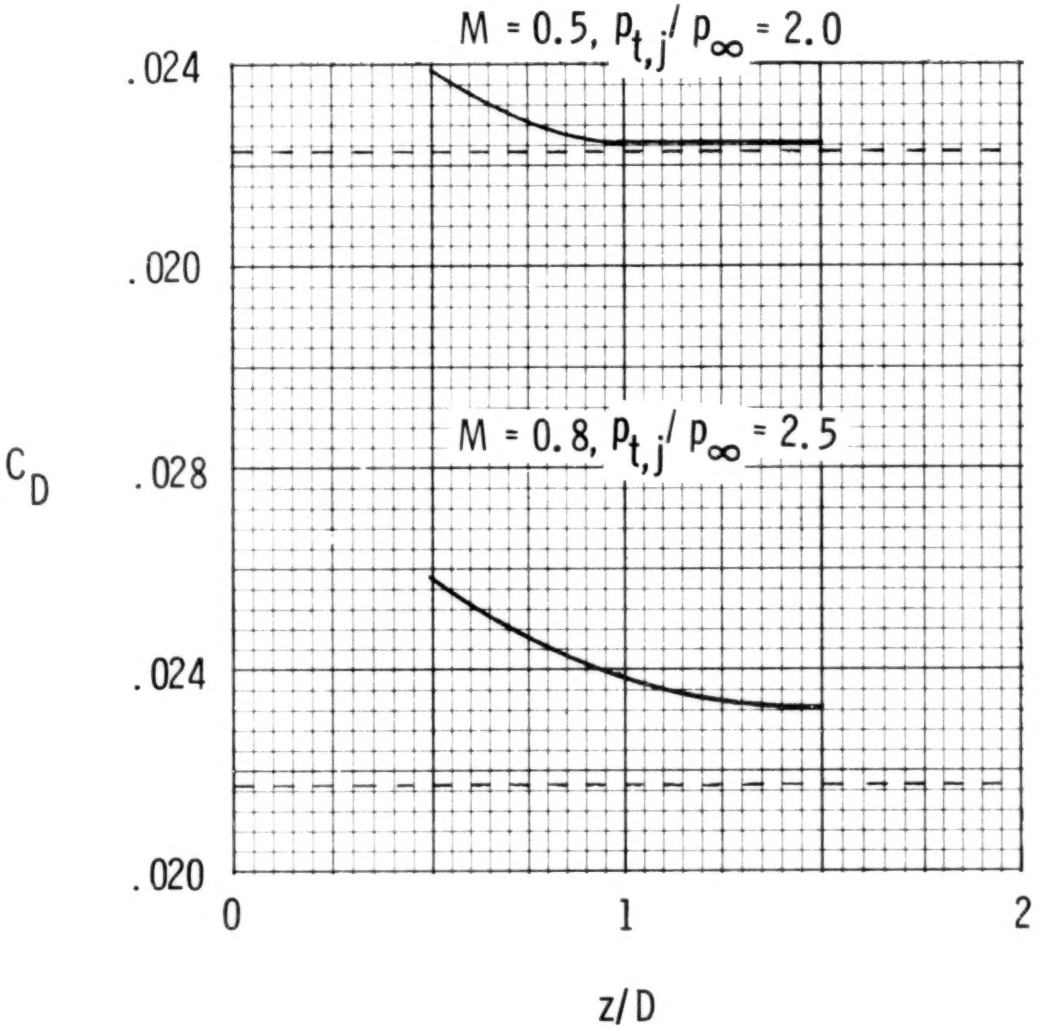

(a) Effect of height. x/D = 0; 2y/b = 0.25.

Figure 19.- Trends in wing-body drag coefficient with nacelle exit position at C_L = 0.3. (Dashed line denotes the baseline.)

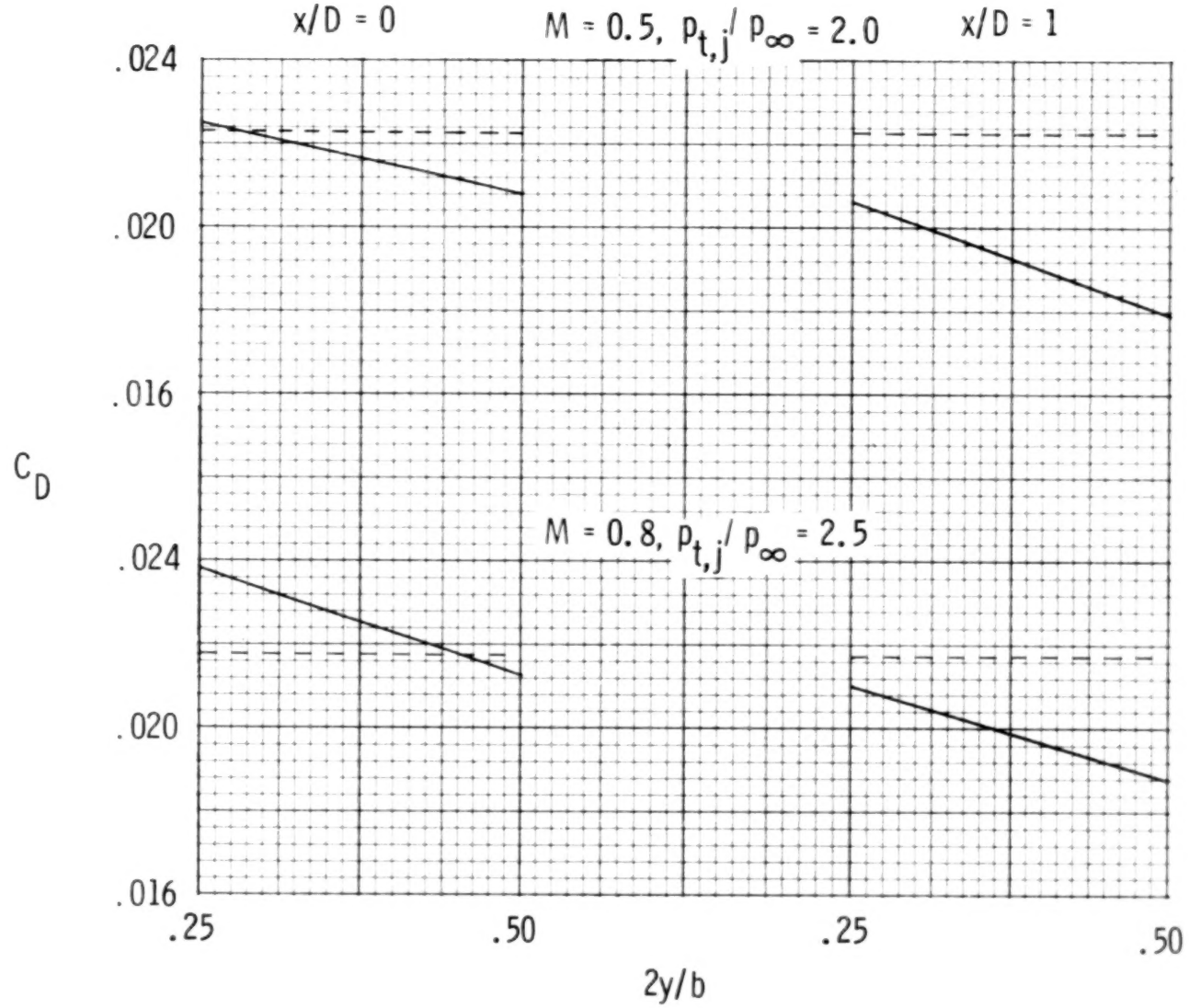

(b) Effect of span. z/D = 1.

Figure 19.- Continued.

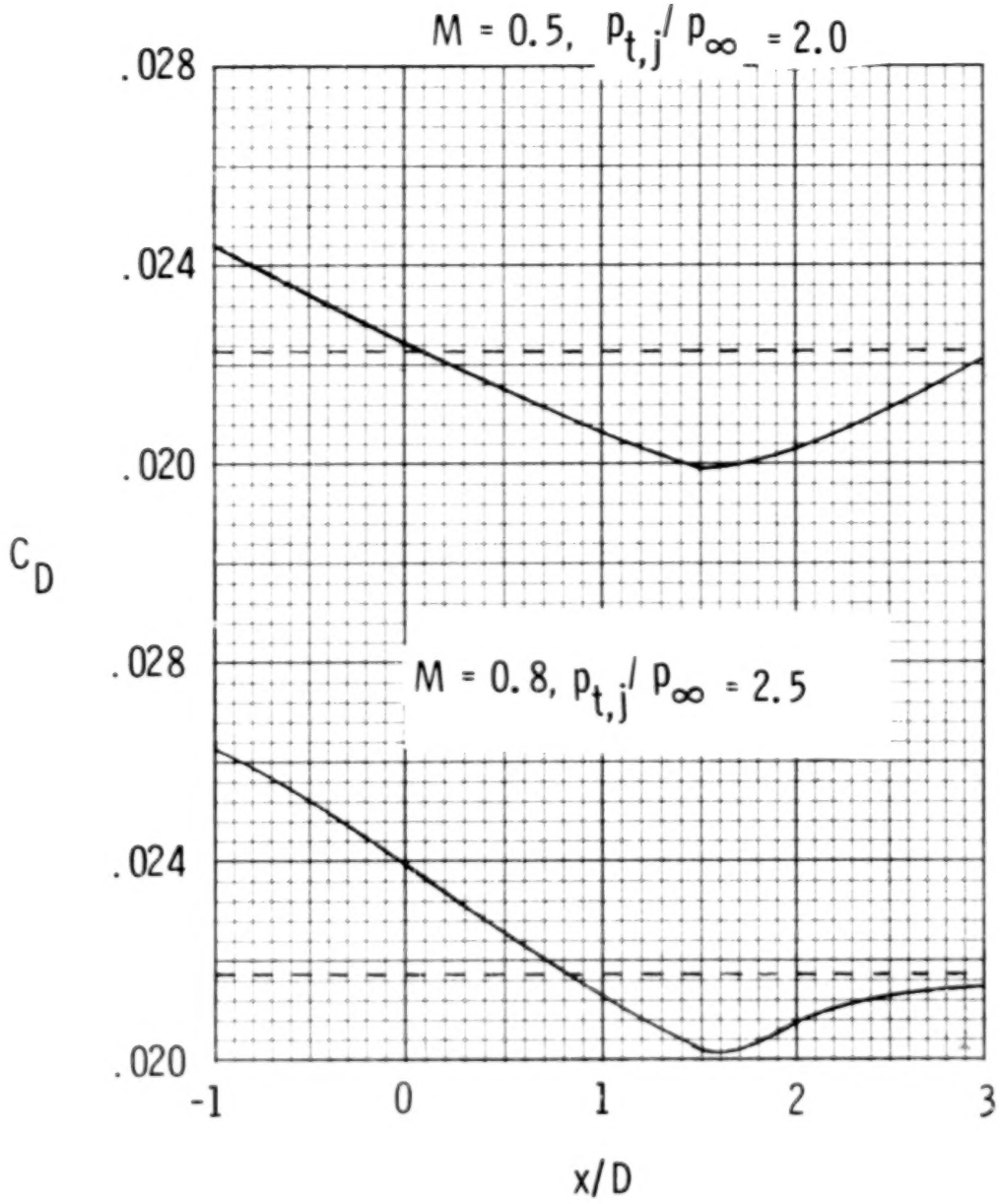

(c) Effect of longitudinal location. 2y/b = 0.25; z/D = 1.

Figure 19.- Concluded.

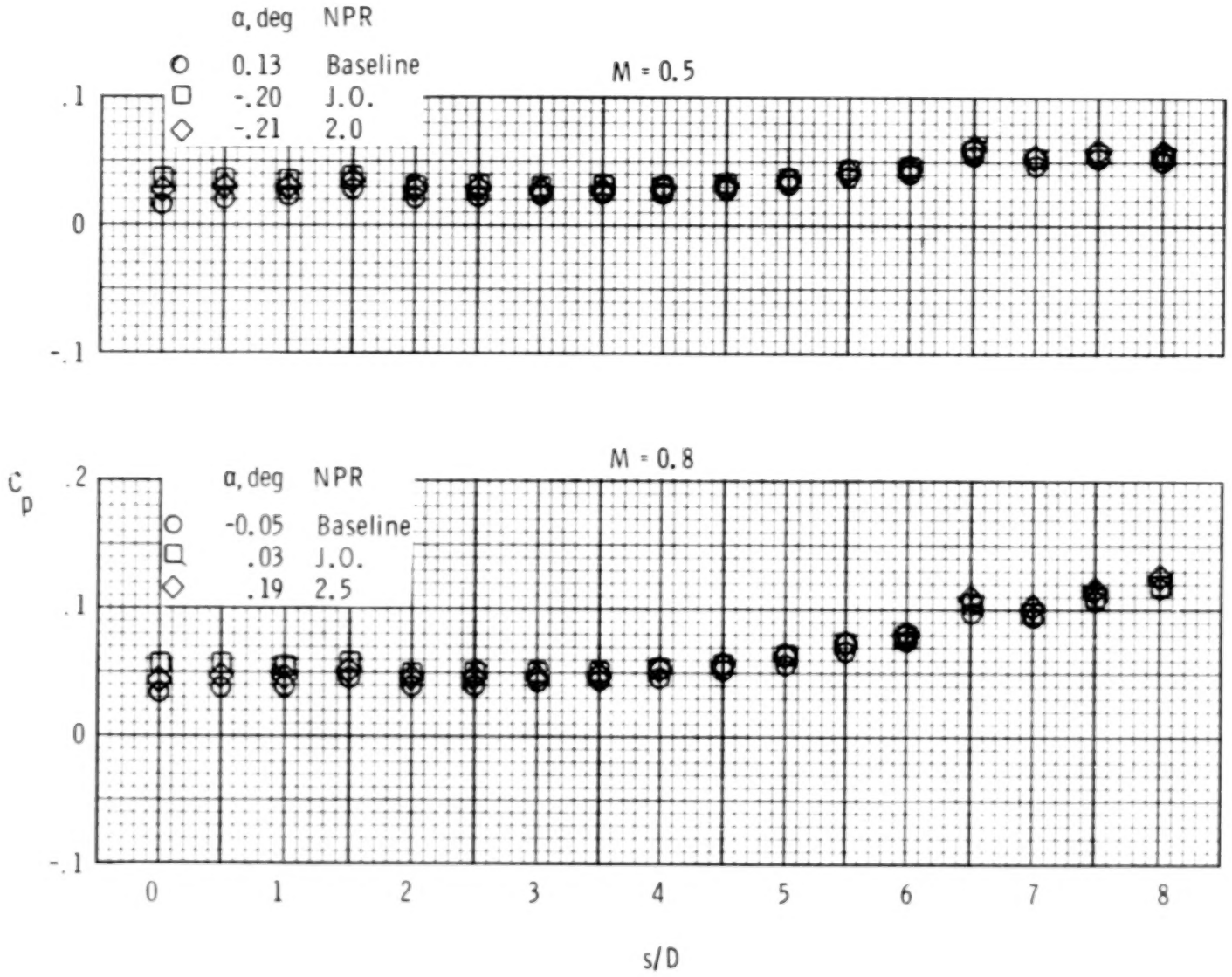

(a) x/D = -1; 2y/b = 0.25; z/D = 1.

Figure 20.- Effect of nacelle installation and jet operation on aft-fuselage pressure coefficients. J.O. denotes jet off; NPR, the nozzle pressure ratio.

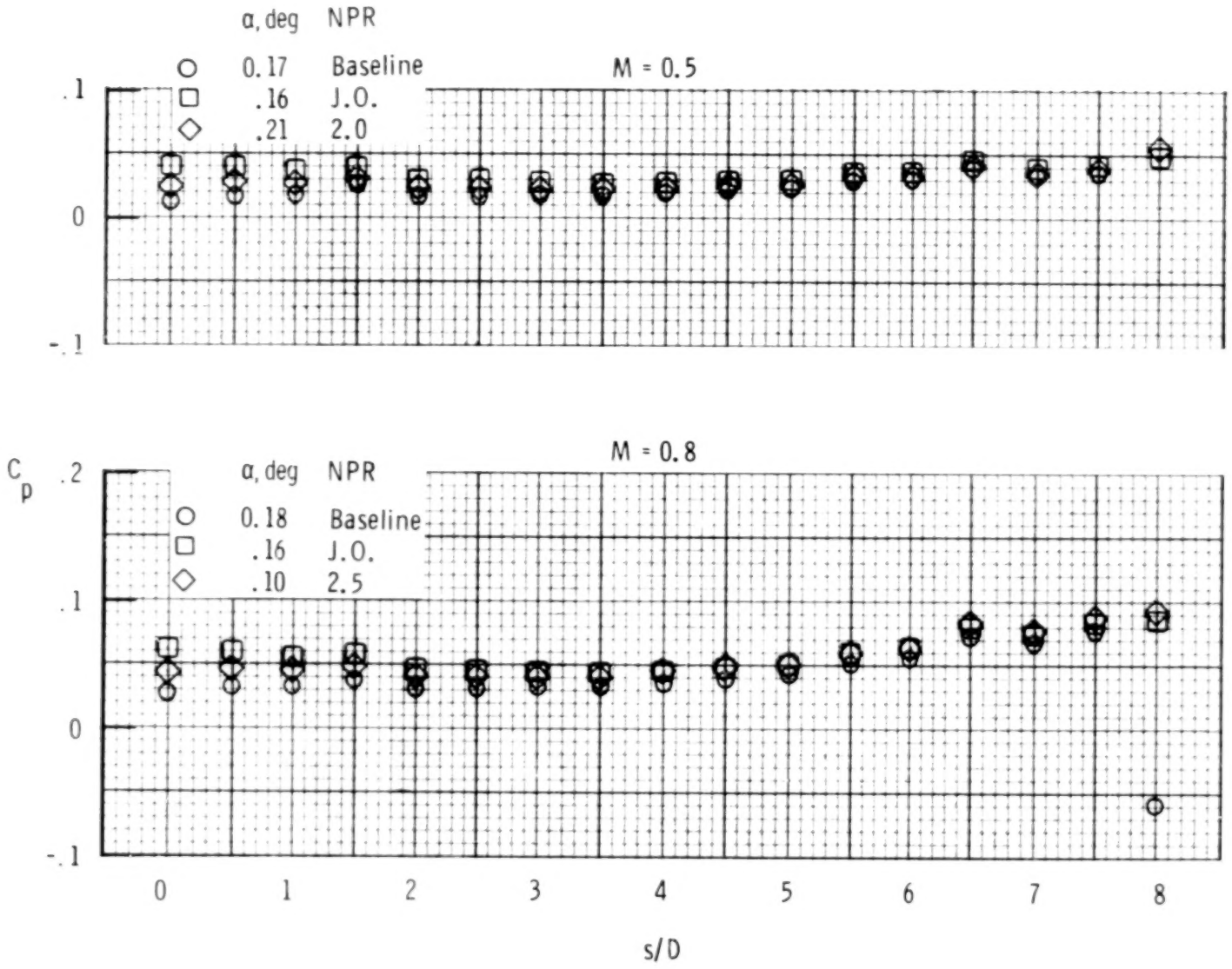

(b) x/D = 0; 2y/b = 0.25; z/D = 1.

Figure 20.- Continued.

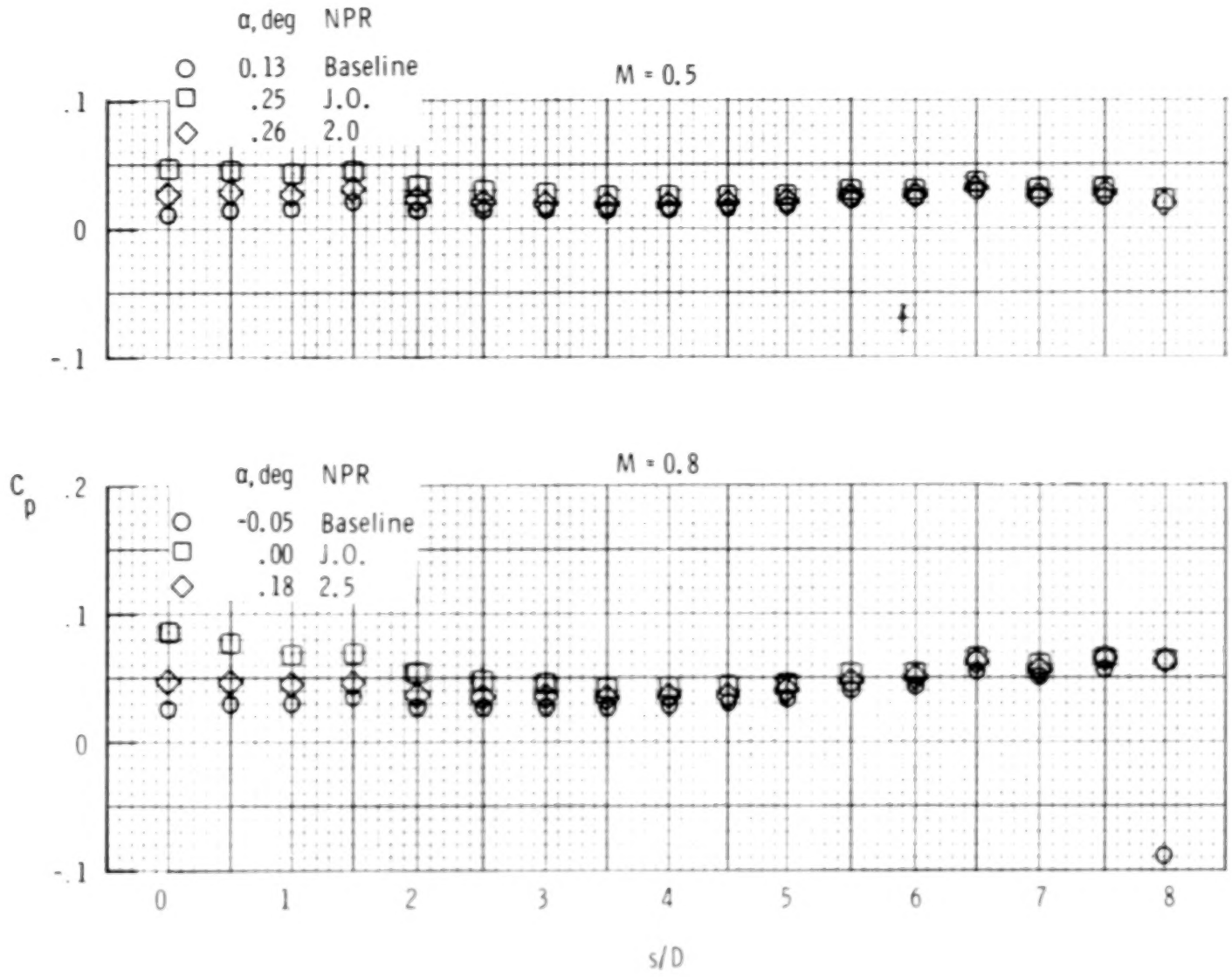

(c) x/D = 1; 2y/b = 0.25; z/D = 1.

Figure 20.- Continued.

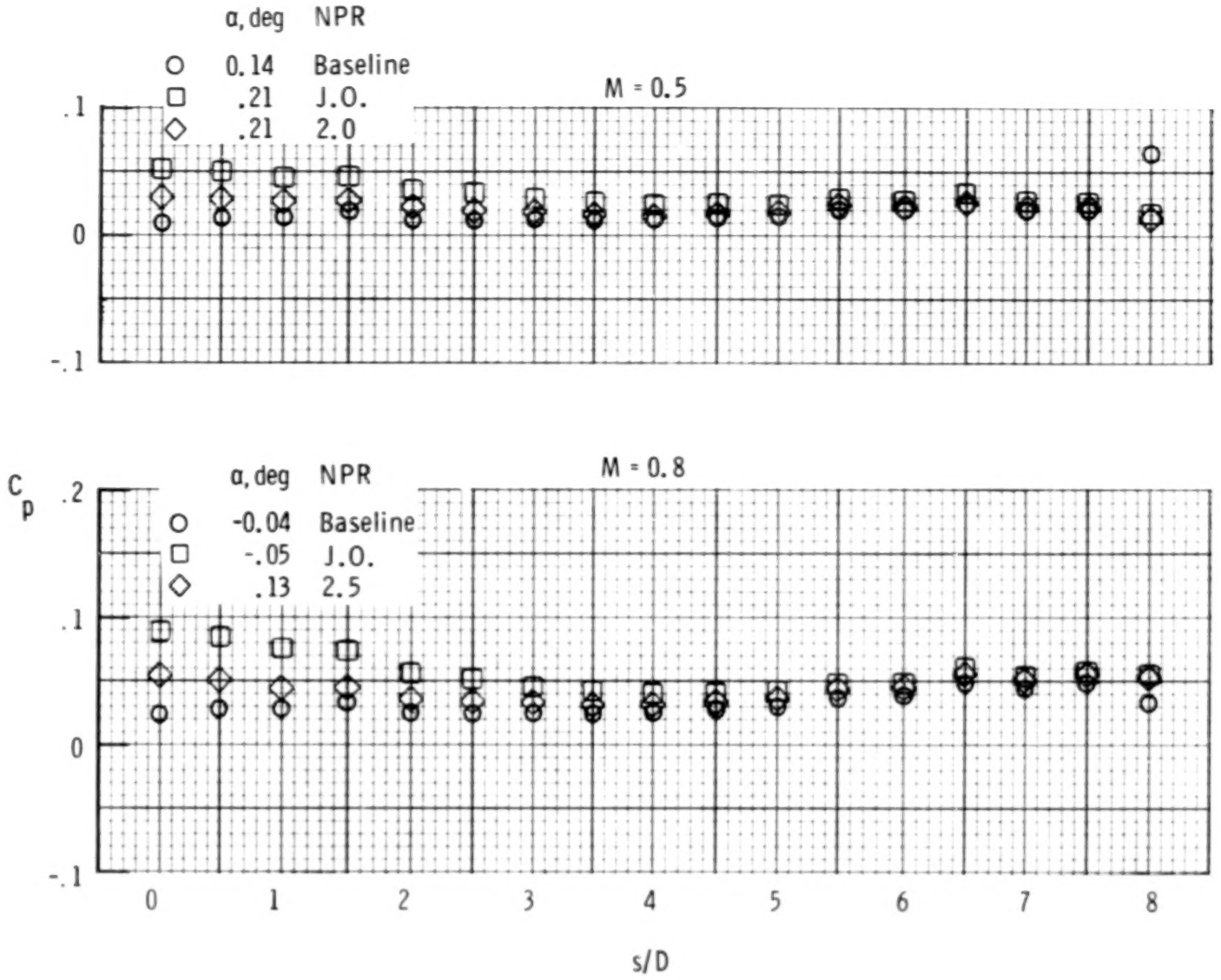

(d) x/D = 1.5; 2y/b = 0.25; z/D = 1.

Figure 20.- Continued.

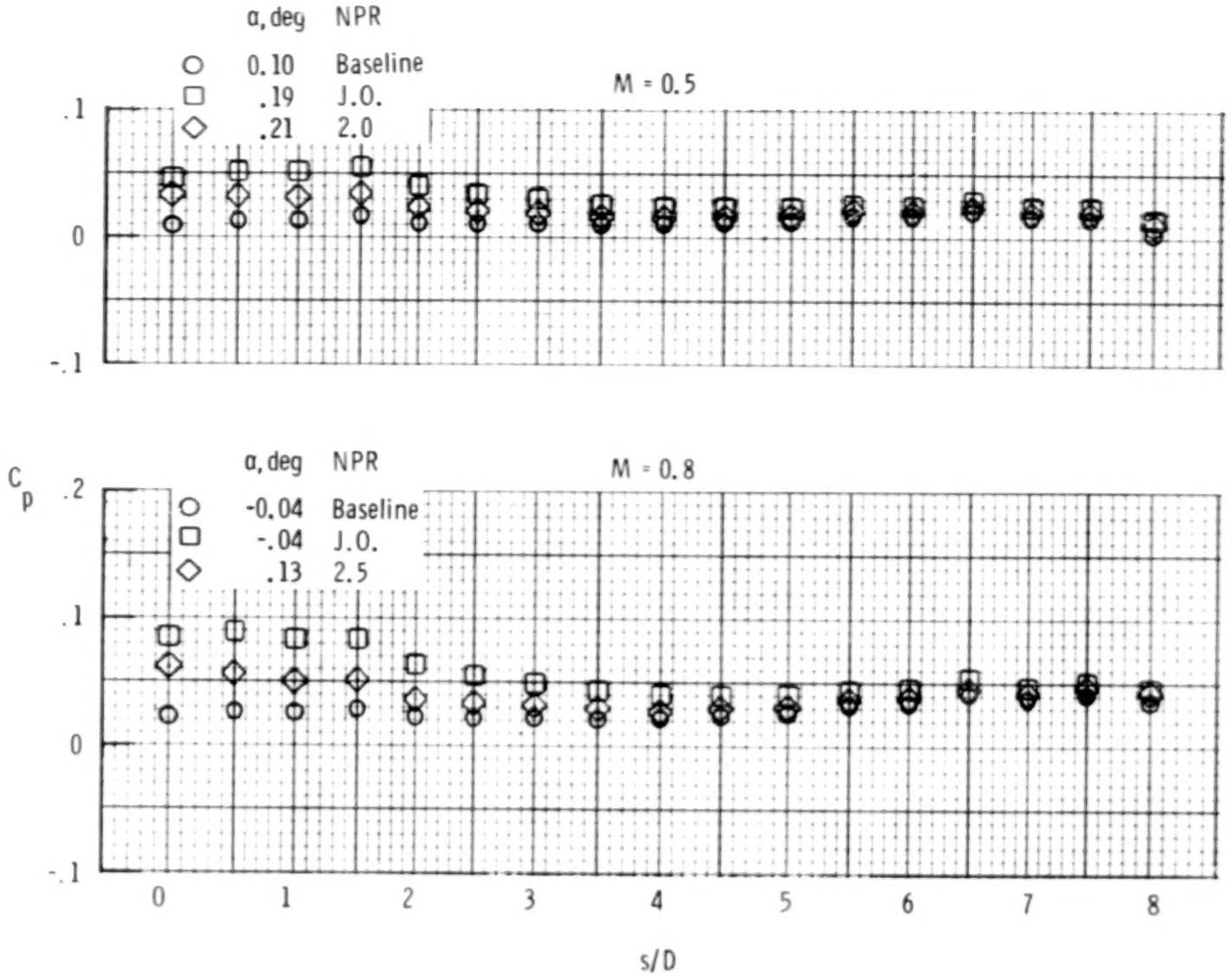

(e) x/D = 2; 2y/b = 0.25; z/D = 1.

Figure 20.- Continued.

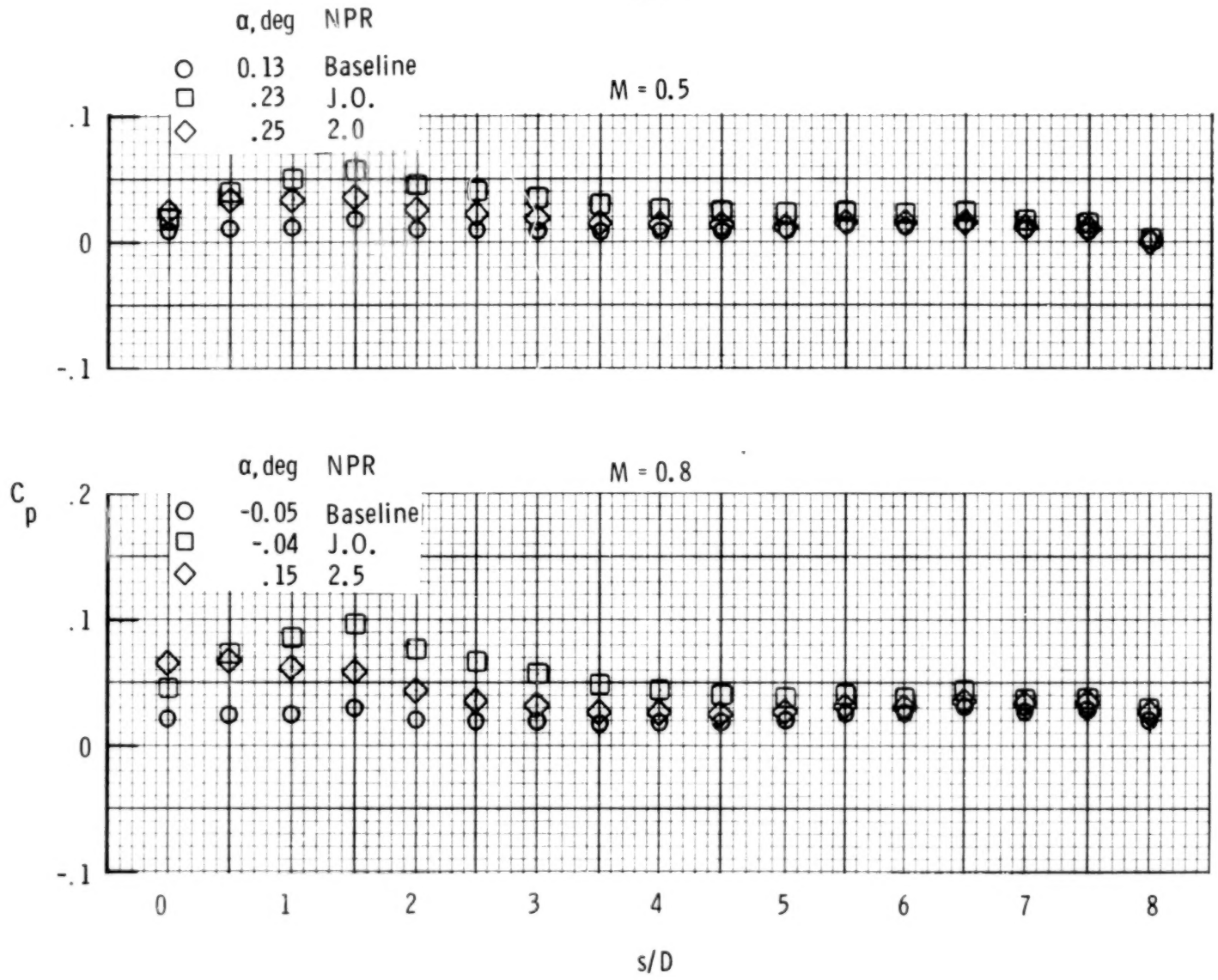

(f) x/D = 3; 2y/b = 0.25; z/D = 1.

Figure 20.- Continued.

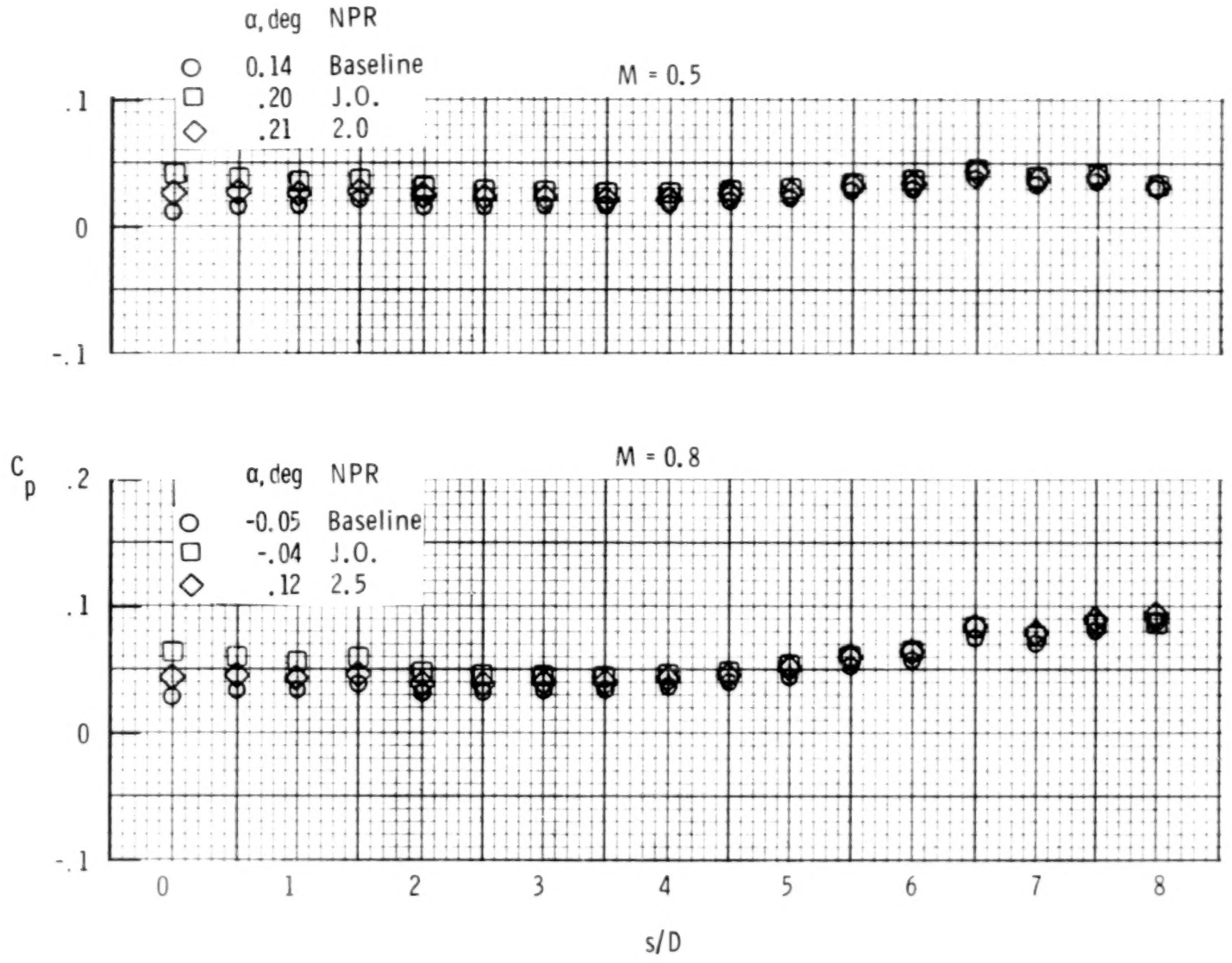

(g) x/D = 0; 2y/b = 0.25; z/D = 0.5.

Figure 20.- Continued.

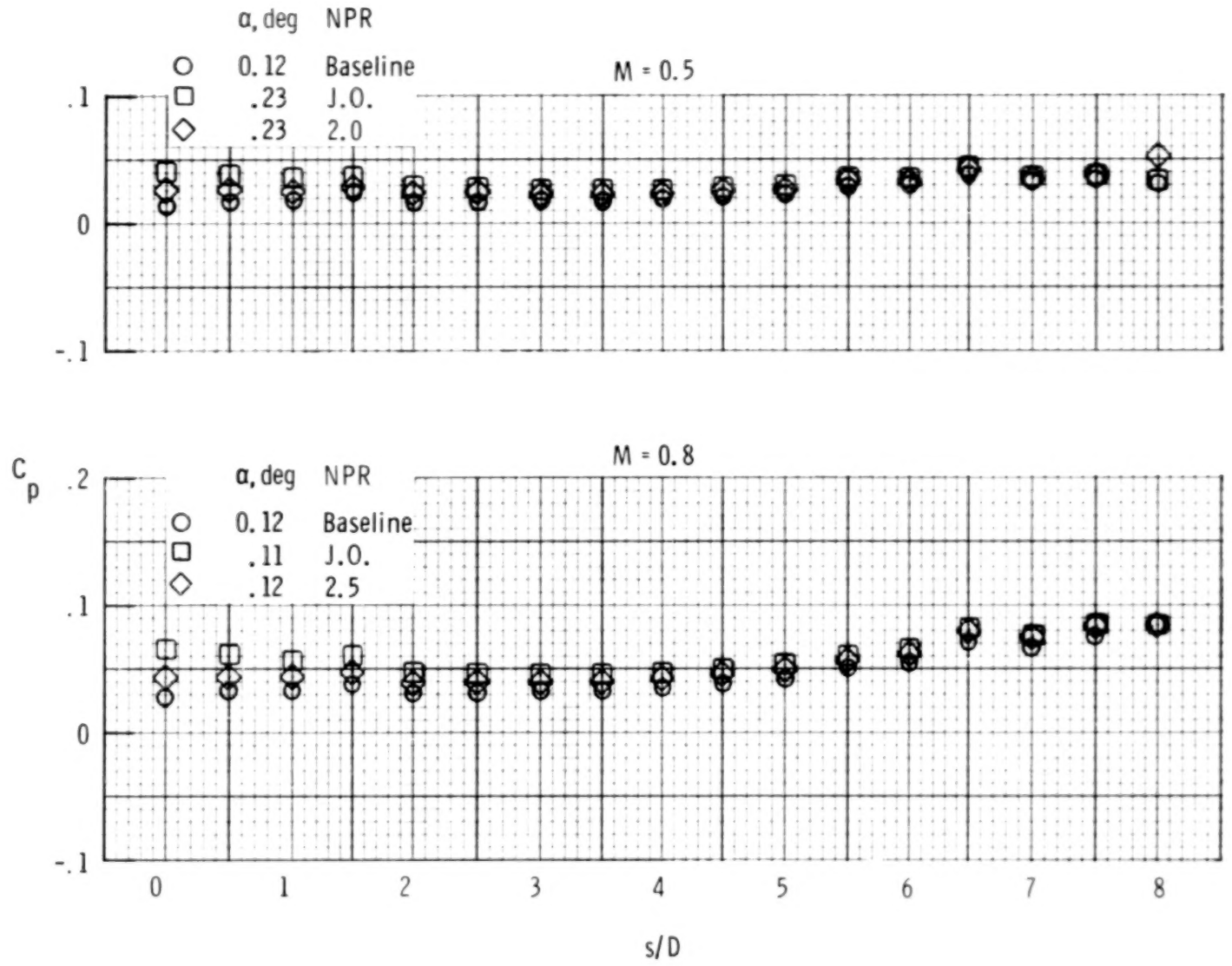

(h) x/D = 0; 2y/b = 0.25; z/D = 1.5.

Figure 20.- Continued.

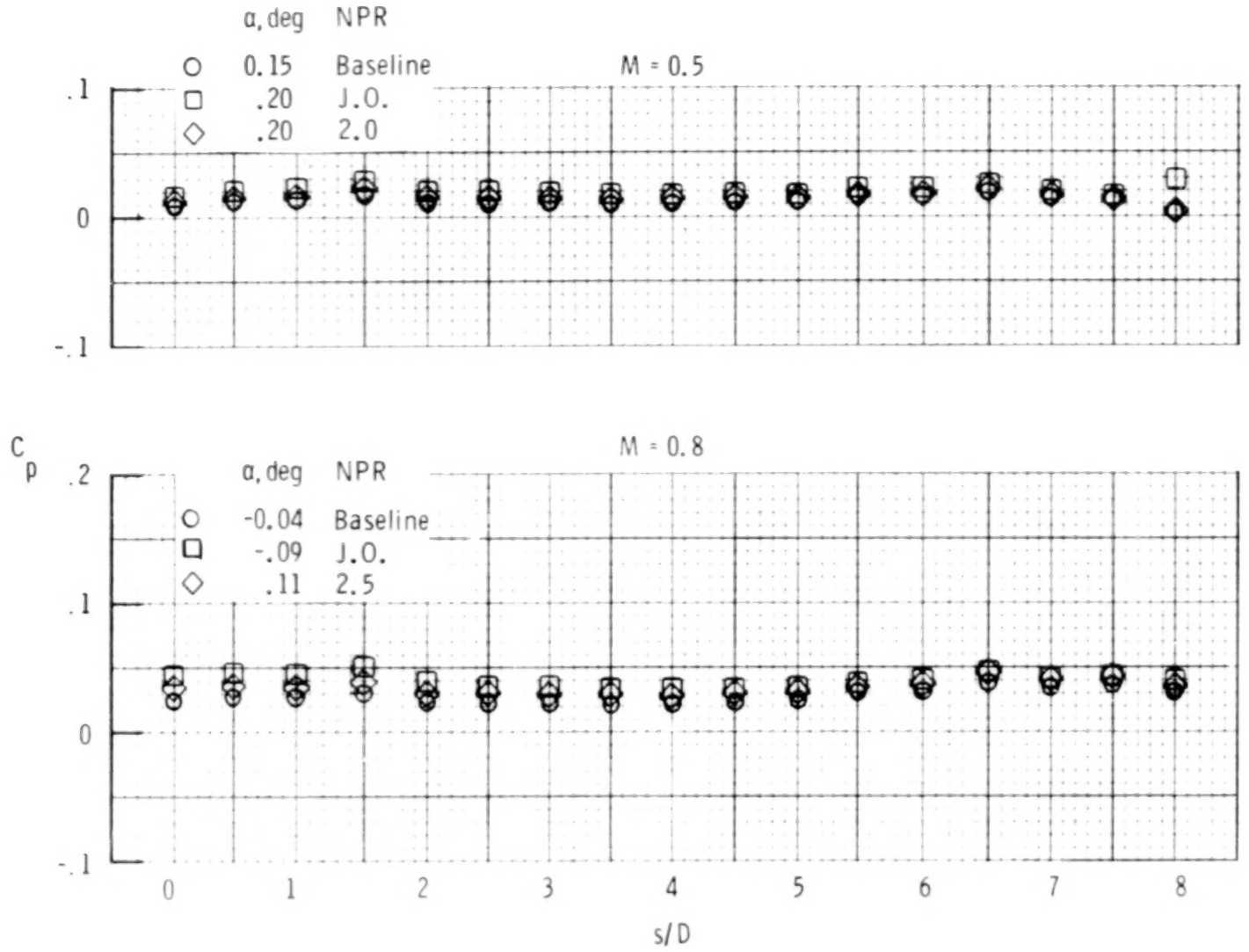

(i) x/D = 0; 2y/b = 0.5; z/D = 1.

Figure 20.- Continued.

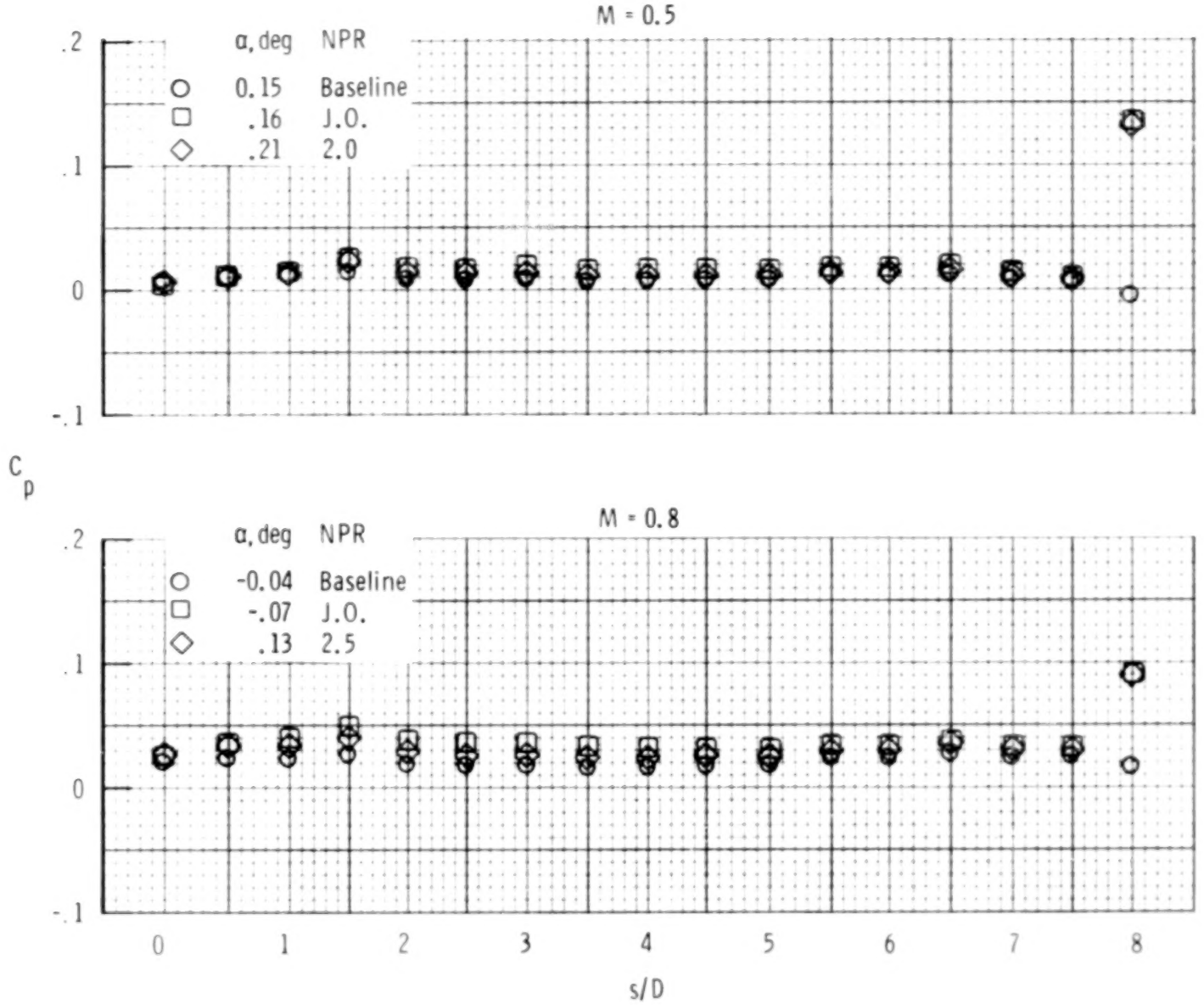

(j) x/D = 1; 2y/b = 0.5; z/D = 1.

Figure 20.- Concluded.

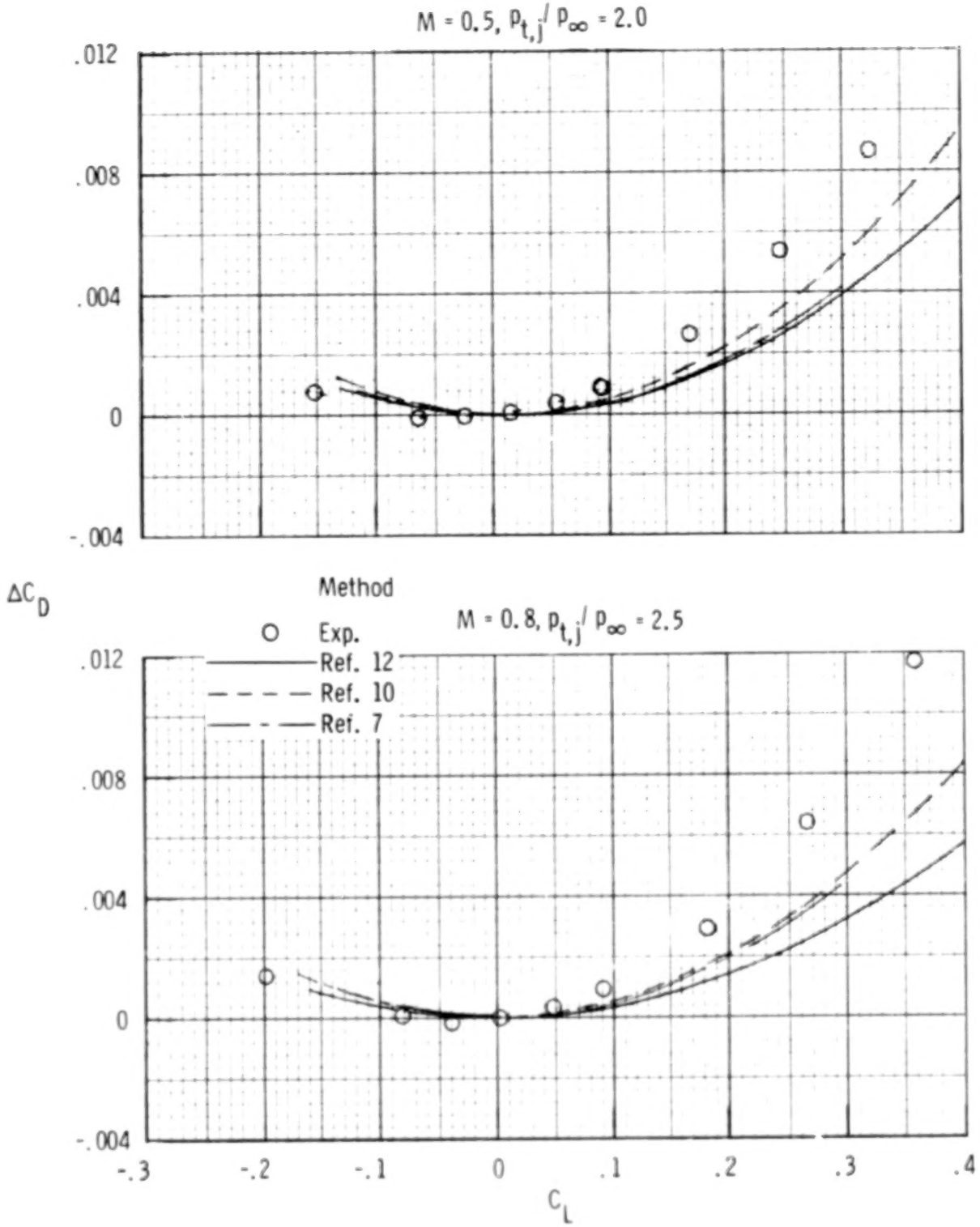

(a) x/D = -1; 2y/b = 0.25; z/D = 1.

Figure 21.- Comparison of experimentally and theoretically determined drag increments.

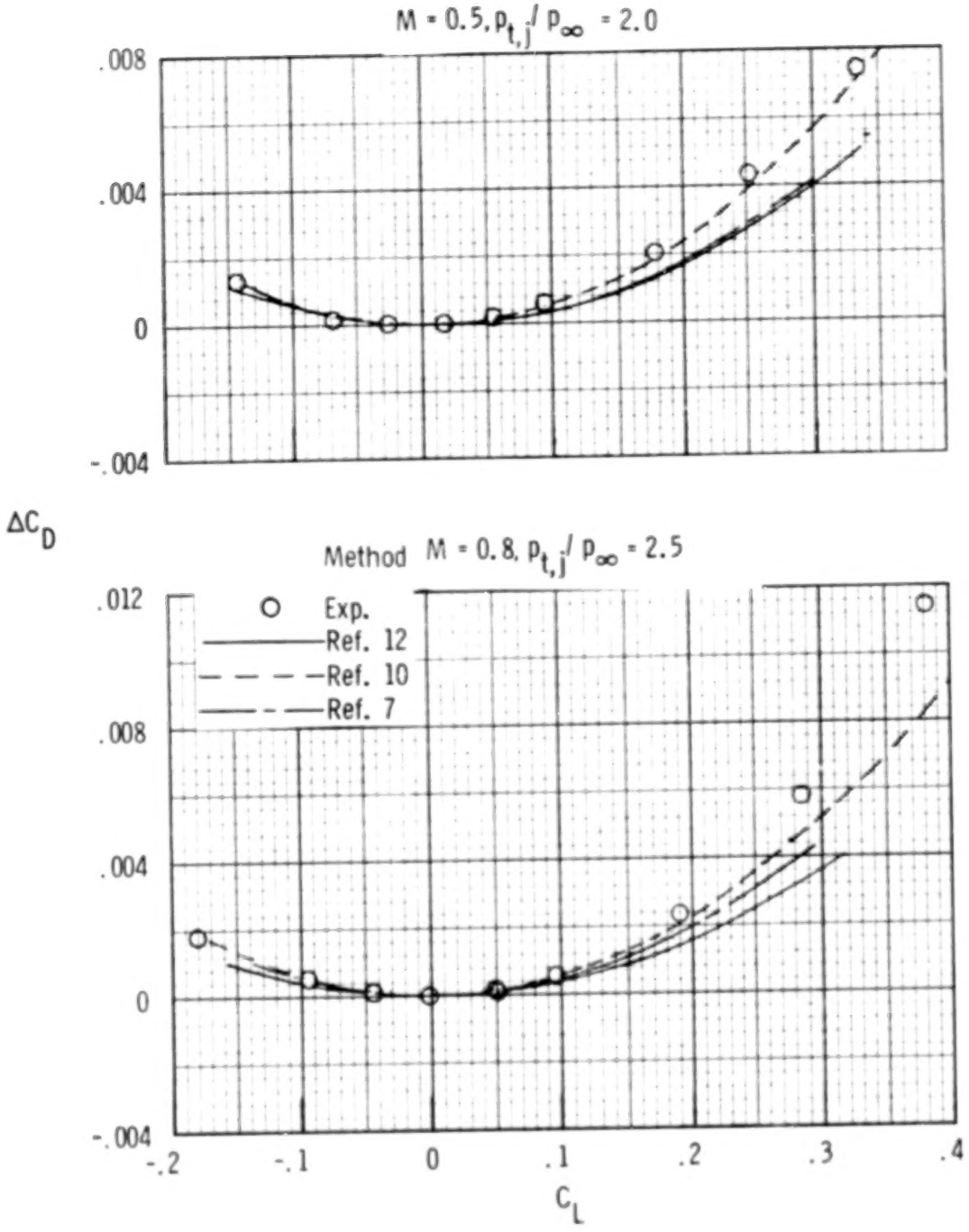

(b) x/D = 0; 2y/b = 0.25; z/D = 1.

Figure 21.- Continued.

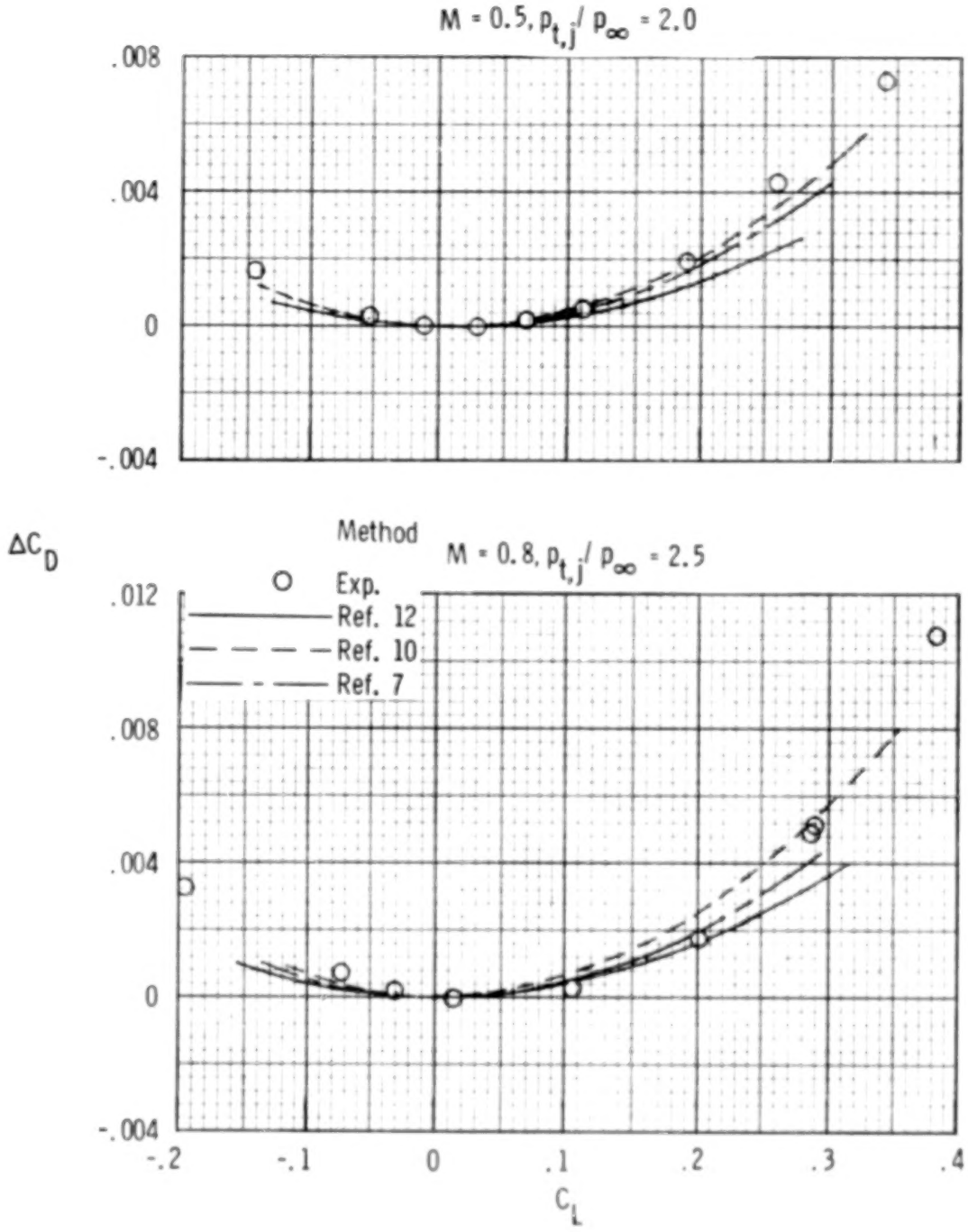

(c) x/D = 1; 2y/b = 0.25; z/D = 1.

Figure 21.- Continued.

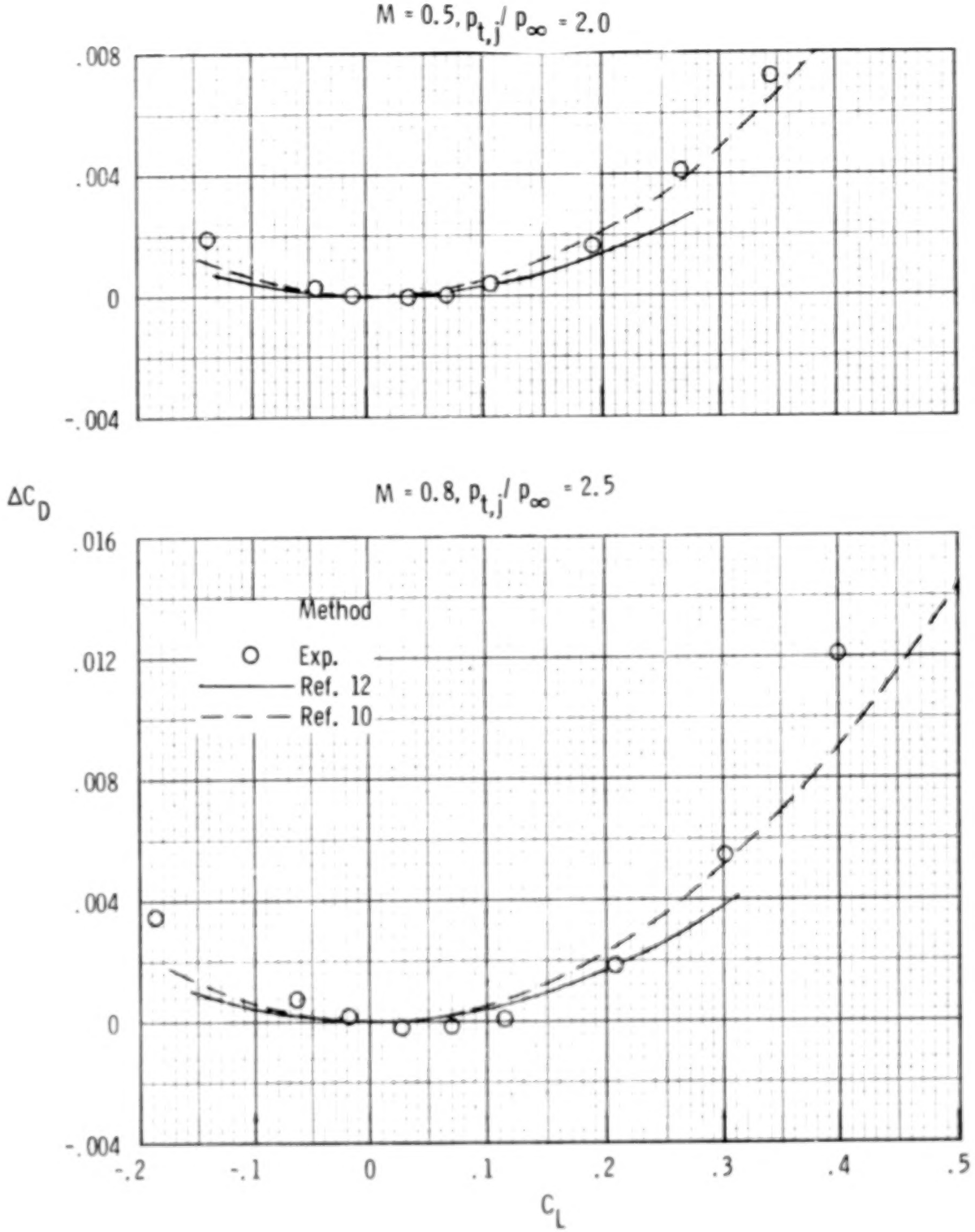

(d) x/D = 1.5; 2y/b = 0.25; z/D = 1.

Figure 21.- Continued.

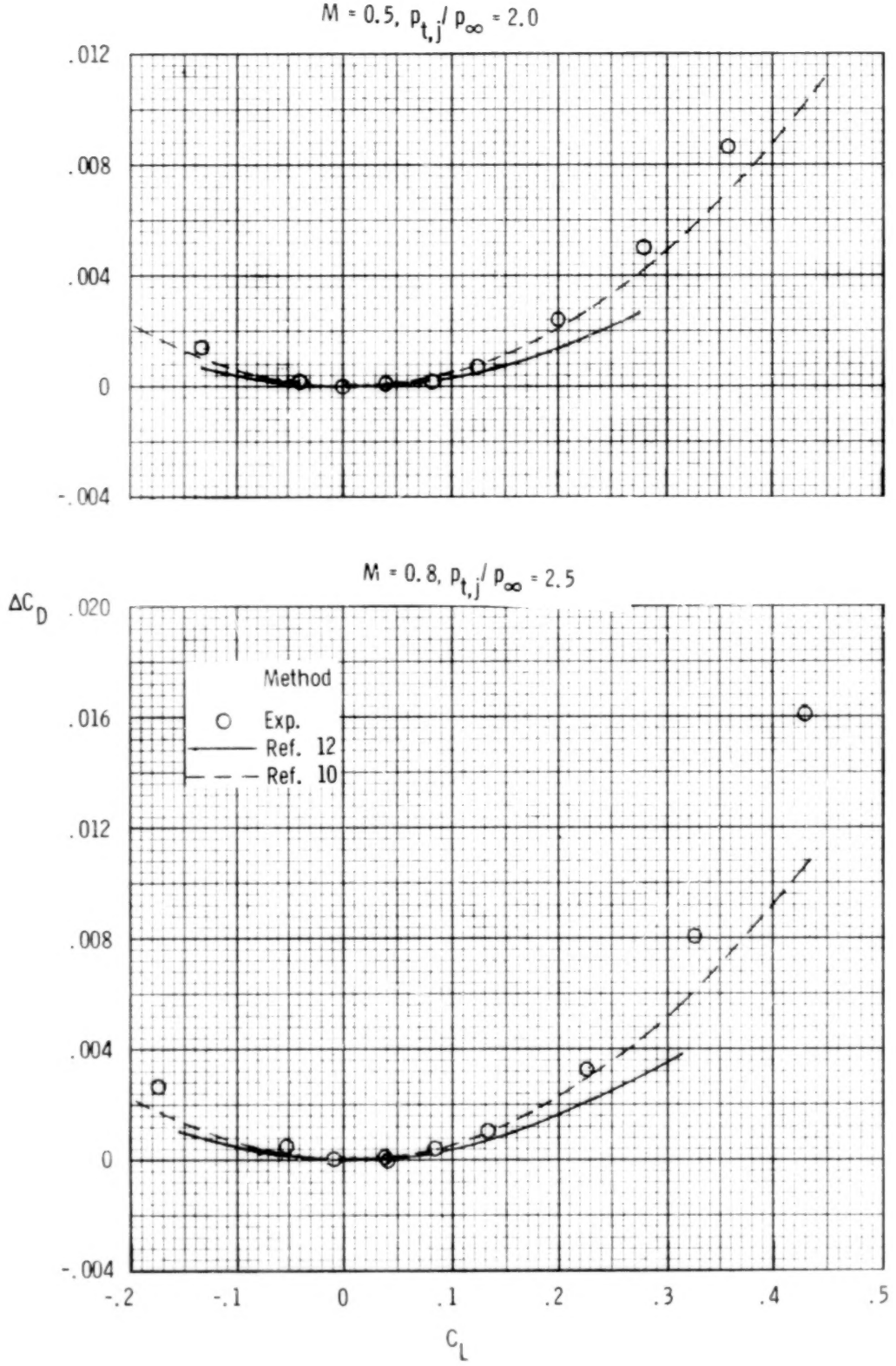

(e) x/D = 2; 2y/b = 0.25; z/D = 1.

Figure 21.- Continued.

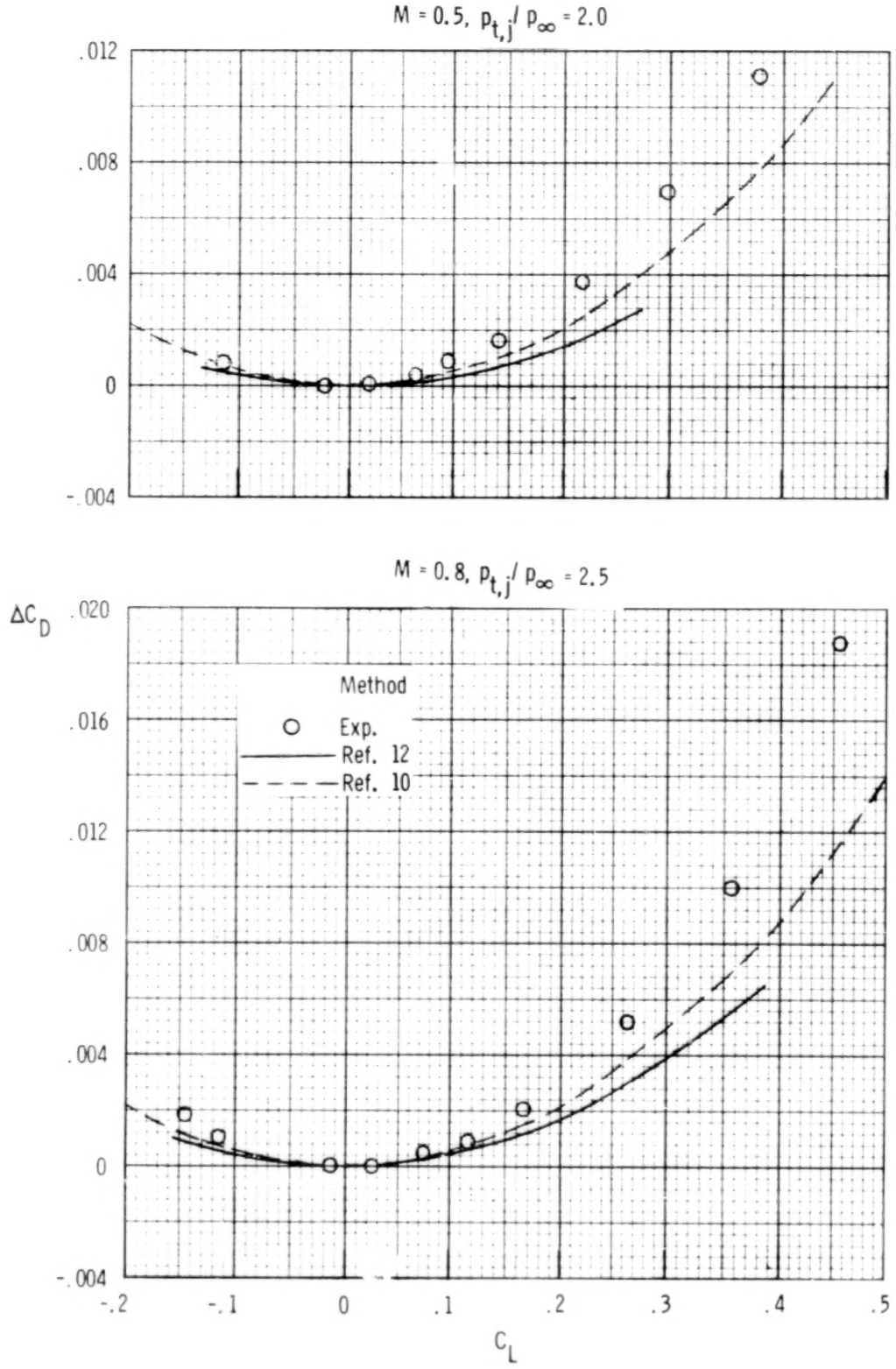

(f) x/D = 3; 2y/b = 0.25; z/D = 1.

Figure 21.- Continued.

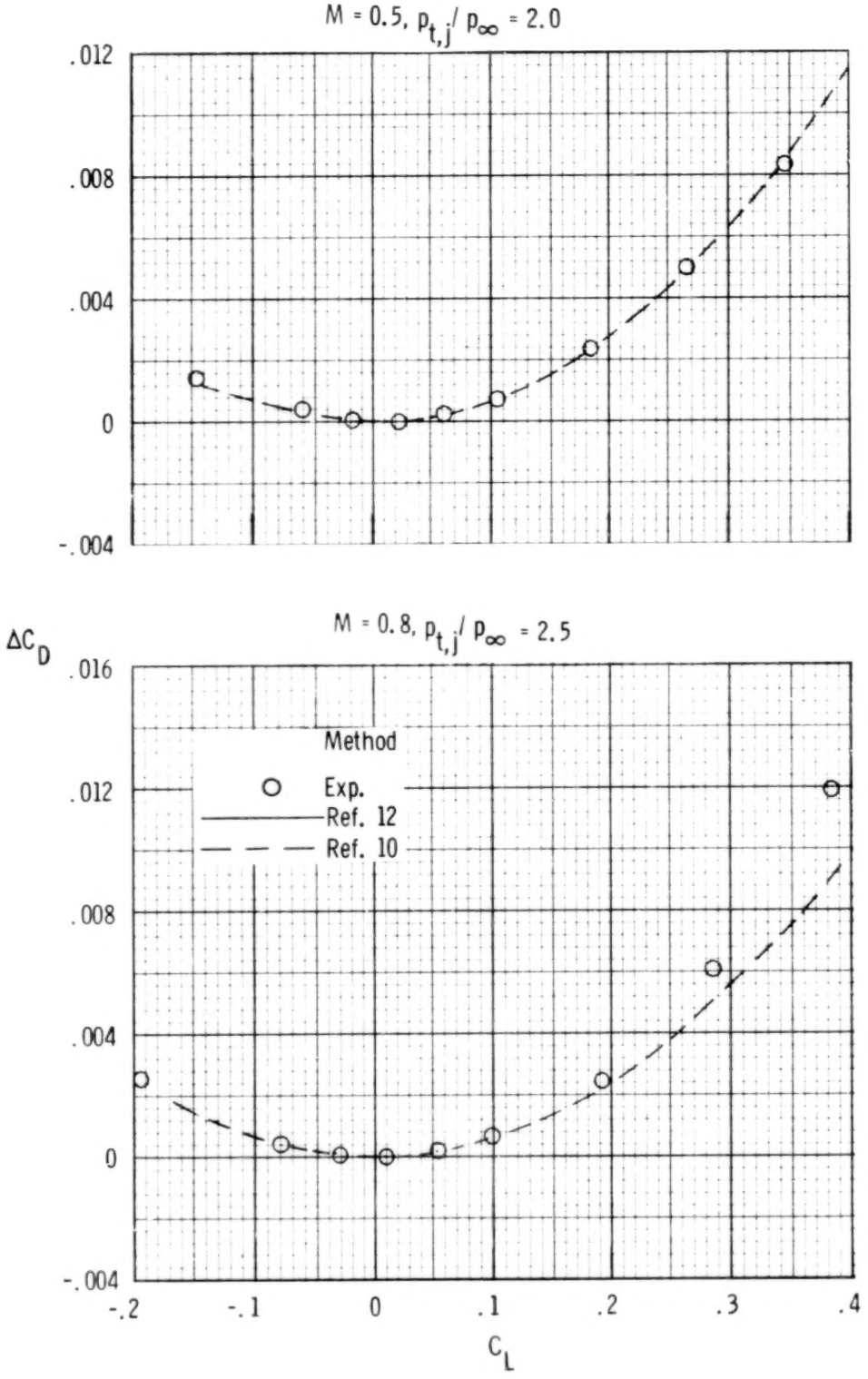

(g) x/D = 0; 2y/b = 0.25; z/D = 0.5.

Figure 21.- Continued.

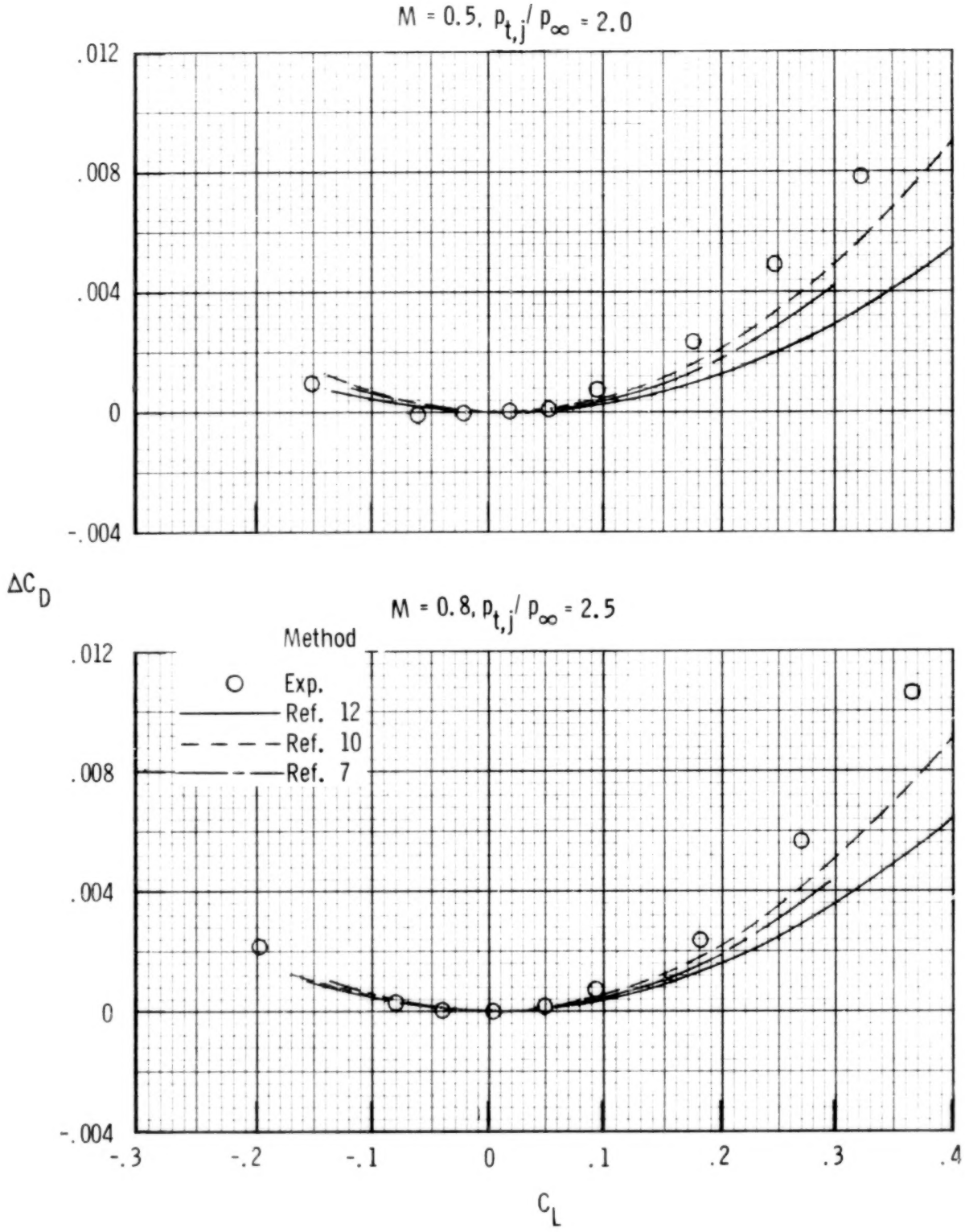

(h) x/D = 0; 2y/b = 0.25; z/D = 1.5.

Figure 21.- Continued.

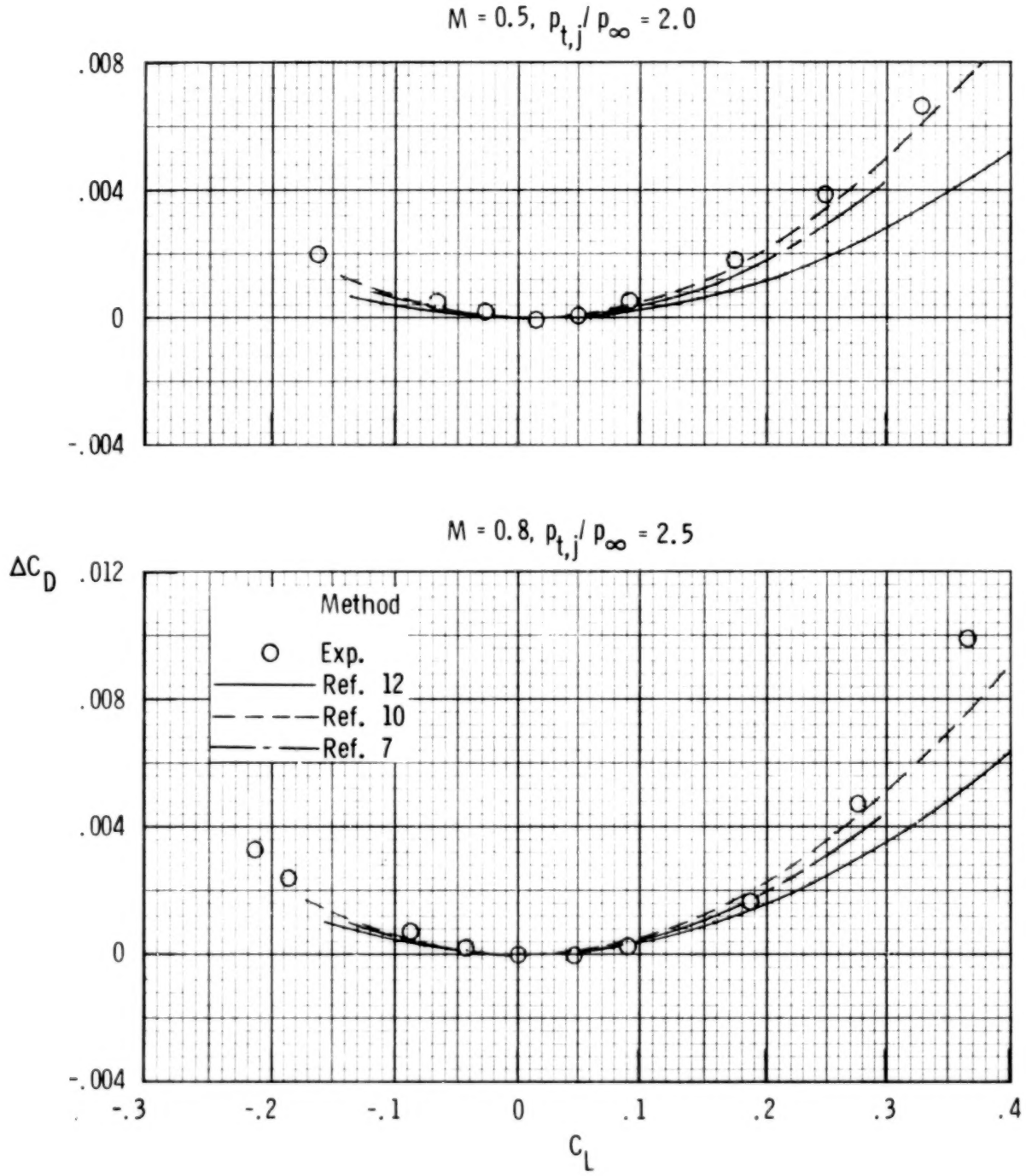

(i) x/D = 0; 2y/b = 0.5; z/D = 1.

Figure 21.- Continued.

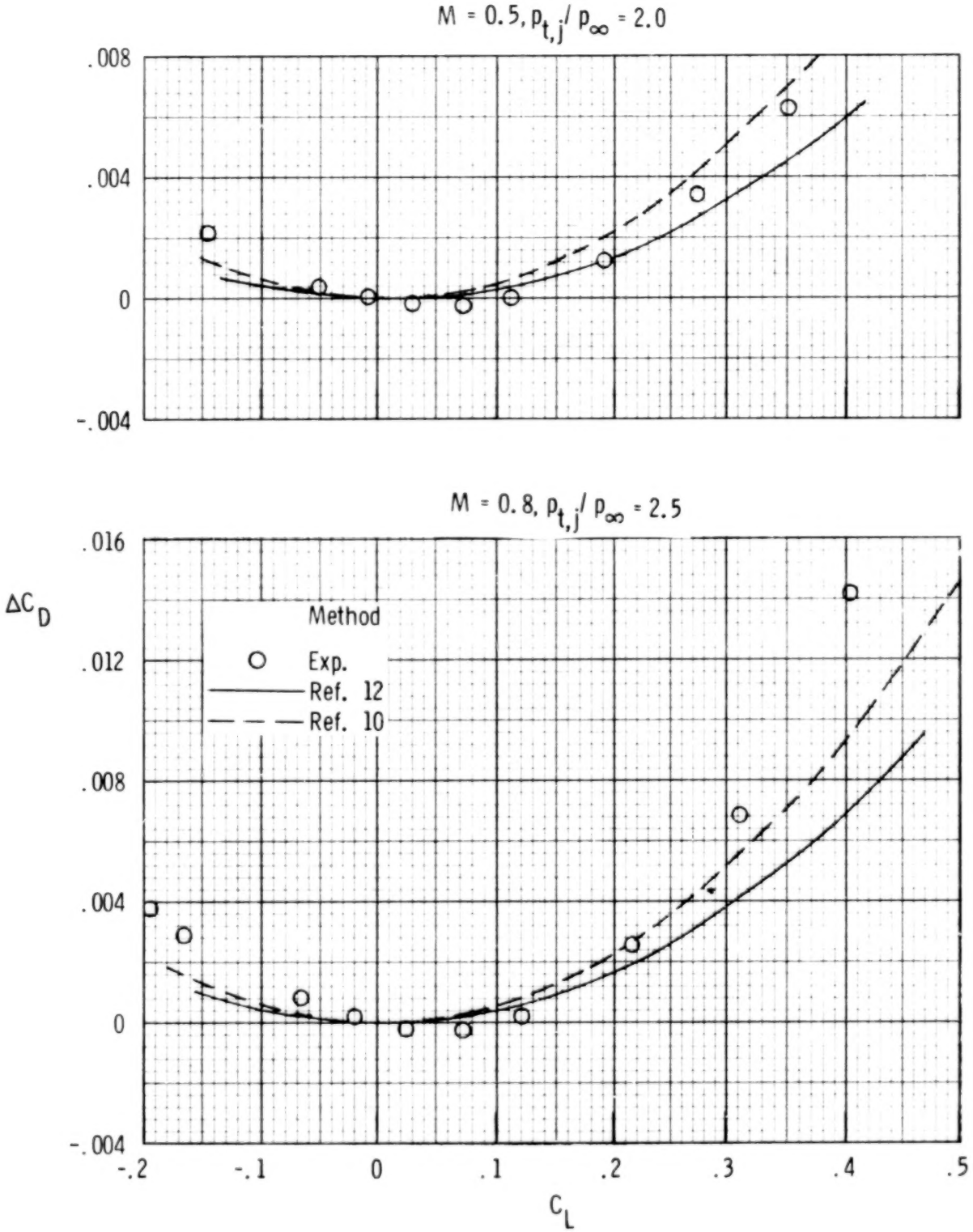

(j) x/D = 1; 2y/b = 0.5; z/D = 1.

Figure 21.- Concluded.

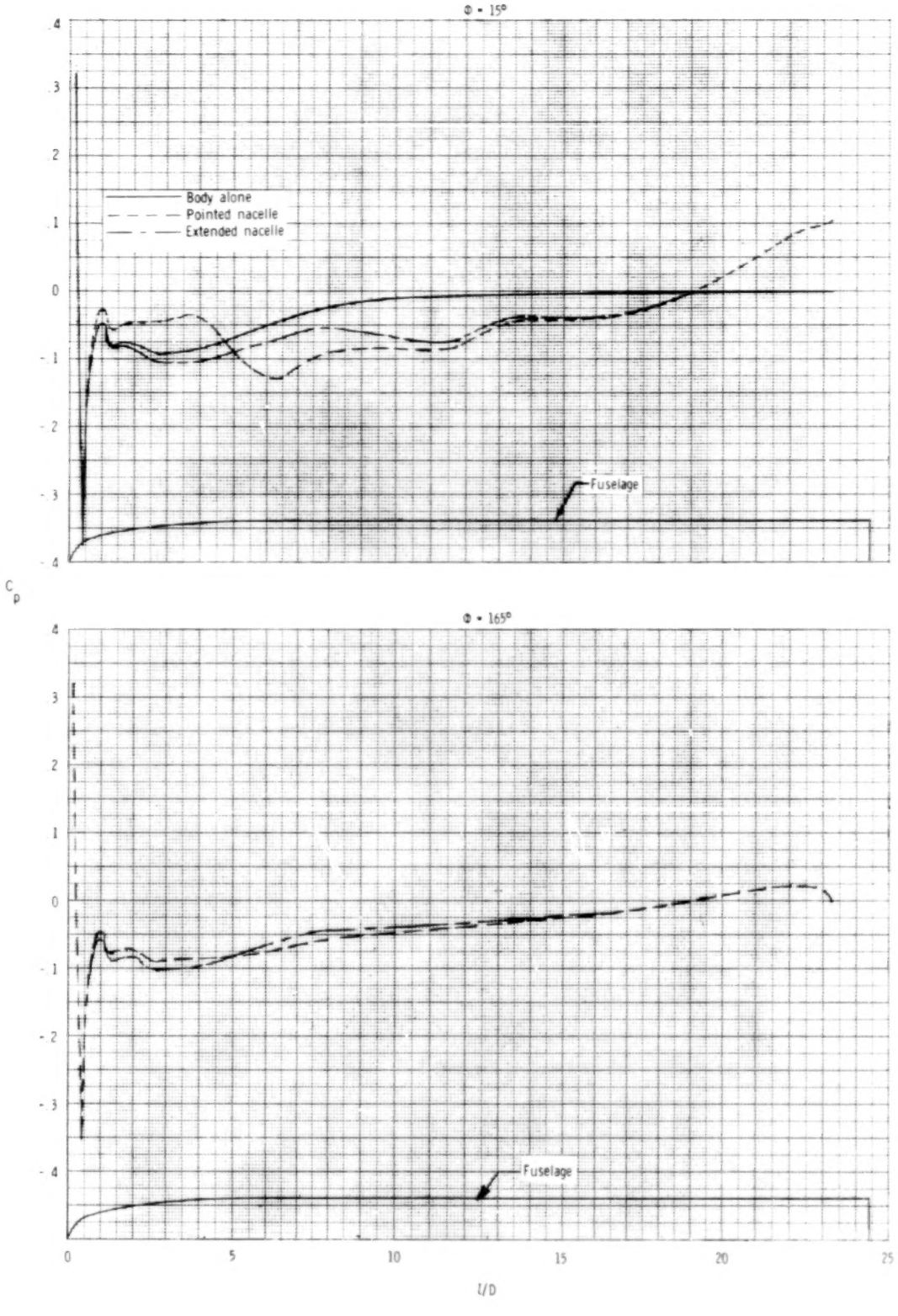

(a) Wing off.

Figure 22.- Effect of nacelle shape on theoretically determined fuselage pressure coefficients.

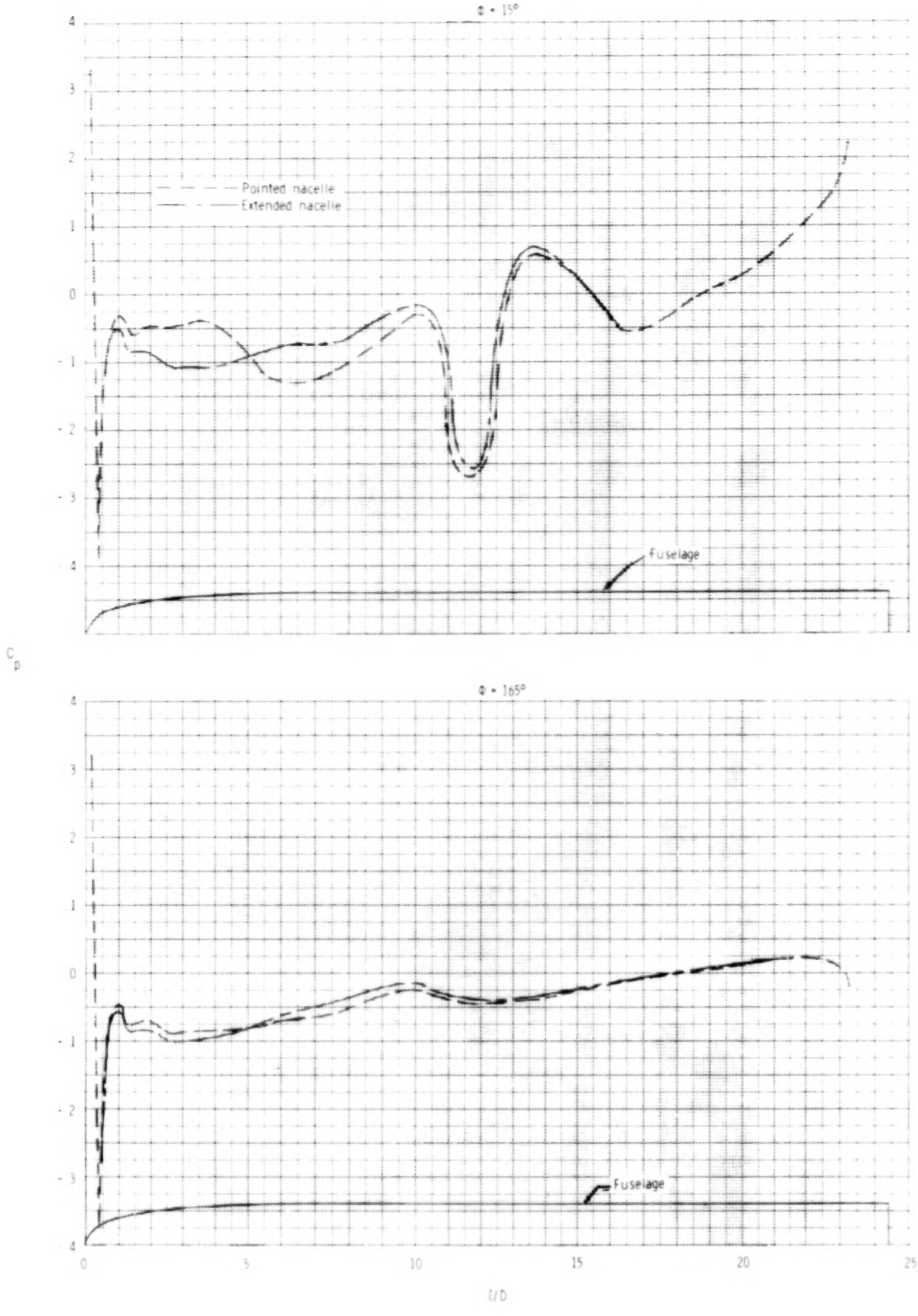

(b) Wing on.

Figure 22.- Concluded.

1. Report No.	2. Government Accession No.	3. Recipient's Catalog No.
NASA TP-1503		

4. Title and Subtitle	5. Report Date
AN EXPERIMENTAL AND THEORETICAL INVESTIGATION OF THE EFFECT OF NONMETRIC OVER-THE-WING NACELLES ON WING-BODY AERODYNAMICS	August 1979
	6. Performing Organization Code
7. Author(s)	8. Performing Organization Report No.
David E. Reubush	L-13010
	10. Work Unit No.
9. Performing Organization Name and Address	505-11-13-04
NASA Langley Research Center Hampton, VA 23665	11. Contract or Grant No.
	13. Type of Report and Period Covered
12. Sponsoring Agency Name and Address	Technical Paper
National Aeronautics and Space Administration Washington, DC 20546	14. Sponsoring Agency Code

15. Supplementary Notes

16. Abstract

Drag reduction benefits due to blowing the jet exhausts over the wing for a transport-type wing-body configuration were investigated in the Langley 16-foot transonic tunnel. In this investigation, a combination of a wing-body model and a powered-nacelle test rig was tested at Mach numbers of 0.50 and 0.80 at angles of attack from -2° to 4° and jet total-pressure ratios from jet off to 3 or 4 (depending on Mach number) for a variety of nacelle locations relative to the wing. In addition, the experimental results were compared with the predictions obtained from several theoretical techniques. Results from this investigation indicate that positioning of the nacelles (nonmetric) can have large effects on the wing-body drag. Some positions yielded higher drag than the baseline position, whereas others yielded lower drag than the baseline position. Results from the theoretical investigation indicate that the theoretical method which utilized a quasi-vortex-lattice for the wing and wing-jet interaction in combination with a jet entrainment model gave generally reasonable predictions of the drag increments.

17. Key Words (Suggested by Author(s))	18. Distribution Statement
Drag Over-the-wing nacelles Subsonic transport Wing-body aerodynamics	Unclassified - Unlimited Subject Category 02

19. Security Classif. (of this report)	20. Security Classif. (of this page)	21. No. of Pages	22. Price*
Unclassified	Unclassified	76	$6.00

* For sale by the National Technical Information Service, Springfield, Virginia 22161

NASA-Langley, 1979